Development of a Membrane-free Fluorescence-based Biosensor for Clinical Analysis

---

Dissertation zur Erlangung des
Doktorgrades der Naturwissenschaften
(Dr. rer. nat.)
an der Fakultät Chemie und Pharmazie
der Universität Regensburg
Deutschland

Vorgelegt von
Dan Strohmaier-Nguyen
aus Mannheim
im Jahr **2025**

Die vorliegende Dissertation entstand in der Zeit von Januar 2019 bis August 2024 am Institut für Analytische Chemie, Chemo- und Biosensorik der Universität Regensburg.

Die Arbeit wurde angeleitet von Prof. Dr. Antje J. Bäumner.

Promotionsgesuch eingereicht im März 2025
Kolloquiumstermin: 30.06.2025

Prüfungsausschuss
Vorsitzender: Prof. Dr. Rainer Müller
Erstgutachterin: Prof. Dr. Antje J. Bäumner
Zweitgutachter: Prof. Dr. Axel Dürkop
Drittprüferin: Prof. Dr. Miriam Breunig

Declaration of Collaborations

Most of the theoretical and experimental work presented in this thesis was conducted solely by the author. However, parts of the results were gained in collaboration with other researchers, which are stated in this section in accordance with §8 Abs. 1 Satz 2 Punkt 7 of the "Ordnung zum Erwerb des akademischen Grades eines Doktors der Naturwissenschaften (Dr. rer. Nat.) an der Universität Regensburg vom 18. Juni 2009".

Innovations in One-Step Point-of-Care Testing within Microfluidics and Lateral Flow Assays for Shaping the Future of Healthcare (Chapter 2)

This chapter has been published. The literature search and writing of the manuscript draft was done by the author. Antje J. Baeumner revised the manuscript and is corresponding author.

Membrane-Free Lateral Flow Assay with the Active Control of Fluid Transport for Ultrasensitive Cardiac Biomarker Detection (Chapter 3)

This chapter has been published. Antje J. Baeumner, Carina Horn and the author developed the concept for this work. Carina Horn and the author planned the experiments. The author did the experimental work and wrote the first draft of the manuscript. Antje J. Baeumner and Carina Horn revised the manuscript. Antje J. Baeumner is corresponding author.

NT-proBNP detection with a one-step magnetic lateral flow channel assay (Chapter 4)

This chapter has been published. Antje J. Baeumner, Carina Horn and the author developed the concept for this work. Carina Horn and the author planned the experiments. The author did the experimental work and wrote the first draft of the manuscript. Antje J. Baeumner and Carina Horn revised the manuscript. Antje J. Baeumner is corresponding author.

Sample-to-answer lateral flow assay with integrated plasma separation and NT-proBNP detection (Chapter 5)

This chapter has been published. Antje J. Baeumner, Carina Horn and the author developed the concept for this work. Carina Horn and the author planned the experiments. The author did the experimental work and wrote the first draft of the manuscript. Antje J. Baeumner and Carina Horn revised the manuscript. Antje J. Baeumner is corresponding author.

Table of Contents

List of Abbreviations and Symbols

In the following, all used abbreviations and symbols, besides the commonly known ones, are explained, while the page number refers to the first appearance in this thesis.

Abbreviation	Meaning	Page
AuNPs	Gold nanoparticles	13
CAGR	Compound annual growth rate	8
CHA	Catalytic hairpin assembly	29
COC	Cyclic olefin copolymer	31
CRISPR/CAS	Clustered regularly interspaced short palindromic repeats/CRISPR-associated system	19
cTnI	Cardiac Troponin I	15
ELISA	Enzyme-linked immunosorbent assay	14
HBS	HEPES-buffered saline	65
HDA	Helicase-dependent amplification	19
HF	Heart failure	64
HRP	Horseradish peroxidase	14
i3DP	Inkjet three-dimensional printing	32
LAMP	Loop-mediated isothermal amplification	19
LFA	Lateral flow assay	1
LOD	Limit of detection	1
MDM	Magnetic digital microfluidic	14
MEF	Metal-enhanced fluorescence	16
MIPs	Molecularly imprinted polymers	8
MNPs	Magnetic nanoparticles	1
MPXV	Monkeypox virus	15
NAATs	Nucleic acid amplification tests	19
NC	Nitrocellulose	1
NCDs	Non-communicable diseases	12
NT-proBNP	N-terminal pro-brain natriuretic peptide	68
oPAD	Origami paper-based analytical device	19

PAA	Polyacrylamide	61
PC	Polycarbonate	31
PDDA	Poly(diallyldimethylammonium chloride)	61
PDMS	Polydimethylsiloxane	30
PEM	Polyelectrolyte multilayer	1
PET	Polyethylene terephthalate	1
PMMA	Polymethyl methacrylate	31
POC	Point of care	60
POCT	Point-of-care testing	1
PPC	Protein-polymer complex	60
pSA	Polystreptavidin	61
PVA	Polyvinyl alcohol	14
QDs	Quantum dots	15
R2R	Roll-to-roll	34
RBCs	Red blood cells	120
RPA	Recombinase polymerase amplification	19
rPAD	Reagent-stored pad	19
RT-LAMP	Reverse transcription loop-mediated isothermal amplification	19
RT-PCR	Reverse transcription polymerase chain reaction	19
SCF	Sucrose-fixed substrate loaded fibers	14
SDA	Strand displacement amplification	19
SERS	Surface-enhanced Raman scattering	17
SLA	Stereolithography	32
SOPs	Standard operating procedures	5
SRB	Sulforhodamine B	13
UCNPs	Upconversion nanoparticles	15
WHO	World Health Organization	8

Summary

This thesis demonstrates the conversion of a conventional lateral flow assay (LFA) into a self-contained and compact membrane-free fluorescence lateral flow channel assay concept for clinical analysis.

While most LFAs rely on membrane and paper materials for protein immobilization, sample preparation, sample flow, and reagent storage, they also bear unfavorable properties. These include variations in flow rate and analysis time due to varying pore structure and sample viscosity. Additionally, obstruction of pores by matrix components, the requirement for relatively high sample volume due to its inherent absorbing properties, and inconsistency in the dispersion of the reagent to the membrane due to batch-to-batch variations further complicate their use. To address these performance-affecting factors, this thesis focuses on developing membrane- and paper-free one-step LFAs utilizing polyelectrolyte multilayer (PEM) and magnetic nanoparticles (MNPs) to enhance the controllability of the immunoreaction and reduce the sample volume. This approach improves overall assay performance and enables straightforward self-testing at home or in rural areas, with an emphasis on patient comfort.

Innovations in One-Step Point-of-Care Testing

The first part of this work reviews innovations in one-step point-of-care testing (POCT) within microfluidics and lateral flow assays (LFAs), examining how they are shaping the future of healthcare. These POCT platforms are carefully evaluated based on various factors, including ease of fabrication, scalability for mass production, simplicity of handling, long-term storage potential, cost-effectiveness, and the capability to integrate sample preparation.

Membrane-free Lateral Flow Assay

The second and third part of this work concentrate on developing membrane-free LFAs by exploring protein immobilization techniques on a flat PET foil, as opposed to the traditionally used nitrocellulose (NC) membrane as the immobilization matrix. By incorporating a PEM to electrostatically immobilize streptavidin and integrating

streptavidin-functionalized MNPs into POCT platforms, low limits of detection (LODs) for both approaches were reached, while also reducing the required sample volume by a factor of 7.5. This makes the platforms more suitable for POCT applications, in which the sample volume is limited or when patients' comfort is of utmost importance.

To be able to replicate the setup of the POCT platforms industrially, the test structure was designed in such a way that all fabrication steps are scalable. The LFAs comprise a PET foil substrate, a spacer with laser-cut capillaries, a cover foil with sample and outlet ports, and pressure-sensitive double-sided adhesive tape. This design enables cost-effective and straightforward manufacturing, allowing for reagent storage on the sensor and preserving the one-step process characteristic of traditional LFAs.

Despite the need for additional hardware, such as the micropump, its integration has enhanced the robustness and reliability of the assay for on-field applications. With limits of detection (LOD) of 56 $pg \cdot mL^{-1}$ for the PEM-based LFA and 43.1 $pg \cdot mL^{-1}$ for the MNP-based LFA in plasma, the platforms demonstrate equal or superior sensitivity compared to traditional LFA methods.

On-Chip Blood Plasma Separation

The fourth part of this work demonstrates the development of an integrated sedimentation-based blood plasma separation system for a fully integrated, ready-to-use POCT platform designed to detect NT-proBNP in undiluted whole blood. To enhance the gravity-based sedimentation, an aggregation agent was used to promote the clumping of red blood cells into bigger clusters. To achieve effective separation within the POCT platform, a physical filter trench was integrated into the system. This trench plays a crucial role in the process, ensuring that the separation of the blood cells is both efficient and reliable. The incorporation of this filter trench not only facilitates the separation of red blood cells but also enhances the overall performance and accuracy of the assay by preventing interference with the optical read-out. The device demonstrated high separation efficiency of 96.23 % and yield of 7.23 µL (=71.9 %). Furthermore, we elaborate on its user-friendly nature and demonstrate its proof-of-concept through an all-dried ready-to-go NT-proBNP lateral flow immunoassay with clinical blood samples.

Zusammenfassung

In dieser Arbeit geht es um die Umwandlung eines herkömmlichen Lateral-Flow-Assays (LFA) in ein eigenständiges und kompaktes membranfreies fluoreszenzbasiertes LFA-Konzept für die klinische Analyse.

Während die meisten LFAs auf Membran- und Papiermaterialien für die Proteinimmobilisierung, Probenvorbereitung, Probenfluss und Lagerung der Reagenzien angewiesen sind, weisen sie auch ungünstige Eigenschaften auf. Dazu gehören Schwankungen in Flussrate und Analysezeit aufgrund variierender Porenstrukturen und Probenviskosität. Darüber hinaus erschweren die Verstopfung der Poren durch Matrixkomponenten, der Bedarf an relativ hohem Probenvolumen aufgrund der inhärenten absorbierenden Eigenschaften und Inkonsistenzen in der Verteilung des Reagenz auf der Membran aufgrund von Chargenunterschieden ihre Anwendung.

Zur Überwindung dieser leistungsbeeinflussenden Faktoren konzentriert sich diese Dissertation auf die Entwicklung von membran- und papierfreien einstufigen LFAs unter Verwendung von Polyelektrolytschichten (PEM) und magnetischen Nanopartikeln (MNPs), um die Kontrollierbarkeit der Immunreaktion zu verbessern und das Probenvolumen zu reduzieren. Dieser Ansatz verbessert die Gesamtleistung des Assays und ermöglicht einen einfachen Selbsttest zu Hause oder in ländlichen Gebieten, wobei der Komfort des Patienten im Vordergrund steht.

Innovationen im One-Step-Point-of-Care-Testing

Zuerst liegt der Fokus dieser Arbeit auf eine Zusammenfassung von Innovationen im einstufigen Point-of-Care-Testing (POCT) im Bereich der Mikrofluidik und Lateral-Flow-Assays (LFAs) und wie sie die Zukunft des Gesundheitswesens formen. Diese POCT-Plattformen werden sorgfältig basierend auf verschiedenen Faktoren bewertet, darunter die Einfachheit der Herstellung, die Skalierbarkeit für die Massenproduktion, die Benutzerfreundlichkeit in der Handhabung, das Potenzial für Langzeitlagerung, die Kosteneffektivität und die Fähigkeit zur Integration der Probenvorbereitung.

Membranfreie Lateral-Flow-Assays

Der zweite und dritte Teil dieser Arbeit konzentriert sich auf die Entwicklung von Proteinimmobilisierungstechniken auf einer flachen PET-Folie anstelle der üblicherweise verwendeten Nitrocellulose (NC)-Membran als Immobilisierungsmatrix. Durch den Einsatz eines Polyelektrolyt-Multischichtsystems (PEM), das Streptavidin elektrostatisch immobilisiert und Integration von Streptavidin-funktionalisierten magnetischen Nanopartikeln (MNPs), wurden niedrige Nachweisgrenzen (LODs) in Immunoassays für beide Ansätze erreicht, wobei gleichzeitig das benötigte Probenvolumen um den Faktor 7,5 reduziert wurde. Dies machen die Plattformen besser geeignet für POCT-Anwendungen, bei denen das Probenvolumen begrenzt ist oder der Komfort der Patienten von größter Bedeutung ist. Um den Aufbau der POCT-Plattformen industriell reproduzierbar zu machen, wurde die Teststruktur so konzipiert, dass alle Herstellungsschritte skalierbar sind. Die LFAs bestehen aus einem PET-Folien-Substrat, einer Folie mit lasergeschnittenen Kapillaren, einer Abdeckfolie mit Proben- und Auslassöffnungen sowie doppelseitigem, druckempfindlichem Kleber. Dieses Design ermöglicht eine kostengünstige und unkomplizierte Herstellung, erlaubt die Lagerung von Reagenzien auf dem Sensor und bewahrt den Ein-Schritt-Prozess, der für traditionelle LFAs charakteristisch ist.

Trotz des Bedarfs an zusätzlicher Hardware, wie einer Mikropumpe, hat dessen Integration die Robustheit und Zuverlässigkeit der Tests im Anwendungsbereich verbessert. Mit Nachweisgrenzen (LOD) von 56 $pg \cdot mL^{-1}$ für den PEM-basierten LFA und 43,1 $pg \cdot mL^{-1}$ für den MNP-basierten LFA in Plasma zeigen die Plattformen eine gleiche oder sogar höhere Empfindlichkeit im Vergleich zu traditionellen LFA-Methoden.

Blutplasma-Trennung

Der vierte experimentelle Teil zeigt die Entwicklung eines integrierten Sedimentationssystems zur Blutplasma-Trennung für eine vollständig integrierte, gebrauchsfertige POCT-Plattform zur Detektion von NT-proBNP in unverdünntem Vollblut. Um die gravitationsbasierte Sedimentation zu verbessern, wurde ein Aggregationsmittel verwendet, das die Verklumpung der roten Blutkörperchen zu größeren Clustern fördert. Zur effektiven Trennung innerhalb der POCT-Plattform

wurde ein physischer Filtergraben in das System integriert. Dieser Filtergraben spielt eine entscheidende Rolle im Prozess, indem er sicherstellt, dass die Trennung der Blutkörperchen effizient und zuverlässig erfolgt. Die Einbindung dieses Filtergrabens erleichtert nicht nur die Trennung der roten Blutkörperchen, sondern verbessert auch die Gesamtleistung und Genauigkeit des Assays, indem Interferenzen mit der optischen Auswertung verhindert werden. Das Gerät zeigte eine hohe Separationsleistung mit einer Effizienz von 96,23 % und einer Ausbeute von 7,23 µL (entsprechen 71,9 %). Darüber hinaus wird die benutzerfreundliche Natur des Systems erläutert und das Konzept anhand eines gebrauchsfertigen NT-proBNP-Lateral-Flow-Immunoassays mit klinischen Blutproben demonstriert.

1 Motivation and Structure of the Thesis

The thesis focuses on the development of a fully integrated membrane and paper material-free fluorescence biosensor for clinical and personal healthcare applications.

Membrane and paper-material-free lateral flow assays (LFAs) represent a significant advancement in diagnostic testing, due to their ability to address several critical limitations associated with traditional membrane-based assays. One major issue with conventional LFAs is the batch-to-batch inconsistencies of membranes, which can lead to variability in sensor performance. Additionally, any changes in the standard operating procedures (SOPs) of membrane manufacturers may alter the pore characteristics, further impacting the reliability of the assay. Traditional membranes also have high sample and analyte absorbing properties, necessitating larger sample volumes, which can be uncomfortable for patients. Moreover, the inconsistency in sample transportation across the membrane can result in uneven flow rates and analysis times. This variability is exacerbated by different hematocrit levels in blood samples, which can affect the immunoreaction and compromise the assay's accuracy. By eliminating these membrane-related issues, membrane-free LFAs offer improved control over sample transportation and immunoreaction conditions, enhancing overall assay performance and patient comfort. One crucial aspect is preserving the one-step detection principle of LFAs, enabling easy operation for patients or untrained personnel. This simplicity is especially beneficial in resource-limited settings, such as remote areas or low- to middle-income countries, where access to centralized laboratories is often restricted.

Chapter 1 covers the motivation behind the thesis and outlines the structure of the work.

Chapter 2 provides a comprehensive overview of one-step point-of-care testing (POCT) platforms, emphasizing their significance in the early detection of diseases. It critically discusses various applications, highlighting the versatility and potential of one-step POCT in different settings. The chapter also addresses the challenges and limitations

faced during the transition from research prototypes to market-ready products, focusing on factors such as scalability, cost-effectiveness, and operational handling.

Chapter 3 focuses on the innovative conversion of a traditional lateral flow assay (LFA) into a membrane-free LFA. The nitrocellulose membrane is replaced with a polyelectrolyte multilayer capable of immobilizing high concentrations of streptavidin for a biotin-streptavidin based immunoassay. Sample transportation is controlled by a micropump, eliminating issues related to membrane inconsistencies. The sensor's performance is evaluated by detecting the heart failure biomarker NT-proBNP and is benchmarked against current LFAs available on the market, demonstrating its enhanced reliability and precision.

Chapter 4 continues the exploration of membrane-free lateral flow assays (LFAs), this time replacing the membrane with streptavidin-functionalized magnetic nanoparticles. These nanoparticles have a high surface-to-volume ratio, facilitating excellent interaction of reagents in the immunoassay within the diffusion-limited LFA. This chapter delves into the benefits of using magnetic nanoparticles, highlighting their potential to enhance assay sensitivity and reliability compared to traditional LFA methods.

Chapter 5 focuses on integrating blood plasma separation into a fully integrated one-step POCT platform and its application in real-life scenarios. Instead of the commonly used filter membrane, which absorbs a significant amount of sample and analyte, a simple gravitation-based sedimentation separation is employed. The sedimentation process is enhanced using an agglutination agent that forms blood cell clusters, reducing the separation time. This innovative platform is then compared to the traditional bench-top centrifugation-based plasma separation method and is evaluated in an immunoassay.

2 Innovations in One-Step Point-of-Care Testing within Microfluidics and Lateral Flow Assays for Shaping the Future of Healthcare

Abstract

Point-of-care testing (POCT) technology, using lateral flow assays and microfluidic systems, facilitates cost-effective diagnosis, timely treatment, ongoing monitoring, and prevention of life-threatening outcomes. Aside from significant advancements demonstrated in academic research, implementation in real-world applications remains frustratingly limited. The divergence between academic developments and practical utility is often due to factors such as operational complexity, low sensitivity, bulky read-out equipment and scale of production. Taking this into consideration, our objective is to present a critical and objective overview of the latest advancements in fully integrated one-step POCT assays for home-testing which would be commercially viable. In particular, aspects of signal amplification, assay design modification, signal read-out, sample preparation and scalable production are critically evaluated and their features and medical applications along with future perspective and challenges with respect to minimal user intervention and mass-production are summarized.

Keywords: one-step, POCT, lateral flow assay, microfluidic, signal amplification, scale-up, fabrication, reader

A shorter version of this chapter has been published.

Strohmaier-Nguyen, D., Horn, C., & Baeumner, A. J. (2024). Innovations in one-step point-of-care testing within microfluidics and lateral flow assays for shaping the future of healthcare. *Biosensors and Bioelectronics*, 116795.
https://doi.org/10.1016/j.bios.2024.116795

Author contributions: DSN did the literature search and wrote the first draft of the manuscript. AJB revised the manuscript and is the corresponding author.

2.1 Introduction

Lateral flow assays (LFA) and microfluidic assays are popular diagnostic systems [1, 2] and should meet the seven World Health Organization (WHO) guidelines for a point-of-care test (POCT) summarized in "ASSURED" (affordable, sensitive, specific, user-friendly, rapid and robust, equipment-free, and deliverable to end users) [3] (Figure 1). In general, the field of application of POCTs has significantly broadened to various operational areas detecting a broad range of analytes. These can be mainly grouped into biological analytes, such as nucleic acids, enzymes, antibodies, small molecules, cells and tissues. With the continuing discovery of new biomarkers, biorecognition elements used for the specific capture of the target marker have been continuously evolving [4]. Natural (antibodies [5], enzymes [6], nucleic acids [7]) and synthetic biorecognition elements (molecularly imprinted polymers (MIPs) [8]) are frequently used in biosensors. Typically, an optical or electrochemical label, that is connected with the biorecognition element, provides a semi-quantitative or quantitative signal that can be easily interpreted by the naked eye, a spectrometer, or electrochemically [9]. The projected revenue for global POCT is anticipated to increase from $45.4 billion in 2022 to $75.5 billion by 2027, exhibiting a compound annual growth rate (CAGR) of 10.7 % [10]. This growth can be attributed to various factors, including advanced technology, heightened health awareness, and an increasing demand from developing countries [11]. Despite their popularity, most commercial POCT systems often do not meet the ASSURED criteria [12] and fail to fulfill requirements (1) in low-resource settings, (2) in settings with shortage of skilled personnel and (3) in automation of operation steps to eliminate user-associated inconstancy in the test results. Mostly, those tests are typically operated in fully automated fashion within centralized health centers for diagnosis. This presents a major challenge, especially in underdeveloped nations where there is often a shortage of both the necessary instrumentation and skilled physicians to conduct these tests, leading to limited diagnostic capabilities. To overcome this burden miniaturization of the detection systems into portable and cost-effective devices or the utilization of even a smartphone offer fast results on-site without the need for trained personnel or complex sample preparation, making them a more convenient option compared to larger and more complex instruments [13]. Most POCT platforms typically

necessitate additional hands-on steps, such as sample preparation, washing, and the introduction of additional solutions to provide sensitive testing. This can lead to intricate operations for the user and increased susceptibility to errors in the detection process [14]. Furthermore, it was noted that the test's performance saw a significant decline attributed to the absence of user expertise, ultimately undermining the test's accuracy [14]. Especially, with the current shortage of healthcare professionals and the additional training and workload for complex POCT procedures may compromise the care provision [15]. In order to enable the test procedure to be conducted by non-specialized personnel or even patients themselves, the integration of sample processing steps and detection into a fully automated one-step POCT platform is an essential prerequisite. Following the sample introduction to the POCT device, amplification and washing steps do not require any sample handling, allowing automated testing with minimal manual interaction. This ensures the elimination of the risk of contamination or user error, which could otherwise lead to inaccurate results [16]. Additionally, to enhance the commercial adoption of one-step POCT systems, it is crucial to hermetically store the immunoassay reagents, either in lyophilized or dried form on the test. This safeguards against biodegradation, ensures the reliability of testing, and facilitates shipping and storage at ambient temperatures [17]. Hence, the optimal POCT system allows specific and sensitive analyte detection, yet eliminating the need for cumbersome and complex equipment and ensuring easy operation for lay patients [18].

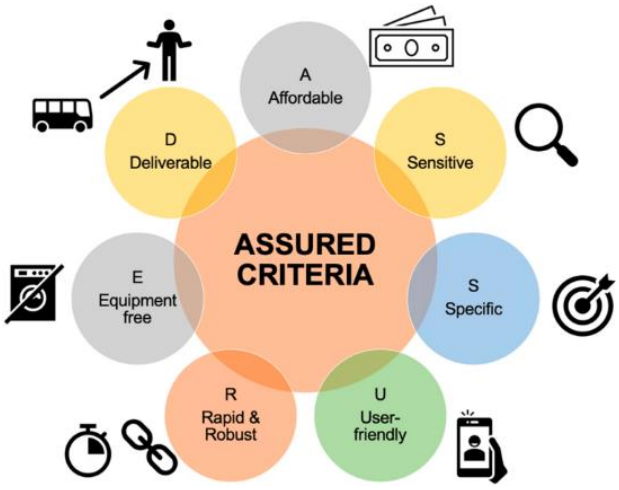

Figure 1: An illustration of the ASSURED criteria for diagnostic platforms. Reproduced/adapted from [19] (https://creativecommons.org/licenses/by/4.0/).

2.2 Complementary recent reviews and focus of this article

In recent years, several notable reviews have emerged in the field of LFA and microfluidics for POCT [9, 20–22]. While most of them, focus on specific disease diagnostic such as COVID-19 [23, 24], hepatitis [25], reviewed specific detection techniques such as nucleic acid detection [26, 27] or primarily emphasize the development and incorporation of new technologies [28] and signal amplification strategies [9] they have limited in-depth discussions on their translation into practical applications and barely consider the operation experience by the end-user. A recent review closely aligns with the content of our review. However, their focus is primarily directed towards simplifying the incubation and washing steps in POCT [18]. Our review instead concentrates on the advancement made in one essential area that is vital to achieving the goal of producing high-performing immunological devices for on-site use: the development of sensing strategies that allow one-step POCT systems with a focus on minimizing user involvement by allowing only the sample to be applied to the assay. At the same time, our review consistently focuses on the aspect of mass production and the associated commercialization of the POCT product, aiming to bridge the gap between research and industry. Moreover, most reviews address paper-based LFAs and microfluidic assays individually [29–32]. Instead, we consolidate the latest state-of-the-art one-step methodologies of both topics devised by the scientific community over the past five years. It highlights strategies that can jointly facilitate the development of one-step POCT platforms designed for home-testing, while addressing the key challenges that lie between prototype creation and mass production. First, we provide examples of one-step POCT devices that have made it to the market. Secondly, our focus shifts to signal amplification advancements that can further enhance the sensor performance and have been successfully integrated into one-step POCT devices. Finally, we explore the effect of test design on the one-step assay and the integration of sample preparation steps into POCT platforms. We also provide a critical analysis of available readout devices and especially fabrication processes which are crucial for any POCT to successfully reach the market. In the conclusion, we analyze and explore prospects for the future.

2.3 Commercial one-step POCT platforms

Although lab-on-chip systems have been in existence for several decades, most of them have not yet been commercialized or regularly utilized as research-grade instruments outside of specialized laboratories. For immunological devices to successfully enter and thrive in the market, they must meet several crucial criteria that ensure their practicality, accessibility, and efficiency. Firstly, they need to be simple to operate, allowing users to perform tests with minimal effort and without specialized training [33]. This leads to the second requirement: the devices must function effectively without the involvement of trained professionals, making them ideal for widespread use in various settings. Additionally, these devices must be cost-effective, ensuring they are affordable for a broad audience, which is critical for large-scale adoption. The ease of fabrication in bulk is another essential factor, as it guarantees that the devices can be mass-produced efficiently, maintaining quality and availability [34]. Lastly, a rapid turnaround time is vital, providing quick results that are necessary for timely decision-making in clinical and on-site applications [22]. By fulfilling these requirements, immunological devices beyond the LFA concept can overcome barriers to market entry and achieve widespread adoption, ultimately advancing the field of Point-of-Care Testing (POCT). To address the mentioned requirements in POCT and in response to the growing trend of health-conscious behavior, commercially available fully-integrated one-step POCT devices have been developed (Table 1) [29]. All devices have in common, that signal generation and analysis are automatically initiated upon sample application to the test and therefore, enable user-independent highly sensitive platforms. In addition, a portable and handheld reader enables on-field analysis, and the proper material and format decision of the sensor format allows profitable industrial scale up production.

Table 1. Examples for commercially available one-step POCT devices

Platform	Reader	Sensing strategy	Sample	Volume (µL)	Biomarkers	Time (min)	Reference
iSTAT	Handheld / portable	electrochemical	Whole blood	17 – 40	lactate, cardiac, hormones	2 – 15	[35]
Triage	Small benchtop / portable	fluorescence	Whole blood or plasma	175 – 250	cardiac	15 – 20	[36]
Atellica VTLi	Handheld / portbable	frustrated total internal reflection imaging	Whole blood or plasma	30	cardiac	8	[37]
LumiraDx	Handheld / portable	fluorescence	Whole blood or plasma	20	cardiac	12	[38]
FREND	Small benchtop / portable	fluorescence	Serum or plasma, nasopharyngeal swab	35 – 70	cardiac, respiratory, urology	3	[39]

2.4 Signal amplification for one-step POCT platforms

The WHO reports that nearly three-quarters of all deaths globally are caused by non-communicable diseases (NCDs), with cardiovascular diseases being the leading cause of NCD deaths annually, along with cancer, chronic respiratory illness, and diabetes [40]. Therefore, early detection of disease biomarkers through highly sensitive analytical devices is crucial in reducing mortality rates. POCT is especially beneficial in low- to middle-income countries where NCD deaths are more prevalent, as POCT is more accessible and convenient compared to conventional laboratory analytical devices, which are often expensive, labor-intensive, and cumbersome. However, the lack of sensitivity and specificity has made POCT unreliable and susceptible to false negatives and false positives [15]. Therefore, developmental focus in the scientific community has been toward improving the assay performance and the pursuit of ever-lower detection limits. While there have been numerous reported record-breaking limits of detection (LODs) for specific analytes, there has unfortunately been an over-emphasis on publications with limited consideration of practical applications, especially in resource or personnel-limited settings. To enhance sensitivity, users often must add an additional signal amplification solution or perform an extra washing step, both of which introduce

additional operational complexities and may elevate the risk of errors [18] rendering the gained LOD performance often times useless. In the following discussion, we will concentrate on the most recent promising developments that demonstrate enhanced sensitivity for one-step POCT platforms. This advancement aims to eliminate complex operational procedures and, consequently, mitigate the potential for errors.

2.4.1 Optical POCT

Presently, most POCT utilize colorimetric signals that are created through colored labels. Antibody-conjugated colloidal gold nanoparticles (AuNPs) are often the preferred choice for quantification, as they have biocompatible properties, are easily modified and functionalized, and exhibit surface plasmon resonance in the visible range. This has made gold nanoparticles the benchmark in the field [41, 42]. Despite its advantageous properties, AuNPs in LFA tests are not without drawbacks. These drawbacks include low AuNP capture efficiency (<5 %) by the recognition elements, speed of flow [43] and insufficient visual contrast detection, leading to subpar sensitivity and detection limits [44]. To increase the color contrast, several novel metallic [45] and non-metallic NPs [46] as well as well-known signal amplification strategies through conjugation, aggregation and growth of nanoparticles have been employed [47]. However, the latter typically require the manual addition of extra amplification solutions [48, 49], introducing complexity and the potential for errors into the assay, as the signal-enhancing reagent must be added at precise timing and temperature conditions [50, 51]. To preserve the user-friendly nature typically associated with LFAs, the integration of the signal amplification step within single-step POCT systems has been crucial [52]. The growth of nanoparticles is accomplished by storing the amplification solution in a dried form on the test and subsequently delivering the reagent to the test zone through manipulation of the test structure or the incorporation of solution-delivering polymers with a sensitivity enhancement of 5-fold up to 543-fold (Figure 2a) [53, 54]. Another amplification approach is the accumulation of multiple nanoparticles that are different in size, on the test line. By storing the NPs on the test, the one-step mechanism is retained and demonstrated a 10-fold up to 30-fold signal enhancement (Figure 2b) [55–57], compared to the traditional LFA. Recently, loading of liposomes with sulforhodamine B (SRB) showed an improvement of the

detection limit of interleukin-6 (IL-6) by an order of magnitude (7 pg·mL^{-1}) when compared to the traditional AuNP based LFA (81 pg·mL$^{-1)}$ (Figure 2c) [58]. Key to this significant lowering of the LOD was the optimization of SRB loading and liposome size. Additionally, enzymatic processes have been shown to increase the sensitivity of immunoassays [59, 60]. However, the addition of the enzyme substrate requires an additional operation step, making also this test procedure more complicated and prone to manual errors [61]. To eliminate the extra addition of the enzyme's substrate, one-step strategies have been realized into POCT platforms [62–66], by implementing wax structures [67, 68] and optimization of the channel geometry to achieve a simple one-step enzyme amplified immunoassay [69]. Another group has demonstrated a fully integrated POCT device for the health monitoring of astronauts through the chemiluminescence process of horseradish peroxidase (HRP) and luminol. The device consists of a disposable LFA cartridge, where the active reagents were stored in reservoirs and a chemiluminescence reader.

The amplification solutions were manually activated through pressure-actuated pouches and controlled through similar valves, thus the assay only requires the addition of the sample [70]. A fully integrated and automated platform based on magnetic digital microfluidic (MDM) technology was demonstrated by the group of [71] (Figure 3a). The platform performs microbead-based ELISA in droplets using highly sensitive biotinylated magnetic nanoparticles, as the mobile substrate.

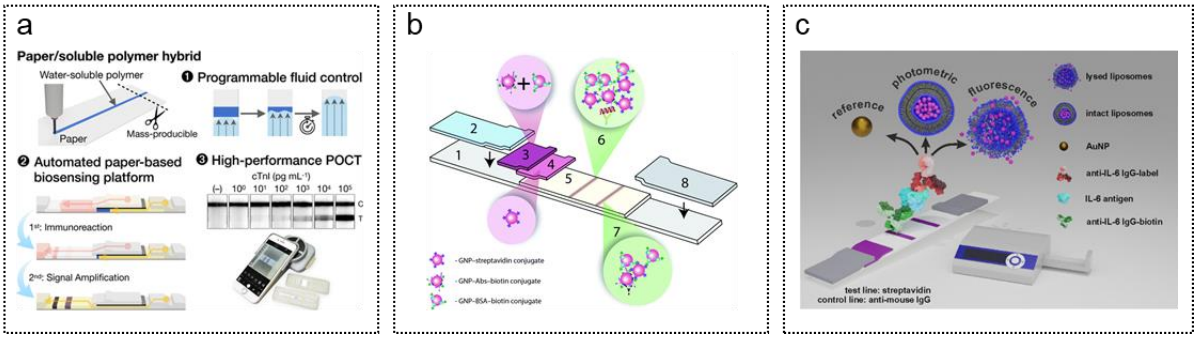

Figure 2: AuNP-based amplification strategies for one-step POCT. An illustration of the workflow of a programmable fluid control for the signal amplification on a lateral flow assay with a dissolvable PVA barrier. Reproduced/adapted from [53] (a). Network of gold nanoparticles. Reproduced from [56] (https://creativecommons.org/licenses/by-nc/3.0/) (b). Loaded liposomes for signal improvement. Reproduced/adapted from [58](https://creativecommons.org/licenses/by/4.0/) (c).

These nanoparticles were controlled by an external magnet, allowing for automated immunoreaction and enzymatic amplification with HRP. By adding sucrose-fixed substrate loaded fibers (SCF) onto the LFA sample pad, automated substrate delivery for the signal amplification with Au@Pt nanozyme at the test line was achieved. The LFA demonstrated similar analytical performance for the detection of acetamiprid with a simplified operation procedure. However it should be noted that the addition of an extra fiber, with high absorbance capacity, may lead to an increase of required sample volume (Figure 3b) [72]. Han et al. introduced a water-swellable polymer for the automated substrate delivery and enabled a 595-fold higher detection limit for cTnI than the gold standard (Figure 3c) [73]. When the immunoreaction is saturated, the polymer releases the reagent solution for the signal amplification. Even though the release of the substrate is automated, and the error susceptibility is reduced by the use of the polymer, the reagent solution still needs to be applied manually to the test.

2.4.2 Photoluminescence

Fluorescence detection has gained widespread prominence in the field of biomedicine and has been integrated into numerous one-step clinical diagnostic instruments, prominently including fluorescent immunoassays. The gain in sensitivity and LOD makes it highly appealing also for the POCT. A variety of fluorescent reporters, including fluorescent dyes, quantum dots (QDs), carbon dots, and upconverting nanoparticles (UCNPs), are employed as amplification signals, due to their enhanced fluorescence output and stability [74, 75]. However, costly optical detection instruments are required to achieve the desired dynamic range and detection limits, preventing its application in low-resource settings and in the at home testing market [76]. In addition to improve readers an abundance of amplification strategies have been proposed recently. Similar to colorimetric approaches, the sheer number of fluorescent labels per binding site at the detection area can be increased through nanocarriers. Nanocarriers pose flexible structures housing a multitude of cavities, holes, or pores, making them suitable for the encapsulation of a diverse range of materials [77]. Currently, the existing nanocarrier options primarily include liposomes [78], mesoporous silica [79], as well as nanomaterials based on polymers [80, 81], metal oxides [82], and carbon [83]. By exploiting the electrostatic multilayer deposition of multiple QDs onto a graphene oxide

nanosheet, a multilayered fluorescent nanofilm improved the sensitivity by 2-3 orders of magnitude for the detection of *Salmonella typhimurium*, compared to the conventional LFA [84]. Yang et al. demonstrated a rapid, on-site, and highly sensitive detection of the MPXV antigen with multilayered SiO2-Au core dual-quantum dot shell nanocomposite. The fluorescence can achieve a 238-fold improvement in sensitivity compared with the AuNP-based LFA (Figure 4a) [85]. Additionally, the sensitivity of fluorescence signals in POCT devices has been improved with the integration of metal-enhanced fluorescence (MEF) technology [76, 86–88]. MEF works by dramatically increasing the fluorescent signal when fluorophores and metallic nanostructures are placed in close specific proximity, enabling the detection of lower concentrations of biomarkers and earlier disease diagnosis through localized surface plasmon resonance of the metal structure and the nanomaterial [89]. For example, a MEF-based microfluidic chip for the detection of cardiac troponin I (cTnI) in spiked human serum was developed. Dense arrays of Au nanorods deposited on the detection area of the microfluidic channel onto which the antibodies were immobilized (Figure 4b) [90]. While MEF has gained much attention, especially for the POCT, a significant challenge lies in attaining uniformity in the size, shape, structure, and morphology of the MEF substrates at the nanoscale level [91]. Another major limitation of fluorescence detection is the autofluorescence of the samples that hinder ultra-sensitive detection [92]. Thus, an extra washing step is required which needs an additional handling process. To circumvent this, a one-step fluorescence immunoassay has been developed where the washing step was eliminated through the installation of switchable peptides that enable fluorescence signal detection in the presence of the analyte (Figure 4c). Thus, the total analysis time could be halved to less than 30 min [93, 94]. To further reduce autofluorescence, lanthanide doped-NPs have been employed into POCT systems due to their large stokes-shift [95, 96].

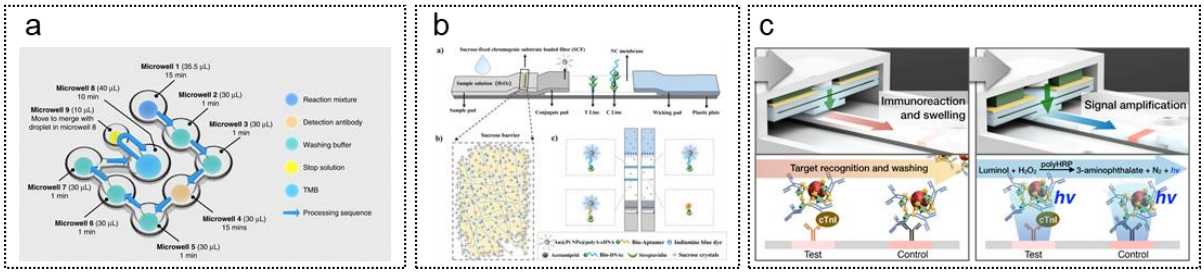

Figure 3: Enzymatic amplification strategies in one-step POCT. Fully automated magnetic microfluidic platform for the controlled reaction workflow. Reproduced/adapted from [71] (https://creativecommons.org/licenses/by/4.0/) (a). Delayed substrate delivery on a paper-based LFA through a dissolvable sucrose barrier. Reproduced/adapted from [72] with permission from Elsevier (b). Time-programmable amplification part based on a water-swellable polymer. Reproduced/adapted from [73] (c).

2.4.3 Surface-enhanced Raman spectroscopy (SERS)

Recently, there has been growing interest in combining POCT devices with surface-enhanced Raman spectroscopy (SERS) [97–101], which allows for highly sensitive detection in laboratory settings. Additionally, the high spatial resolution and narrow Raman scattering bands of SERS make it a promising tool for multiplexing [102]. A few examples have been published, such as the a SERS-based LFA for the detection SARS-CoV-2 IgM/IgG [103].

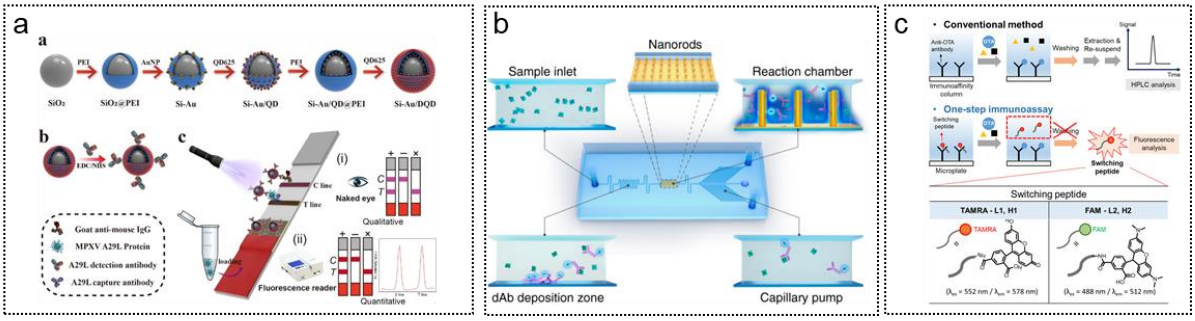

Figure 4: Fluorescence one-step POCT. Signal amplification by embedding multiple QDs into a nanocarrier made out of SiO_2 nanoparticles. Reproduced/adapted from [85] (https://creativecommons.org/licenses/by/4.0/) (a). MEF-based microfluidic platform for highly sensitive detection. Reproduced/adapted from [90] (https://creativecommons.org/licenses/by/4.0/) (b). One-step immunoassay with switching peptides to avoid an additional washing step [93] (https://creativecommons.org/licenses/by/4.0/) (c).

With that set up, the detection limit was improved by a factor of 800 compared to the traditional LFA. Quantitative analysis was performed with a portable Raman reader that houses a 785 nm laser for the excitation. To reduce the sample volume, Su et al. have integrated SERS detection within a microfluidic platform. A microfluidic SERS platform with integrated blood-plasma separation was able to detect creatinine with only 3 µL whole blood within 2 minutes [104]. However, SERS detection has several limitations that hinder its in-field application. Reproducibility is challenging due to the size variation of metal colloids, uncontrollable aggregation of particles and the uneven distribution of signaling molecules on particle surfaces. Additionally, the sensitivity of SERS in POCT is relatively bad compared to conventional SERS, due to the reduced resolution of portable readers. Further, the analyte is often affected by the POCT's material properties and the design of the platform that is known as "memory effect" [105]. To realistically use SERS in real-world scenarios, further developments are needed to address the mentioned limitations. If achieved, SERS could become a valuable addition to the POCT portfolio.

Fluorescence, MEF, and SERS are innovative concepts with potential, but their requirement for a reader limits their applicability in certain types of POCT, such as home testing and resource-limited settings. However, they remain intriguing and pertinent for POCT conducted in doctor's offices, analytical laboratories, and similar settings.

2.4.4 Electrochemical sensors

Electrochemical methods hold significant potential for affordable, compact, user-friendly portable devices suitable for various applications [106]. Their main advantages over optical methods are the simplicity of the hardware needed and the ability to detect in optically scattering and colored samples. Hence, electrochemical measurements can be conducted on colored or turbid samples like whole blood, without being disrupted by fat globules, red blood cells, hemoglobin, or bilirubin [107]. Wang et al. demonstrated this nicely with a budget-friendly, and portable microfluidic paper-based electrochemical apparatus, allowing for the immediate isolation of proteins and the direct electrochemical identification of Pb(II) in protein-rich urine samples (Figure 5a) [108]. Beck et al. proposed superior signal amplification with silver nanoparticles when

compared to conventional gold nanoparticles in an one-step electrochemical flow channel device (Figure 5b) [109, 110]. Here, all reagents were dried on the sensor, preserving the one-step LFA methodology. Yakoh et al. created a device capable of sequentially storing and transporting reagents to the detection channel autonomously, without requiring external power (Figure 5c) [111]. This device consists of two main parts: an origami folding paper (oPAD) and a mobile reagent-stored pad (rPAD). This three-dimensional capillary-driven device streamlines the cumbersome process of multi-step reagent manipulation in complex assays. Even though only buffers were utilized in this scenario, and not actual human samples, the straightforward yet adaptable design allowed for achieving good sensitivity while maintaining the one-step approach.

2.4.5 Nucleic acid amplification

Complementary to the widespread nanomaterial-based amplification methods, nucleic acid amplification techniques (NAATs) have been proved as reliable and strong detection tool. Currently, the real-time polymerase chain reaction (RT-PCR), the gold standard for virus infection detection, stands out due to its extraordinary sensitivity and specificity. However, RT-PCR suffers from cumbersome machines and skilled professionals and is therefore inapplicable in a POCT setting that does not rely on laboratory-based devices [112]. Recently, isothermal nucleic acid amplification strategies such as loop-mediated isothermal amplification (LAMP), strand-displacement amplification (SDA), recombinase polymerase amplification (RPA), helicase dependent amplification (HDA), and CRISPR/CAS have gained massive attention in diagnostic testing as their isothermal character facilitates the integration in POCT devices and ensures a cost- and time-effective approach [20, 113]. Especially, in the COVID-19 pandemic nucleic acid based detection methods ensured accurate and fast results [112]. The key advantage of nucleic acid amplification lies in the generation of a large number of copies of the target and therefore, improving the sensor sensitivity [114]. The main challenge for NAATs is the integration of the multiple step process ((I) nucleic acid purification, (II) amplification, (III) detection) of nucleic acid amplification methods in the one-step POCT device to reduce the hands-on interference and potential contamination [115, 116]. Unfortunately, these steps still are often performed

separately off-device and manual pipetting is required, but there is great potential for integrating the entire handling into a POCT device, eliminating the need for human intervention [117]. Recently, a range of fully integrated one-step platforms based on NAATs have emerged, offering streamlined and user-friendly solutions [26, 118]. For example, Seok et al. designed a reverse transcription LAMP (RT-LAMP)-based lab-on-paper for molecular diagnostics of Zika, Dengue, and Chikungunya viruses from human serum [119]. The entire nucleic acid testing process, encompassing sampling, extraction, amplification, and detection, is seamlessly executed on a single paper chip within 60 minutes at 65 °C. Utilizing the engineered structure of paper materials and dried chemicals on the all-in-one chip, serum samples containing the target virus RNA are effortlessly introduced via automatic flow from distilled water injection. An autonomous and fully integrated sample-to-answer device, for the specific detection of HIV-1 virus from human whole blood was developed to streamline the whole detection process [120]. Following sample addition, the result can be observed within 90 minutes. Additionally, users need to execute only four steps to commence testing: loading the sample and rehydrating mixture, adding wash buffer, sealing the inlets with adhesive, and activating the temperature control circuit by connecting to a power source like a computer, cellphone, or portable battery. Focusing on multiplexing, Xie et al. developed a magnetic-based all-in-one platform for the detection of foodborne pathogens [121]. Using this platform, the time required from sample collection to obtaining results was approximately 60 minutes, and the entire process on the chip was completely automated.

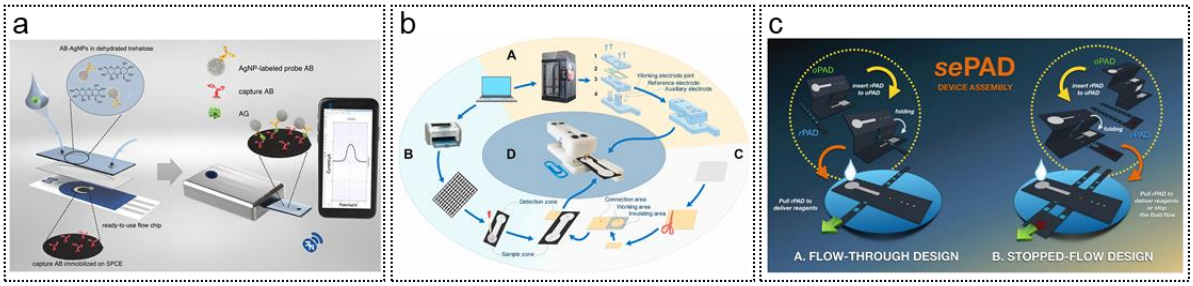

Figure 5: Electrochemical one-step POCT. Microfluidic biosensor for the detection of NT-proBNP via Ag- nanoparticles. Reproduced/adapted from [110] (a). Paper-based electrochemical sensor with on-line isolation of proteins in urine for the detection of Pb. Reproduced/adapted from [108] (b). An origami folding paper (oPAD) and a movable reagent-stored pad (rPAD) for the sequential transport of reagents. Reproduced/adapted from [111] (c).

2.4.5.1 Commercial one-step NAAT devices

These advancements have resulted in the emergence of several scalable production devices that have now entered the market (Figure 6) [26, 122]. USTAR has developed an EC-certified COVID-19 RNA paper-based test that allows for PCR-quality detection at home using a portable kit without the need for additional instruments. Results can be observed within 35 minutes, and the product offers a sensitivity of 95.4 % and a specificity of 99.8 %. However, it's worth noting that the user is required to add two additional buffers to the assay, resulting in two additional steps for the user to complete [123]. Visby Medical™ has launched a portable and fully integrated PCR-platform for the simultaneously detection of three respiratory health biomarkers, such as COVID-19, influenza A and influenza B. The device enables accurate testing with the results being available under 30 minutes [124]. Similarly, Cue Health has released a handheld, portable PCR platform capable of detecting COVID-19 in just 20 minutes. The test kit includes a reader and an assay that can be inserted into the reader after sample addition [125]. Detect® has introduced a fully integrated one-step POCT device, eliminating any sample handling. The device consists of a heater and a lateral flow assay. After collecting the sample through the nasal swab, the tube is closed with the provided detect cap that contains the reagents for the NAT. The tube is then placed into the heater for 55 minutes for the reaction to take place. After that, the tube and an additional reagent are transferred to the lateral flow assay where, the PCR-quality result can be observed after 10 minutes [126]. A similar but much more convenient method to test for COVID-

19 is introduced by the Lucira POCT device by Pfizer. This test is based on RT-LAMP and is also able to detect 3 viruses with only one test within 30 min. The test is initiated with the addition of the sample and no training is required, thus enabling home-testing [127]. BIOPIX-T introduced the PEBBLE qcLAMP, a compact and lightweight diagnostic system designed for rapid molecular detection of infectious diseases like COVID-19 and Influenza A at the point of care or demand. The platform performs a real-time quantitative colorimetric loop-mediated isothermal amplification (qcLAMP) within 30 minutes and the reader enables an innovative approach for heating the test vials and interpreting the results [128].

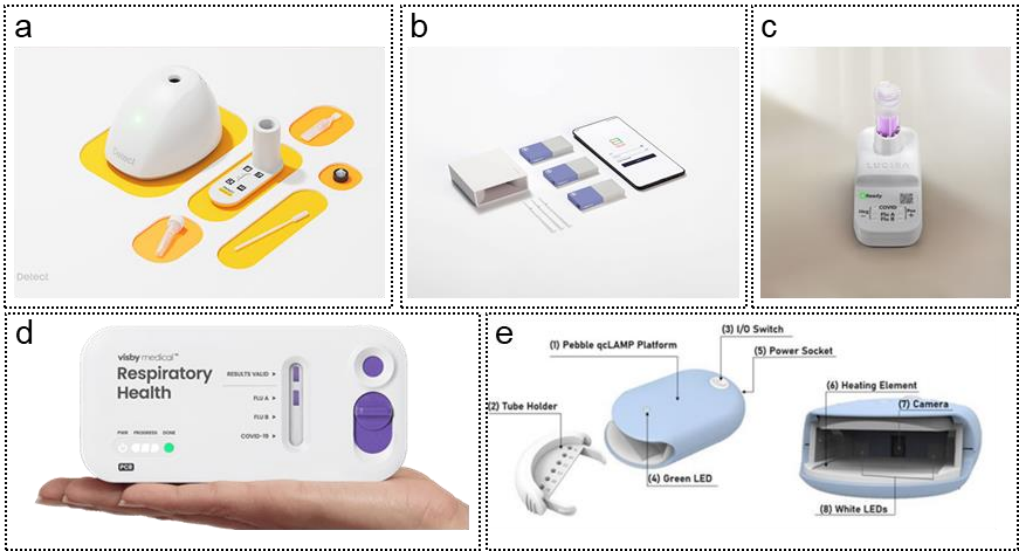

Figure 6: Commercial one-step NAAT devices. Molecular PCR platform [126] (a), Reader and tests [125] (b), Reader and assay [127] (c), Reader and assay [124] (d), Molecular diagnostic device Pebble [128] (e)

2.4.6 Design Modification and fluid control

Aside from tag-related amplification methods, recent research have focused on test structure modifications for enhancing the sensitivity of conventional LFAs [129]. The improvement is mainly attributed to the increase in kinetics of the immunoreaction. For example, to slow down the flow in paper-based LFAs physical barriers such as wax barriers (Figure 7a) [130–132], cotton thread [133–135], laser patterning [136, 137], pressed NC membrane [138] have been reported. Modification of the size ratio of the

test line and stacking the pads vertically have also shown positive impact on the sensor performance [139, 140]. While nitrocellulose remains the predominant material for capturing bioreceptors like antibodies in LFAs [141], it also bears some limitations such as fluctuations in flow rate and analysis time due to differences in pore structure and sample viscosity. Pore blockage caused by matrix components, the membrane's innate absorbent properties leading to a relatively high sample volume, and inconsistency in dispersing the labeled sample across the membrane due to batch-to-batch variations and buffer reagents [142]. Thus, there has been a notable trend in exploring alternative membrane materials recently. For example, electrospun polymer nanofibers [143–145], *bombyx mori* cocoons and electrospun silk fibroin [146], cotton thread [147]. Yet, an extensive assessment of these alternative materials regarding the sensitivity, reliability and long-term stability is necessary before considering them as dependable substrate for immunoassays [129]. To overcome these limitations, other researchers have focused their work on channel-based assays, where any membrane- and fleece material was omitted. The most popular immunoassays are built in so-called microfluidics, where microchannels simultaneously house sample processing and detection. This technology's strengths lie in its cost-effective and scalable manufacturing, simple adaptability for functionalization, faster reaction kinetics, and its flexibility in adjusting flow rates by changing the geometry of the channel or external fluid flow control system (Figure 7b/c) [148–153]. In a study by Strohmaier-Nguyen et al. sample-absorbing fleece and membrane materials were eliminated for the detection of NT-proBNP in a lateral flow channel assay [154]. By drying antibodies on the test and a multilayered polymer film as the test line, the one-step characteristic has been preserved. Unlike traditional lateral flow assays, the assay developed in this study requires only 20 µL of sample volume (as opposed to 150 µL), easily obtained through a simple finger prick, thereby making it suitable for home testing. Similarly, Hemming et al. transformed the conventional LFA into a fluorescence-based capillary-driven microfluidic without any fleece- and membrane materials [155]. Through a self-coalescence mechanism involving rehydration of reagents to form a homogenous concentration profile and capturing beads in the detection zone, a detection limit of 4 $ng \cdot mL^{-1}$ cTnI was achieved using only 1 µL sample volume. The group of Kim et al. developed a microfluidic immunoassay

with a fluid vent control to amplify the signal of the immunoassay by pausing the sample flow [156]. All reagents were dried within the sensor, allowing the immunoassay to be initiated upon sample introduction. In the developed platform, meticulous fluid flow control ensured continuous delivery of reagents to the detection area. This approach led to an improved immunoreaction and 10 times higher LOD than the commercial LFA kit.

2.4.7 Sample preparation

Sample preparation, a crucial aspect of precise biomedical analysis, provides the recovery and concentration of the desired biomarker from the sample through purification of the sample and elimination of potential interferences (e.g., non-target contaminants) [157]. Incorporating this step into one-step platforms is a must and provides the opportunity for accurate and highly sensitive testing, however, is an immensely challenging task. The complexity of preparing the sample varies typically mainly based on the source of the sample (predominantly here whole blood, urine, or saliva).

2.4.7.1 Blood

Whole blood stands as one of the most intricate body fluids utilized in clinical analyses [158] and usually demands plasma separation from blood cells to prevent impediments in the detection process and signal read-out such as high non-specific autofluorescence signals [159] and colorimetric background signals. In traditional paper-based POCT platforms, plasma separation is often accomplished using a porous filtration membrane. This straightforward strategy is hampered by membrane clogging, increased blood volume requirements due to dead volume in the membrane, and analyte loss caused by non-specific adsorption. In recent years, there has been a rise in literature focused on miniaturized methods for plasma extraction [160–163]. However, most of these methods necessitate pre-dilution of the blood sample. While this reduces the concentration of blood cells, it also decreases the concentration of the target analyte, and it presents an extra sample processing step. It thus ultimately impairs the sensor

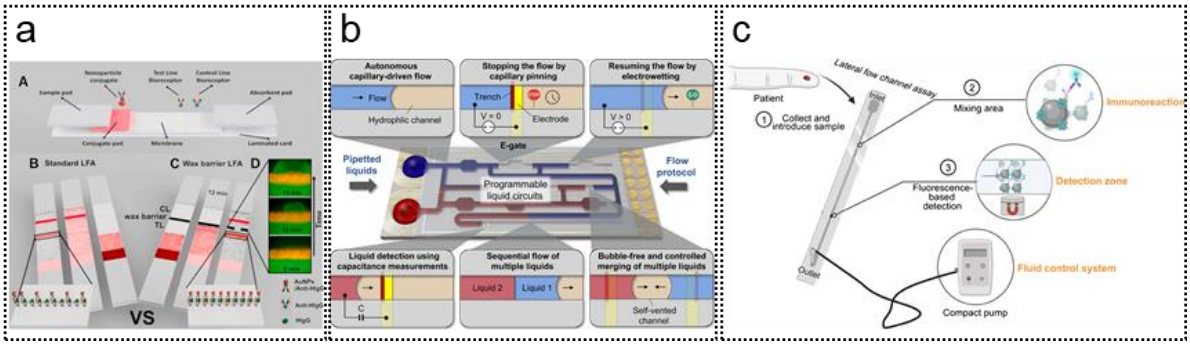

Figure 7: Sensitivity enhancement through design modification and fluid flow control. LFA with wax barriers. Reproduced/adapted from [130] (a). Programmable microfluidic with electro-actuated valves and self-vented channels. Reproduced/adapted from [149] (https://creativecommons.org/licenses/by-nc/2.0/) (b). Magnetic bead-based platform with active fluid control. Reproduced/adapted from [153] (https://creativecommons.org/licenses/by/4.0/) (c).

performance and adds inconsistencies to the POCT platform. Thus recently researchers focuses on integrated plasma separation techniques without the need for a blood sample pre-dilution [104, 164–167]. The integration of an acoustic microstreaming into a microfluidic device for the detection of HIV-1 p24 protein enabled the isolation of plasma from undiluted whole blood and achieved approximately 31.8 % plasma yield with 99.9 % plasma purity in a span of five minutes. They showcased a detection threshold of 17 pg·mL^{-1}, with the acoustic microstreaming also serving as both a micropump and micromixer, facilitating controlled sample flow and enhanced kinetics of the immunoreaction [168]. Lenz et al. have integrated centrifugal cross-flow filtration to separate serum form whole blood with a purity of 99.99 % and showed higher biomarker retention when compared to the serum that was separated with the benchtop centrifugation [169]. A magnetic separation technique was devised to extract plasma from whole blood. By coating magnetic nanoparticles with antibodies targeting red blood cells, plasma with 99.9 % purity was obtained. In a ferritin test conducted on the lateral flow assay, it exhibited a superior detection limit compared to the filtration membrane [170]. A significant drawback of the setup is that the biomarker's bioanalysis was conducted off-chip, rather than being integrated into the separation module. By combining the commercially available filter membrane with a microfluidic device, the researcher successfully extracted 20 µL plasma from 100 µL undiluted whole blood in

16 min [171]. To actively pull the extracted plasma from the membrane, nano-sized gaps were incorporated on both ends of the microchannel. Thus, the whole platform enables powerless application. To overcome the inherent sample absorbing characteristics of the filter membrane, a sedimentation-based plasma separation enables efficient separation and sensitive detection with minimal sample volume was developed for the detection of NT-proBNP in whole blood (Figure 8a) [172].

2.4.7.2 Saliva

The conventional collection of saliva is done off-chip and requires additional saliva collector and running buffer in order to initiate the immunoassay on the POCT platform [173]. This step is more cumbersome for the user as the saliva needs to be added to the test separately. In order to achieve more effective regulation and ensure consistent performance in saliva-based testing, it is essential to standardize collection methods, facilitated by the use of standardized collection devices [174]. To overcome this burden, the company inne.io has developed a fully integrated minilab for home-testing to track fertility hormones in saliva. The saliva collector houses a sample absorbing pad that is integrated into the LFA (Figure 8b) [175]. After sampling, the collector is folded onto the LFA, thereby initiating the immunoassay. In combination with the reader, the results are automatically sent to the smartphone. Vinoth et al. created a portable electrochemical microfluidic device, featuring an integrated filtration membrane for the electrochemical monitoring of various salivary biomarkers [177]. The samples are gathered using a plastic dropper, then introduced into the device inlet and allowed to traverse through the microfluidic channels. Another all-in-one electrochemical-based platform for the detection of cotinine was developed by integrating the commercial available cotton-swab-type collector with a 3D printed housing for seamlessness and straightforward introduction of the sample to the assay [178].

Figure 8: Integrated sample preparation. Sedimentation-based plasma separation in a microfluidic platform. Reproduced/adapted from [172] (https://creativecommons.org/licenses/by/4.0/) (a). Portable reader and integrated saliva collector and preconcentration step in a LFA. Reproduced/adapted from (inne.io) (b). Integrated preconcentration for a urine-based assay. Reproduced/adapted from [181] (https://creativecommons.org/licenses/by/4.0/) (c).

2.4.7.3 Urine

The preparation of urine for POCT analysis is simpler and does not require pre-processing**.** However, there may be cases where the target analyte is present only in very low concentration making a preconcentration step necessary [176, 179–181]. By using gradients as the driving force for the preconcentration of proteins have been successfully demonstrated. Specifically proteins were enriched 100-fold using both electric field and pH gradient or by pressure gradients water and interferences were filtered through membrane and the protein of interest was preconcentrated up to 100-fold (Figure 8c) [181]. Most of the on-chip preconcentration steps are a good alternative for the cumbersome bench-top instruments, however, they are still complex as they require additional running or washing buffers, complex geometries or specific parts of the platform need to be manually assembled afterwards. Thus, many further improvements need to be made in order to fulfill the requirements of the one-step POCT.

2.5 Reader

There is a substantial trend towards the migration of testing from the traditional centralized laboratory setups, characterized by expensive instrumentation, intricate sampling protocols, and highly trained technicians, to resource-constrained settings,

including remote areas and households. In these settings, portable devices and readers can be operated by individuals with minimal or no training to receive reliable test results [182]. In LFAs or microfluidics-based immunoassays, a reader or analyzer is a crucial instrument for obtaining quantitative results that are not subject to the error tolerance or inaccuracy of subjective read-out. Traditional analytical systems are typically expensive, large, complex, and demand highly regulated infrastructure and skilled medical personnel. Technological advancements have led to the development and commercialization of numerous miniaturized, compact, and even handheld readers [183] [184]. However, many readers are not sufficiently portable or involve expensive manufacturing processes, consequently raising the overall cost of POCT devices. This makes them less accessible for rural settings or home testing. In 2021, the global mobile user count reached 7.1 billion, with projections indicating a probable increase in this number in the coming years [185]. Utilizing this globally accessible and connected portable device offers a significant opportunity to harness the technology for the development of POCT devices, promising user-oriented diagnostic testing [186–189].

2.5.1 Optical Reader

The cameras of smartphones, when used with specific casings to maintain the appropriate camera-to-sensor distance or enable analysis without external light interference, have been extensively employed in the evaluation of optical biosensors as they can recognize subtle variations in color hue [190]. Additional devices, such as a simple dark box made from black cardboard, can reduce interference from ambient light [191], allow direct measurements on a microfluidic platform [192, 193], or even connect to portable SPR attachments (Figure 9a) [194], facilitating on-field testing.

Fluorescence POCT systems have long been proposed as they offer significantly lower LODs in comparison to colorimetric or reflectance approaches. However, the bulkiness and costs of traditional readers have prevented wide-spread applicability in the POCT. Thus, miniaturization of light source, camera, filters and electronics are crucial and are nicely demonstrated recently [195]. Through Bluetooth connectivity fast and easy result management could be done via smartphone [196] [197–199] as the display was outsourced to the smartphone which ultimately lowered the price of the reader per device. Main drawback of this setup is the extra costs in the production of the camera

system and thus the increase of the burden of purchase for low-income facilities. Thus, a more cost-efficient prototype for the fluorescence analysis was proposed using the smartphone as reader [200–202]. However, considering the differences between phone manufacturers, this approach has many regulatory hurdles though. Similarly, when other functions are outsourced to the phone, such as fluid flow control in a microfluidic platform [203], costs are reduced, but regulatory approval may become even more difficult.

2.5.2 Nucleic Acid-based Reader

In the case of NAAT assays, portable readers include those additional functions needed to run the assays, such as traditional heaters [204–206] or chemical heaters, thereby reducing the complexity of the device [207, 208]. In fact, a platform with a chemical heating process enabled instrument-free detection of H1N1 virus in low resource settings, where no instrument for heating is necessary [209].

2.5.3 SERS Reader

With the increasing focus of SERS-based assays, the readout of the RAMAN signal became more important. However, the main challenge with integrating SERS-POCT in real-world scenarios is the long recording and integration time of the results [210]. To overcome this limitation, a portable SERS reader for fast data acquisition by exploiting a line illumination along the test line with a custom-designed fiber optical probe with a line focus was developed (Figure 9b) [211]. Also multiplexing has been enabled by a cost-efficient and automated set up [212]. Because portable Raman spectrometers have lower sensitivity compared to laboratory-based confocal ones due to the miniaturization process, sample pre-amplification is highly desirable before LFA detection. For example, by combining SERS with the isothermal amplification catalytic hairpin assembly (CHA), the detection limit was 3 orders of magnitude lower than the SERS-LFA without amplification [213].

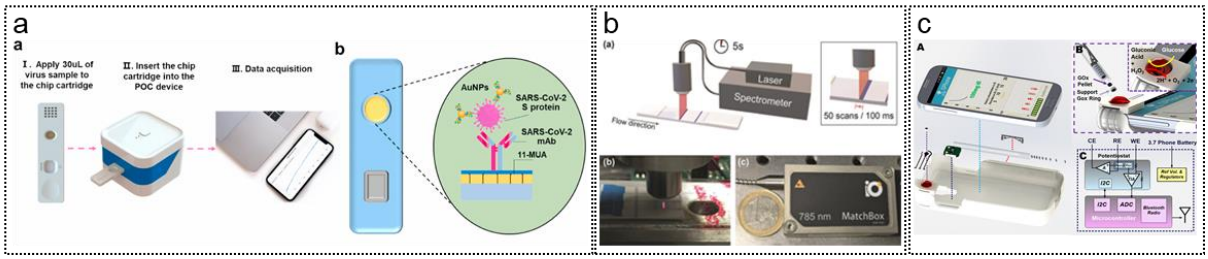

Figure 9: POCT readers. Portable SPR-Reader. Reproduced/adapted from [194] (a). SERS-Reader with line illumination. Reproduced/adapted from [211] (b). Smartphone-based reader. Reproduced/adapted from [214] (c)

2.5.4 Electrochemical Reader

Electrochemical sensors utilize smartphones not only for their potentiometric capabilities at the point of care and for signal processing, but also as the primary power source for the entire biosensor platform [215, 216]. In general, the smartphone is completed with an electrochemical workstation, that provides the connection to the sensor (Figure9c) [214, 217–220]. Since the results are transmitted wirelessly to the smartphone interface, this approach facilitates the separation of testing and readout based on location, a crucial factor in rapidly communicable diseases. By integrating the electrochemical readout of the smartphone with a miniaturized LED as the light source photoelectrochemical biosensing is also possible [221].

2.5.5 Thermal Reader

Thermal sensing utilizes a heat transducer and a laser to generate heat when in contact with the analyte. This allows the smartphone, acting as the thermal reader, to detect the resulting thermal signal [222]. For example a thermal smartphone-based reader have been developed for the sensitive detection of exosomes [223]. This set up consists of a 3D-printing strip holder, an excitation laser, and a smartphone-accessible thermal detector.

The lasers for excitation and thermal detection were integrated together in the opposite side mode. The dimensions of the smartphone-based thermal reader were 72 mm (L), 50 mm (W), and 60 mm (H), with a total weight of 56.4 g. A smartphone thermal detector, in which the laser and the thermal detection was located on the same side

[224]. The platform enabled rapid and low-cost detection of anti-SARS-CoV-2 antibody. The size of the assembled reader is 80 mm by 110 mm by 100 mm.

2.6 Fabrication

Considering the vast number of publications, principles and platform technologies offered the pace of expansion and commercial adoption of these technologies has notably trailed behind dramatically. This delay can be attributed, at least in part, to the challenges associated with transitioning from small-scale benchtop fabrication techniques to large-scale mass production. Therefore, thinking about cost-effective and scalable manufacturing processes are essential to facilitate the path to commercialization ab initio should be an adopted strategy [225–227]. In general, academically published microfluidics and LFAs are made three major groups: polydimethylsiloxane (PDMS), thermoplastics, and paper materials. Unsurprisingly, not every material platform lends itself easily to mass production. While industrial processes often mandate roll-to-roll fabrication, it is worthwhile taking a deeper look into the materials dominating the research space with respect to their use in manufacturing processes.

2.6.1 Material

2.6.1.1 Paper

Paper-based systems have been investigated as costly material and are advantageous due to their simplicity, accessibility, significantly low costs, high porosity, high physical absorption, ease of manipulation and sterilization, potential for chemical or biological modifications, bio-affinity, biocompatibility, light weights, and the ability to operate without supporting equipment [228]. Yet, the limited mechanical stability and the susceptibility to deterioration constrains its utility in high-pressure settings and severe conditions [229]. Additionally, the non-uniform porosity of the paper may result in variable fluid flow, thereby diminishing the precision of the acquired results [230]. To circumvent this issue, there has been a recent trend towards the manufacturing and development of POCT platforms, primarily composed of polymers, which provide numerous benefits compared to conventional paper, such as enhanced uniformity, preferable surface chemistry, and greater regulation of physical characteristics.

2.6.1.2 Polymers

Polydimethylsiloxane (PDMS) is an inexpensive material that is easy to mold, making it ideal for prototyping. [231]. However, PDMS possesses a porous structure, which allows for the diffusion of a wide range of molecules, making it an adsorptive material and incompatible with organic solvents. Additionally, the evaporation of water through channel walls can lead to a change in the concentration of the solution, which presents another issue. To overcome these problems, the focus shifted to the integration of thermoplastics into the fabrication of POCT devices. Poly(methyl methacrylate) (PMMA), polyethylene terephthalate (PET), poly carbonate (PC) and cyclic olefin copolymer (COC) have been the typical examples for large-scale manufacturing processes due to their cost-efficiency and biocompatibility. Thermoplastics are rigid polymer substances characterized by robust mechanical stability, minimal water absorption, and resistance to organic solvents, acids, and bases. These qualities are pivotal in numerous bioanalytical microfluidic applications [232]. Typically, the material choice dictates the manufacturing process. Sensor device fabrication methods can be broadly categorized into small-scale and large-scale production.

2.6.2 Small-scale production

2.6.2.1 Soft lithography

Soft lithography is a widely utilized method for fabricating microfluidic devices, employing flexible and elastomeric materials like PDMS to produce microfluidic patterns [231]. Typically, after mixing the PDMS polymer with the curing agent, the liquid is poured on the SU-8 mold and cured at 40 – 80 °C for 1-2 h, following by peeling of the elastomer for demolding [233]. However, due to the long fabrication steps, this process is limited to laboratory settings. To overcome this, researchers have shown the possibility for scaling-up PDMS sensor fabrication through roll-to-roll fabrication [234] and flexographic printing plate [235].

2.6.2.2 Ablation techniques

Fast prototyping can be achieved through ablation techniques that can be grouped into mechanical milling [236] and energy-based ablation [237]. After designing the sensor's structure, typically with CAD software, the design guides the laser in removing

substrate material. Laser ablation presents numerous benefits such as its applicability to a wide range of materials, cost-effectiveness and quick manufacturing process. However, laser ablation processes suffer from poor optical quality of the micromachined surface due to material melting, vaporization, and ejection induced by laser irradiation. This leads to the formation of pores and material residue deposition, resulting in high surface roughness and restricting the use of laser-cut devices [238].

2.6.2.3 3D printing

Over the past few years, there has been an increasing trend in using 3D printing to manufacture microfluidic devices, primarily because of its ability to produce highly accurate and complex structures [239]. While soft lithography is confined to planar 2-dimensional complexities, 3D printing can rapidly produce "truly 3-dimensional" features such as crossover (overhanging) features. 3D printing involves the creation of three-dimensional objects through the layer-by-layer deposition of materials. Among all 3D printing methods [240–243], Fused Deposition Modeling (FDM) [244], stereolithography (SLA), and Inkjet 3D printing (i3DP) stand out as the most widely utilized.

2.6.3 Large-scale production

2.6.3.1 Hot Embossing and Imprinting

Replication methods, where masters and molds with defined nanostructures can be utilized to replicate subsequent products can significantly lowered production time and expenses [245]. Usually, during the hot embossing procedure, the features of a mold are transferred onto a polymer substrate under high temperature and pressure conditions [246]. All components are cooled to a temperature below the polymer's glass transition, after which the processed polymer is removed from the mold. Since this step requires the time-inefficient heating and cooling ramp, the imprinting technique has been utilized at lower temperature by increasing the applied pressure in order to shorten the fabrication time [247]. Nevertheless, hot embossing faces limitations, including extended cycle durations, complexities in generating micro-patterns with significant aspect ratios, and struggles in separating the mold from the substrate without causing damage during the de-embossing phase [248].

2.6.3.2 Injection Molding

Injection molding, presents a potentially more economically feasible option and has demonstrated its capability to facilitate the mass production of microfluidic devices across a diverse array of materials [249]. Typically, injection molding entails the injection of liquefied plastic into a cavity shaped by two molds, typically composed of metal [250], [251]. While injection molding offers swift and consistent production of microstructures, it only yields individual chips through this sequential method. Additionally, handling chips becomes intricate during each subsequent post-processing step [252]. Moreover, the demolding stage represents a pivotal phase that significantly impacts the quality of polymer microstructures [253].

2.6.3.3 Roll-to-Roll

Roll-to-roll (R2R) manufacturing encompasses a range of foil-based processes that employ both additive and subtractive techniques to construct functional structured devices for quick and cost-effective mass production [252, 254, 255]. R2R fabrication, such as R2R hot embossing, featuring two rollers sandwiching a polymer film, represents the ultimate goal for continuous and high-throughput production of patterned polymeric films [256]. R2R manufacturing has been also implemented in the fabrication of paper-based microfluidics for the direct transfer of wax from commercially available wax ribbon to the surface of a paper substrate. In contrast to traditional approaches for paper-based microfluidics this proposed fabrication technique enables the batch production of paper-based microfluidic chips at a more rapid pace [257]. Another group developed the first energy-efficient room-temperature printing-imprinting integrated roll-to-roll manufacturing platform for mass production of a polydimethylsiloxane (PDMS)-based platform [258]. Nonetheless, it is important to note that PDMS as a substrate is still not ideal for scalable fabrication setups and thermoplastics have gained significant attention in the development of current biosensors.

In summary, the selection of material is critical in determining economic cost, fabrication time, handling properties, reliability, bonding efficiency, and ease of use. In addition to the established roll-to-roll (R2R) production process for the industrial fabrication of biosensors, other scalable manufacturing techniques, such as 3D printing

and laser processing, have recently gained importance. The current goal is to further develop these methods and potentially combine them with R2R processes to enhance flexibility in meeting individual requirements.

2.6.4 Perspective

Before a commercial POCT system can be produced through mass fabrication, manufacturers must overcome several challenges, including material selection, meeting sensor performance criteria, ensuring ease of production, simplifying test operation, and developing integration solutions. They are accountable for maintaining product quality, especially for medical devices, while also focusing on minimizing costs and boosting profit margins [34]. It cannot be emphasized enough that changes in material, process, and production techniques all influence the performance of a test system, in part dramatically. Finely tuned optimized assays may result in bad performing assays when production techniques are altered. It is therefore of utmost importance for novel POCT concepts to consider mass producibility already while inventing new assays, without which these may never be of help to the society at large.

(I) Material and geometric structure for ease of production

The development of POCT devices involves a complex chain of processes, requiring various manufacturing techniques like ablation tools, hot embossing, and roll-to-roll integration. An effective design can significantly reduce effort. Rectangular channels are preferable due to the challenges of achieving rounded structures when using methods like laser ablation or micromilling. Larger channels can simplify tooling, replication, and integration.

A thorough understanding of the assays being performed on a chip and their material requirements is also important in selecting the appropriate material for production. It is crucial to fully understand the surface properties (e.g., hydrophobicity), light absorbance, mechanical characteristics, and manufacturability (e.g., replication fidelity, surface treatment, bonding methods) of a material used to minimize the potential costs associated with redevelopment. For example, while PDMS is commonly used in lab settings, thermoplastics are generally preferred for industrial scale-up. By addressing these material and design considerations during the design and prototyping stages,

while keeping potential scale-up challenges in mind, setbacks can be mitigated, and costs saved.

Manufacturing feasibility should be considered from the start of product development, with expert advice to streamline the process and reduce scale-up failures, especially in academic projects that have application in mind and are not only seeking basic understanding or the innovation of new principles. In fact, early involvement of professionals experienced in manufacturing and scale-up would be desirable, as this can save time and effort in converting prototypes into commercial products and assess early on, whether a new assay system has the possibility to be more than a proof-of-principle.

(II) Performance and complexity of POCT device and its operation

For successful commercialization, factors such as performance, system complexity and ease of use of the test must be considered. POCTs with low system requirements, allowing for the miniaturization of necessary hardware, offer broader application possibilities and can be used in low-resource settings [259]. High accuracy, sensitivity and specificity in combination with easy test handling, where the sample is simply applied to the test—ideally non- or minimally invasive samples—does not require trained personnel for execution or sampling [260]. This is particularly advantageous given the current shortage of skilled personnel in medical facilities.

2.7 Conclusion

Currently, most of the POCT devices remain bulky bench-top instruments or require skilled personnel to operate multiple handling steps. This is because innovations in POCT primarily prioritize cost reduction and sensitivity improvement, which often necessitate multiple operational steps and complex manufacturing. However, there is a growing post-pandemic trend toward developing compact, portable and user-friendly devices, signifying a shift away from complex platforms to on-site, and home-based testing settings. This transformation suggests a positive outlook for accessibility and ease of use, minimizing the need for highly skilled personnel to operate multiple handling steps. Recent research has narrowed the gap between the complexity of devices demonstrated in one-step assay systems and that of bench-top assays. The advancements attained in academic research are now ready to be seamlessly integrated

with commercially viable options and gain more and more importance. New sensing technologies, including new labels, test structure and miniaturized read-out systems have overcome the limitations of conventional assays and enable highly sensitive one-step POCT platforms. Furthermore, advancements in materials and technical equipment facilitate commercialization in the market. Another crucial factor for the successful marketing and sustainability of one-step POCT devices is to mitigate the risk of sample contamination by untrained personnel. The scale down of all analytical steps such as sample preparation, reagent mixing, separation, chemical reaction and signal detection into a POCT system, eliminate any manual operation and enable reliable testing in rural areas or in home settings.

2.8 References

1. Koczula KM, Gallotta A (2016) Lateral flow assays. Essays Biochem 60:111–120. https://doi.org/10.1042/EBC20150012

2. Yang S-M, Lv S, Zhang W, Cui Y (2022) Microfluidic Point-of-Care (POC) Devices in Early Diagnosis: A Review of Opportunities and Challenges. Sensors 22:1620. https://doi.org/10.3390/s22041620

3. Land KJ, Boeras DI, Chen X-S, Ramsay AR, Peeling RW (2019) REASSURED diagnostics to inform disease control strategies, strengthen health systems and improve patient outcomes. Nat Microbiol 4:46–54. https://doi.org/10.1038/s41564-018-0295-3

4. Morales MA, Halpern JM (2018) Guide to Selecting a Biorecognition Element for Biosensors. Bioconjug Chem 29:3231–3239. https://doi.org/10.1021/acs.bioconjchem.8b00592

5. Dkhar DS, Kumari R, Mahapatra S, Divya null, Kumar R, Tripathi T, Chandra P (2022) Antibody-receptor bioengineering and its implications in designing bioelectronic devices. Int J Biol Macromol 218:225–242. https://doi.org/10.1016/j.ijbiomac.2022.07.109

6. Gupta U, Gupta V, Arun RK, Chanda N (2022) Recent advances in enzymatic biosensors for point-of-care detection of biomolecules. Biotechnol Bioeng 119:3393–3407. https://doi.org/10.1002/bit.28251

7. Yoo H, Jo H, Soo Oh S (2020) Detection and beyond: challenges and advances in aptamer-based biosensors. Mater Adv 1:2663–2687. https://doi.org/10.1039/D0MA00639D

8. Denmark DJ, Mohapatra S, Mohapatra SS (2020) Point-of-Care Diagnostics: Molecularly Imprinted Polymers and Nanomaterials for Enhanced Biosensor Selectivity and Transduction. EuroBiotech J 4:184–206

9. Nguyen V-T, Song S, Park S, Joo C (2020) Recent advances in high-sensitivity detection methods for paper-based lateral-flow assay. Biosens Bioelectron 152:112015. https://doi.org/10.1016/j.bios.2020.112015

10. (2023) Markets and Markets. In: Point Care Diagn. Mark. Size. https://www.marketsandmarkets.com/Market-Reports/point-of-care-diagnostic-market-106829185.html

11. Luppa PB (2018) Point-of-care testing: prionciples and clinical applications, 1st edition. Springer, New York, NY

12. Nilghaz A, Guan L, Tan W, Shen W (2016) Advances of Paper-Based Microfluidics for Diagnostics—The Original Motivation and Current Status. ACS Sens 1:1382–1393. https://doi.org/10.1021/acssensors.6b00578

13. Zhang J, Lan T, Lu Y (2020) Translating in vitro diagnostics from centralized laboratories to point-of-care locations using commercially-available handheld meters. TrAC Trends Anal Chem 124:115782. https://doi.org/10.1016/j.trac.2019.115782

14. Fox JW, Cohen DM, Marcon MJ, Cotton WH, Bonsu BK (2006) Performance of Rapid Streptococcal Antigen Testing Varies by Personnel. J Clin Microbiol 44:3918–3922. https://doi.org/10.1128/JCM.01399-06

15. Ortiz DA, Loeffelholz MJ (2023) Practical Challenges of Point-of-Care Testing. Clin Lab Med 43:155–165. https://doi.org/10.1016/j.cll.2023.02.002

16. Sharma S, Zapatero-Rodríguez J, Estrela P, O'Kennedy R (2015) Point-of-Care Diagnostics in Low Resource Settings: Present Status and Future Role of Microfluidics. Biosensors 5:577–601. https://doi.org/10.3390/bios5030577

17. Yager P, Edwards T, Fu E, Helton K, Nelson K, Tam MR, Weigl BH (2006) Microfluidic diagnostic technologies for global public health. Nature 442:412–418. https://doi.org/10.1038/nature05064

18. Kimura H, Asano R (2022) Strategies to simplify operation procedures for applying labeled antibody-based immunosensors to point-of-care testing. Anal Biochem 654:114806. https://doi.org/10.1016/j.ab.2022.114806

19. Bhardwaj T, Ramana LN, Sharma TK (2022) Current Advancements and Future Road Map to Develop ASSURED Microfluidic Biosensors for Infectious and Non-Infectious Diseases. Biosensors 12:357. https://doi.org/10.3390/bios12050357

20. Liu L, Yang D, Liu G (2019) Signal amplification strategies for paper-based analytical devices. Biosens Bioelectron 136:60–75. https://doi.org/10.1016/j.bios.2019.04.043

21. Roy L, Buragohain P, Borse V (2022) Strategies for sensitivity enhancement of point-of-care devices. Biosens Bioelectron X 10:100098. https://doi.org/10.1016/j.biosx.2021.100098

22. Sachdeva S, Davis RW, Saha AK (2021) Microfluidic Point-of-Care Testing: Commercial Landscape and Future Directions. Front Bioeng Biotechnol 8:602659. https://doi.org/10.3389/fbioe.2020.602659

23. Pérez-López B, Mir M (2021) Commercialized diagnostic technologies to combat SARS-CoV2: Advantages and disadvantages. Talanta 225:121898. https://doi.org/10.1016/j.talanta.2020.121898

24. Shaffaf T, Forouhi S, Ghafar-Zadeh E (2021) Towards Fully Integrated Portable Sensing Devices for COVID-19 and Future Global Hazards: Recent Advances, Challenges, and Prospects. Micromachines 12:915. https://doi.org/10.3390/mi12080915

25. Duchesne L, Lacombe K (2018) Innovative technologies for point-of-care testing of viral hepatitis in low-resource and decentralized settings. J Viral Hepat 25:108–117. https://doi.org/10.1111/jvh.12827

26. Li Z, Bai Y, You M, Hu J, Yao C, Cao L, Xu F (2021) Fully integrated microfluidic devices for qualitative, quantitative and digital nucleic acids testing at point of care. Biosens Bioelectron 177:112952. https://doi.org/10.1016/j.bios.2020.112952

27. Liu C-W, Tsutsui H (2023) Sample–to-answer sensing technologies for nucleic acid preparation and detection in the field. SLAS Technol 28:302–323. https://doi.org/10.1016/j.slast.2023.06.002

28. Sena-Torralba A, Álvarez-Diduk R, Parolo C, Piper A, Merkoçi A (2022) Toward Next Generation Lateral Flow Assays: Integration of Nanomaterials. Chem Rev 122:14881–14910. https://doi.org/10.1021/acs.chemrev.1c01012

29. Torul H, Arslan ZÇ, Tezcan T, Kayiş EÇ, Çalımcı M, Gumustas A, Yildirim E, Külah H, Tamer U (2023) Microfluidic-based blood immunoassays. J Pharm Biomed Anal 228:115313. https://doi.org/10.1016/j.jpba.2023.115313

30. Omidfar K, Riahi F, Kashanian S (2023) Lateral Flow Assay: A Summary of Recent Progress for Improving Assay Performance. Biosensors 13:837. https://doi.org/10.3390/bios13090837

31. Liu D, Wang Y, Li X, Mengmeng Li, Qiaoyi Wu, Song Y, Zhu Z, Yang C, Yang CJ (2022) Integrated microfluidic devices for in vitro diagnostics at point of care. Aggregate. https://doi.org/10.1002/agt2.184

32. Zhang Y, Liu Y (2022) Advances in integrated digital microfluidic platforms for point-of-care diagnosis: a review. Sens Diagn 1:648–672. https://doi.org/10.1039/D2SD00031H

33. Zhang JY, Bender AT, Boyle DS, Drain PK, Posner JD (2021) Current state of commercial point-of-care nucleic acid tests for infectious diseases. The Analyst 146:2449–2462. https://doi.org/10.1039/D0AN01988G

34. Cong H, Zhang N (2022) Perspectives in translating microfluidic devices from laboratory prototyping into scale-up production. Biomicrofluidics 16:021301. https://doi.org/10.1063/5.0079045

35. Abbott. In: -STAT 1. https://www.globalpointofcare.abbott/ww/en/product-details/apoc/i-stat-system.html. Accessed 10 Jun 2024

36. Hitado GmbH. In: Hitado GmbH Quidel Triage® MeterPro. https://www.hitado.de/quidel-triage-meterpro/qu-828-sb0020. Accessed 10 Jun 2024

37. Siemens Healthineers. In: Atellica® VTLi High-Sensit. Troponin Assay. https://www.siemens-healthineers.com/cardiac/cardiac-assays/vtli-hsctni

38. LumiraDx. In: Point Care Test. - Gener. Diagn. https://www.lumiradx.com/us-en/. Accessed 11 Jun 2024

39. NanoEntek. In: FREND Syst. - Microfluid. Immunofluoresc. Anal. https://www.nanoentek.com/theme/nanont2_en/shop/02/product01_view.php?it_id=1560265562. Accessed 10 Jun 2024

40. (2023) World Health Organization. In: Non Commun. Dis. https://www.who.int/news-room/fact-sheets/detail/noncommunicable-diseases. Accessed 17 Oct 2023

41. Amendola V, Pilot R, Frasconi M, Maragò OM, Iatì MA (2017) Surface plasmon resonance in gold nanoparticles: a review. J Phys Condens Matter 29:203002. https://doi.org/10.1088/1361-648X/aa60f3

42. Zhou W, Gao X, Liu D, Chen X (2015) Gold Nanoparticles for In Vitro Diagnostics. Chem Rev 115:10575–10636. https://doi.org/10.1021/acs.chemrev.5b00100

43. Moghadam BY, Connelly KT, Posner JD (2015) Two Orders of Magnitude Improvement in Detection Limit of Lateral Flow Assays Using Isotachophoresis. Anal Chem 87:1009–1017. https://doi.org/10.1021/ac504552r

44. Qin Z, Chan WCW, Boulware DR, Akkin T, Butler EK, Bischof JC (2012) Significantly Improved Analytical Sensitivity of Lateral Flow Immunoassays by Thermal Contrast. Angew Chem Int Ed Engl 51:4358–4361. https://doi.org/10.1002/anie.201200997

45. Beck F, Loessl M, Baeumner AJ (2023) Signaling strategies of silver nanoparticles in optical and electrochemical biosensors: considering their potential for the point-of-care. Microchim Acta 190:91. https://doi.org/10.1007/s00604-023-05666-6

46. Wu JZ, Ghopry SA, Liu B, Shultz A (2023) Metallic and Non-Metallic Plasmonic Nanostructures for LSPR Sensors. Micromachines 14:1393. https://doi.org/10.3390/mi14071393

47. Zhou Y, Ding L, Wu Y, Huang X, Lai W, Xiong Y (2019) Emerging strategies to develop sensitive AuNP-based ICTS nanosensors. TrAC Trends Anal Chem 112:147–160. https://doi.org/10.1016/j.trac.2019.01.006

48. Tng DJH, Yin BCY, Cao J, Ko KKK, Goh KCM, Chua DXW, Zhang Y, Chua MLK, Low JGH, Ooi EE, Soo KC (2022) Amplified parallel antigen rapid test for point-of-care salivary detection of SARS-CoV-2 with improved sensitivity. Mikrochim Acta 189:14. https://doi.org/10.1007/s00604-021-05113-4

49. Panferov VG, Byzova NA, Biketov SF, Zherdev AV, Dzantiev BB (2021) Comparative Study of In Situ Techniques to Enlarge Gold Nanoparticles for Highly Sensitive Lateral Flow Immunoassay of SARS-CoV-2. Biosensors 11:229. https://doi.org/10.3390/bios11070229

50. Ren W, Ballou DR, FitzGerald R, Irudayaraj J (2019) Plasmonic enhancement in lateral flow sensors for improved sensing of E. coli O157:H7. Biosens Bioelectron 126:324–331. https://doi.org/10.1016/j.bios.2018.10.066

51. Zhou Y, Chen Y, Liu Y, Fang H, Huang X, Leng Y, Liu Z, Hou L, Zhang W, Lai W, Xiong Y (2021) Controlled copper in situ growth-amplified lateral flow sensors for sensitive, reliable, and field-deployable infectious disease diagnostics. Biosens Bioelectron 171:112753. https://doi.org/10.1016/j.bios.2020.112753

52. Panferov VG, Zherdev AV, Dzantiev BB (2023) Post-Assay Chemical Enhancement for Highly Sensitive Lateral Flow Immunoassays: A Critical Review. Biosensors 13:866. https://doi.org/10.3390/bios13090866

53. Han G-R, Koo HJ, Ki H, Kim M-G (2020) Paper/Soluble Polymer Hybrid-Based Lateral Flow Biosensing Platform for High-Performance Point-of-Care Testing. ACS Appl Mater Interfaces 12:34564–34575. https://doi.org/10.1021/acsami.0c07893

54. Panraksa Y, Apilux A, Jampasa S, Puthong S, Henry CS, Rengpipat S, Chailapakul O (2021) A facile one-step gold nanoparticles enhancement based on sequential patterned lateral flow immunoassay device for C-reactive protein detection. Sens Actuators B Chem 329:129241. https://doi.org/10.1016/j.snb.2020.129241

55. Shen Y, Shen G (2019) Signal-Enhanced Lateral Flow Immunoassay with Dual Gold Nanoparticle Conjugates for the Detection of Hepatitis B Surface Antigen. ACS Omega 4:5083–5087. https://doi.org/10.1021/acsomega.8b03593

56. Taranova NA, Slobodenuyk VD, Zherdev AV, Dzantiev BB (2021) Network of gold conjugates for enhanced sensitive immunochromatographic assays of troponins. RSC Adv 11:16445–16452. https://doi.org/10.1039/D1RA02212A

57. Chotithammakul S, Cortie MB, Pissuwan D (2021) Comparison of Single- and Mixed-Sized Gold Nanoparticles on Lateral Flow Assay for Albumin Detection. Biosensors 11:209. https://doi.org/10.3390/bios11070209

58. Rink S, Kaiser B, Steiner M-S, Duerkop A, Baeumner AJ (2022) Highly sensitive interleukin 6 detection by employing commercially ready liposomes in an LFA

format. Anal Bioanal Chem 414:3231–3241. https://doi.org/10.1007/s00216-021-03750-5

59. Bollella P (2022) Enzyme-based amperometric biosensors: 60 years later … Quo Vadis? Anal Chim Acta 1234:340517. https://doi.org/10.1016/j.aca.2022.340517

60. Calabria D, Calabretta MM, Zangheri M, Marchegiani E, Trozzi I, Guardigli M, Michelini E, Di Nardo F, Anfossi L, Baggiani C, Mirasoli M (2021) Recent Advancements in Enzyme-Based Lateral Flow Immunoassays. Sensors 21:3358. https://doi.org/10.3390/s21103358

61. Joung H-A, Oh YK, Kim M-G (2014) An automatic enzyme immunoassay based on a chemiluminescent lateral flow immunosensor. Biosens Bioelectron 53:330–335. https://doi.org/10.1016/j.bios.2013.10.004

62. Parandakh A, Ymbern O, Jogia W, Renault J, Ng A, Juncker D (2023) 3D-printed capillaric ELISA-on-a-chip with aliquoting. Lab Chip 23:1547–1560. https://doi.org/10.1039/D2LC00878E

63. Liu D, Zhang Y, Zhu M, Yu Z, Ma X, Song Y, Zhou S, Yang C (2020) Microfluidic-Integrated Multicolor Immunosensor for Visual Detection of HIV-1 p24 Antigen with the Naked Eye. Anal Chem 92:11826–11833. https://doi.org/10.1021/acs.analchem.0c02091

64. Rocca M, Temiz Y, Salva ML, Castonguay S, Gervais T, Niemeyer CM, Delamarche E (2021) Rapid quantitative assays for glucose-6-phosphate dehydrogenase (G6PD) and hemoglobin combined on a capillary-driven microfluidic chip. Lab Chip 21:3573–3582. https://doi.org/10.1039/D1LC00354B

65. Uddin MJ, Bhuiyan NH, Shim JS (2021) Fully integrated rapid microfluidic device translated from conventional 96-well ELISA kit. Sci Rep 11:1986. https://doi.org/10.1038/s41598-021-81433-y

66. Lee M-J, Soum V, Lee S-N, Choi J-H, Shin J-H, Shin K, Oh B-K (2022) Pumpless three-dimensional photo paper–based microfluidic analytical device for automatic detection of thioredoxin-1 using enzyme-linked immunosorbent assay. Anal Bioanal Chem 414:3219–3230. https://doi.org/10.1007/s00216-021-03747-0

67. Preechakasedkit P, Siangproh W, Khongchareonporn N, Ngamrojanavanich N, Chailapakul O (2018) Development of an automated wax-printed paper-based lateral flow device for alpha-fetoprotein enzyme-linked immunosorbent assay. Biosens Bioelectron 102:27–32. https://doi.org/10.1016/j.bios.2017.10.051

68. Ishii M, Preechakasedkit P, Yamada K, Chailapakul O, Suzuki K, Citterio D (2018) Wax-Assisted One-Step Enzyme-Linked Immunosorbent Assay on Lateral Flow Test Devices. Anal Sci 34:51–56. https://doi.org/10.2116/analsci.34.51

69. Panraksa Y, Jang I, Carrell CS, Amin AG, Chailapakul O, Chatterjee D, Henry CS (2022) Simple manipulation of enzyme-linked immunosorbent assay (ELISA) using an automated microfluidic interface. Anal Methods 14:1774–1781. https://doi.org/10.1039/D2AY00326K

70. Zangheri M, Mirasoli M, Guardigli M, Di Nardo F, Anfossi L, Baggiani C, Simoni P, Benassai M, Roda A (2019) Chemiluminescence-based biosensor for monitoring astronauts' health status during space missions: Results from the International Space Station. Biosens Bioelectron 129:260–268. https://doi.org/10.1016/j.bios.2018.09.059

71. Hu X, Gao X, Chen S, Guo J, Zhang Y (2023) DropLab: an automated magnetic digital microfluidic platform for sample-to-answer point-of-care testing—development and application to quantitative immunodiagnostics. Microsyst Nanoeng 9:1–12. https://doi.org/10.1038/s41378-022-00475-y

72. Mao M, Sun F, Wang J, Li X, Pan Q, Peng C, Wang Z (2023) Delayed delivery of chromogenic substrate to nanozyme amplified aptamer lateral flow assay for acetamiprid. Sens Actuators B Chem 385:133720. https://doi.org/10.1016/j.snb.2023.133720

73. Han G-R, Ki H, Kim M-G (2020) Automated, Universal, and Mass-Producible Paper-Based Lateral Flow Biosensing Platform for High-Performance Point-of-Care Testing. ACS Appl Mater Interfaces 12:1885–1894. https://doi.org/10.1021/acsami.9b17888

74. Gong X, Cai J, Zhang B, Zhao Q, Piao J, Peng W, Gao W, Zhou D, Zhao M, Chang J (2017) A review of fluorescent signal-based lateral flow immunochromatographic strips. J Mater Chem B 5:5079–5091. https://doi.org/10.1039/c7tb01049d

75. Supianto M, Lee HJ (2022) Recent research trends in fluorescent reporters-based lateral flow immunoassay for protein biomarkers specific to acute myocardial infarction. Bull Korean Chem Soc 43:4–10. https://doi.org/10.1002/bkcs.12430

76. Semeniak D, Cruz DF, Chilkoti A, Mikkelsen MH (2023) Plasmonic Fluorescence Enhancement in Diagnostics for Clinical Tests at Point-of-Care: A Review of Recent Technologies. Adv Mater n/a:2107986. https://doi.org/10.1002/adma.202107986

77. Chen X, Miao X, Ma T, Leng Y, Hao L, Duan H, Yuan J, Li Y, Huang X, Xiong Y (2021) Gold Nanobeads with Enhanced Absorbance for Improved Sensitivity in Competitive Lateral Flow Immunoassays. Foods Basel Switz 10:1488. https://doi.org/10.3390/foods10071488

78. Xing H, Hwang K, Lu Y (2016) Recent Developments of Liposomes as Nanocarriers for Theranostic Applications. Theranostics 6:1336–1352. https://doi.org/10.7150/thno.15464

79. Gubala V, Giovannini G, Kunc F, Monopoli MP, Moore CJ (2020) Dye-doped silica nanoparticles: synthesis, surface chemistry and bioapplications. Cancer Nanotechnol 11:1. https://doi.org/10.1186/s12645-019-0056-x

80. Chen Z, Zhang Z, Zhai X, Li Y, Lin L, Zhao H, Bian L, Li P, Yu L, Wu Y, Lin G (2020) Rapid and Sensitive Detection of anti-SARS-CoV-2 IgG, Using Lanthanide-Doped Nanoparticles-Based Lateral Flow Immunoassay. Anal Chem 92:7226–7231. https://doi.org/10.1021/acs.analchem.0c00784

81. Zhou Y, Chen Y, Liu W, Fang H, Li X, Hou L, Liu Y, Lai W, Huang X, Xiong Y (2021) Development of a rapid and sensitive quantum dot nanobead-based double-antigen sandwich lateral flow immunoassay and its clinical performance for the detection of SARS-CoV-2 total antibodies. Sens Actuators B Chem 343:130139. https://doi.org/10.1016/j.snb.2021.130139

82. Zou J, Liu X, Ren X, Tan L, Fu C, Wu Q, Huang Z, Meng X (2021) Rapid and simultaneous detection of heart-type fatty acid binding protein and cardiac troponin using a lateral flow assay based on metal organic framework@CdTe nanoparticles. Nanoscale 13:7844–7850. https://doi.org/10.1039/D1NR00702E

83. Arshad F, Nabi F, Iqbal S, Khan RH (2022) Applications of graphene-based electrochemical and optical biosensors in early detection of cancer biomarkers. Colloids Surf B Biointerfaces 212:112356. https://doi.org/10.1016/j.colsurfb.2022.112356

84. Yu Q, Xia X, Xu C, Wang W, Zheng S, Wang C, Gu B, Wang C (2023) Introduction of a multilayered fluorescent nanofilm into lateral flow immunoassay for ultrasensitive detection of Salmonella typhimurium in food samples. Anal Methods Adv Methods Appl 15:3631–3641. https://doi.org/10.1039/d3ay00738c

85. Yang X, Cheng X, Wei H, Tu Z, Rong Z, Wang C, Wang S (2023) Fluorescence-enhanced dual signal lateral flow immunoassay for flexible and ultrasensitive detection of monkeypox virus. J Nanobiotechnology 21:450. https://doi.org/10.1186/s12951-023-02215-4

86. Campu A, Muresan I, Craciun A-M, Vulpoi A, Cainap S, Astilean S, Focsan M (2023) Innovative, Flexible, and Miniaturized Microfluidic Paper-Based Plasmonic Chip for Efficient Near-Infrared Metal Enhanced Fluorescence Biosensing and Imaging. ACS Appl Mater Interfaces 15:55925–55937. https://doi.org/10.1021/acsami.3c08658

87. Guo L, Shi Y, Liu X, Han Z, Zhao Z, Chen Y, Xie W, Li X (2018) Enhanced fluorescence detection of proteins using ZnO nanowires integrated inside microfluidic chips. Biosens Bioelectron 99:368–374. https://doi.org/10.1016/j.bios.2017.08.003

88. Zhao D, Wu Z, Yu J, Wang H, Li Y, Duan Y (2020) Highly sensitive microfluidic detection of carcinoembryonic antigen via a synergetic fluorescence enhancement

strategy based on the micro/nanostructure optimization of ZnO nanorod arrays and in situ ZIF-8 coating. Chem Eng J 383:123230. https://doi.org/10.1016/j.cej.2019.123230

89. Jeong Y, Kook Y-M, Lee K, Koh W-G (2018) Metal enhanced fluorescence (MEF) for biosensors: General approaches and a review of recent developments. Biosens Bioelectron 111:102–116. https://doi.org/10.1016/j.bios.2018.04.007

90. Wang Y, Zhao J, Zhu Y, Dong S, Liu Y, Sun Y, Qian L, Yang W, Cao Z (2021) Monolithic integration of nanorod arrays on microfluidic chips for fast and sensitive one-step immunoassays. Microsyst Nanoeng 7:1–10. https://doi.org/10.1038/s41378-021-00291-w

91. Deng W, Xie F, Baltar HTMCM, Goldys EM (2013) Metal-enhanced fluorescence in the life sciences: here, now and beyond. Phys Chem Chem Phys 15:15695–15708. https://doi.org/10.1039/C3CP50206F

92. Loiseau A, Asila V, Boitel-Aullen G, Lam M, Salmain M, Boujday S (2019) Silver-Based Plasmonic Nanoparticles for and Their Use in Biosensing. Biosensors 9:78. https://doi.org/10.3390/bios9020078

93. Kim T-H, Bong J-H, Kim H-R, Shim W-B, Kang M-J, Pyun J-C (2022) One-step immunoassay based on switching peptides for analyzing ochratoxin A in wines. J Anal Sci Technol 13:43. https://doi.org/10.1186/s40543-022-00352-3

94. Liu Q, Zhou X, Wu H, Zheng B (2020) Blocking-free and self-contained immunoassay platform for one-step point-of-care testing. Biosens Bioelectron 165:112394. https://doi.org/10.1016/j.bios.2020.112394

95. Jin B, Du Z, Zhang C, Yu Z, Wang X, Hu J, Li Z (2022) Eu-Chelate Polystyrene Microsphere-Based Lateral Flow Immunoassay Platform for hs-CRP Detection. Biosensors 12:977. https://doi.org/10.3390/bios12110977

96. Liu Q, Cheng S, Chen R, Ke J, Liu Y, Li Y, Feng W, Li F (2020) Near-Infrared Lanthanide-Doped Nanoparticles for a Low Interference Lateral Flow Immunoassay Test. ACS Appl Mater Interfaces 12:4358–4365. https://doi.org/10.1021/acsami.9b22449

97. Gunawardhana L, Kourentzi K, Danthanarayana AN, Brgoch J, Shan X, Willson RC, Shih W-C (2021) SERS-Based Ultrasensitive Lateral Flow Assay for Quantitative Sensing of Protein Biomarkers. IEEE J Sel Top Quantum Electron 27:1–8. https://doi.org/10.1109/JSTQE.2021.3062548

98. Khlebtsov B, Khlebtsov N (2020) Surface-Enhanced Raman Scattering-Based Lateral-Flow Immunoassay. Nanomaterials 10:2228. https://doi.org/10.3390/nano10112228

99. Panneerselvam R, Sadat H, Höhn E-M, Das A, Noothalapati H, Belder D (2022) Microfluidics and surface-enhanced Raman spectroscopy, a win–win combination? Lab Chip 22:665–682. https://doi.org/10.1039/D1LC01097B

100. Sun J, Gong L, Wang W, Gong Z, Wang D, Fan M (2020) Surface-enhanced Raman spectroscopy for on-site analysis: A review of recent developments. Luminescence 35:808–820. https://doi.org/10.1002/bio.3796

101. Khlebtsov BN, Bratashov DN, Byzova NA, Dzantiev BB, Khlebtsov NG (2019) SERS-based lateral flow immunoassay of troponin I by using gap-enhanced Raman tags. Nano Res 12:413–420. https://doi.org/10.1007/s12274-018-2232-4

102. Langer J, Jimenez de Aberasturi D, Aizpurua J, Alvarez-Puebla RA, Auguié B, Baumberg JJ, Bazan GC, Bell SEJ, Boisen A, Brolo AG, Choo J, Cialla-May D, Deckert V, Fabris L, Faulds K, García de Abajo FJ, Goodacre R, Graham D, Haes AJ, Haynes CL, Huck C, Itoh T, Käll M, Kneipp J, Kotov NA, Kuang H, Le Ru EC, Lee HK, Li J-F, Ling XY, Maier SA, Mayerhöfer T, Moskovits M, Murakoshi K, Nam J-M, Nie S, Ozaki Y, Pastoriza-Santos I, Perez-Juste J, Popp J, Pucci A, Reich S, Ren B, Schatz GC, Shegai T, Schlücker S, Tay L-L, Thomas KG, Tian Z-Q, Van Duyne RP, Vo-Dinh T, Wang Y, Willets KA, Xu C, Xu H, Xu Y, Yamamoto YS, Zhao B, Liz-Marzán LM (2020) Present and Future of Surface-Enhanced Raman Scattering. ACS Nano 14:28–117. https://doi.org/10.1021/acsnano.9b04224

103. Liu H, Dai E, Xiao R, Zhou Z, Zhang M, Bai Z, Shao Y, Qi K, Tu J, Wang C, Wang S (2021) Development of a SERS-based lateral flow immunoassay for rapid and ultra-sensitive detection of anti-SARS-CoV-2 IgM/IgG in clinical samples. Sens Actuators B Chem 329:129196. https://doi.org/10.1016/j.snb.2020.129196

104. Su X, Xu Y, Zhao H, Li S, Chen L (2019) Design and preparation of centrifugal microfluidic chip integrated with SERS detection for rapid diagnostics. Talanta 194:903–909. https://doi.org/10.1016/j.talanta.2018.11.014

105. Wang C, Weng G, Li J, Zhu J, Zhao J (2024) A review of SERS coupled microfluidic platforms: From configurations to applications. Anal Chim Acta 1296:342291. https://doi.org/10.1016/j.aca.2024.342291

106. Singh A, Sharma A, Ahmed A, Sundramoorthy AK, Furukawa H, Arya S, Khosla A (2021) Recent Advances in Electrochemical Biosensors: Applications, Challenges, and Future Scope. Biosensors 11:336. https://doi.org/10.3390/bios11090336

107. Yao H, Jenkins SH, Pesce AJ, Halsall HB, Heineman WR (1993) Electrochemical homogeneous enzyme immunoassay of theophylline in hemolyzed, icteric, and lipemic samples. Clin Chem 39:1432–1434

108. Wang W, Ding S, Wang Z, Lv Q, Zhang Q (2021) Electrochemical paper-based microfluidic device for on-line isolation of proteins and direct detection of lead in urine. Biosens Bioelectron 187:113310. https://doi.org/10.1016/j.bios.2021.113310

109. Beck F, Horn C, Baeumner AJ (2022) Ag nanoparticles outperform Au nanoparticles for the use as label in electrochemical point-of-care sensors. Anal Bioanal Chem 414:475–483. https://doi.org/10.1007/s00216-021-03288-6

110. Beck F, Horn C, Baeumner AJ (2022) Dry-reagent microfluidic biosensor for simple detection of NT-proBNP via Ag nanoparticles. Anal Chim Acta 1191:339375. https://doi.org/10.1016/j.aca.2021.339375

111. Yakoh A, Chaiyo S, Siangproh W, Chailapakul O (2019) 3D Capillary-Driven Paper-Based Sequential Microfluidic Device for Electrochemical Sensing Applications. ACS Sens 4:1211–1221. https://doi.org/10.1021/acssensors.8b01574

112. Esbin MN, Whitney ON, Chong S, Maurer A, Darzacq X, Tjian R (2020) Overcoming the bottleneck to widespread testing: a rapid review of nucleic acid testing approaches for COVID-19 detection. RNA 26:771–783. https://doi.org/10.1261/rna.076232.120

113. Zheng C, Wang K, Zheng W, Cheng Y, Li T, Cao B, Jin Q, Cui D (2021) Rapid developments in lateral flow immunoassay for nucleic acid detection. The Analyst 146:1514–1528. https://doi.org/10.1039/D0AN02150D

114. J. Asiello P, J. Baeumner A (2011) Miniaturized isothermal nucleic acid amplification, a review. Lab Chip 11:1420–1430. https://doi.org/10.1039/C0LC00666A

115. Wu J, Kodzius R, Cao W, Wen W (2014) Extraction, amplification and detection of DNA in microfluidic chip-based assays. Microchim Acta 181:1611–1631. https://doi.org/10.1007/s00604-013-1140-2

116. Dong T, Wang GA, Li F (2019) Shaping up field-deployable nucleic acid testing using microfluidic paper-based analytical devices. Anal Bioanal Chem 411:4401–4414. https://doi.org/10.1007/s00216-019-01595-7

117. Cunha ML, da Silva SS, Stracke MC, Zanette DL, Aoki MN, Blanes L (2022) Sample Preparation for Lab-on-a-Chip Systems in Molecular Diagnosis: A Review. Anal Chem 94:41–58. https://doi.org/10.1021/acs.analchem.1c04460

118. Wang N, Zhang J, Xiao B, Chen A (2024) Microfluidic-assisted integrated nucleic acid test strips for POCT. Talanta 267:125150. https://doi.org/10.1016/j.talanta.2023.125150

119. Seok Y, Batule BS, Kim M-G (2020) Lab-on-paper for all-in-one molecular diagnostics (LAMDA) of zika, dengue, and chikungunya virus from human serum. Biosens Bioelectron 165:112400. https://doi.org/10.1016/j.bios.2020.112400

120. Phillips EA, Moehling TJ, Ejendal KFK, Hoilett OS, Byers KM, Basing LA, Jankowski LA, Bennett JB, Lin L-K, Stanciu LA, Linnes JC (2019) Microfluidic rapid and

autonomous analytical device (microRAAD) to detect HIV from whole blood samples. Lab Chip 19:3375–3386. https://doi.org/10.1039/C9LC00506D

121. Xie M, Chen T, Cai Z, Lei B, Dong C (2024) An All-in-One Platform for On-Site Multiplex Foodborne Pathogen Detection Based on Channel-Digital Hybrid Microfluidics. Biosensors 14:50. https://doi.org/10.3390/bios14010050

122. Li N, Lu Y, Cheng J, Xu Y (2020) A self-contained and fully integrated fluidic cassette system for multiplex nucleic acid detection of bacteriuria. Lab Chip 20:384–393. https://doi.org/10.1039/c9lc00994a

123. USTAR BIOTECHNOLOGIES (HANGZHOU) LTD. In: COVID-19 RNA Test. https://en.bioustar.com/product/COVID-19-RNA-Test-82.html. Accessed 18 Sep 2023

124. Visby Medical. In: Respir. Health Test — POC Rapid PCR Device. https://www.visbymedical.com/respiratory-health-test/. Accessed 11 Jun 2024

125. Cue Health. In: Real-Time COVID-19 Test. https://cuehealth.com/products/how-cue-detects-covid-19. Accessed 11 Jun 2024

126. Detect. In: Accurate Access. Diagn. https://www.detect.com/. Accessed 18 Sep 2023

127. LUCIRA®. In: LUCIRA® Pfizer COVID-19 Flu Home Test. https://www.lucirabypfizer.com/. Accessed 5 Apr 2024

128. Bioopix-T. In: Pebble. https://biopix-t.com/. Accessed 5 Apr 2024

129. Díaz-González M, de la Escosura-Muñiz A (2021) Strip modification and alternative architectures for signal amplification in nanoparticle-based lateral flow assays. Anal Bioanal Chem 413:4111–4117. https://doi.org/10.1007/s00216-021-03421-5

130. Sena-Torralba A, Ngo DB, Parolo C, Hu L, Álvarez-Diduk R, Bergua JF, Rosati G, Surareungchai W, Merkoçi A (2020) Lateral flow assay modified with time-delay wax barriers as a sensitivity and signal enhancement strategy. Biosens Bioelectron 168:112559. https://doi.org/10.1016/j.bios.2020.112559

131. Tran BT, Rijiravanich P, Puttaraksa N, Surareungchai W (2022) Wax gates in laminated microfluidic paper-based immunosensors. Microchem J 178:107343. https://doi.org/10.1016/j.microc.2022.107343

132. Strong EB, Knutsen C, Wells JT, Jangid AR, Mitchell ML, Martinez NW, Martinez AW (2019) Wax-Printed Fluidic Time Delays for Automating Multi-Step Assays in Paper-Based Microfluidic Devices (MicroPADs). Inventions 4:20. https://doi.org/10.3390/inventions4010020

133. Zhang S-F, Liu L-N, Tang R-H, Liu Z, He X-C, Qu Z-G, Li F (2019) Sensitivity enhancement of lateral flow assay by embedding cotton threads in paper. Cellulose 26:8087–8099. https://doi.org/10.1007/s10570-019-02677-6

134. Tan W, Powles E, Zhang L, Shen W (2021) Go with the capillary flow. Simple thread-based microfluidics. Sens Actuators B Chem 334:129670. https://doi.org/10.1016/j.snb.2021.129670

135. Chen H, Liu Y, Feng S, Cao Y, Wu T, Liu Z (2022) Cotton thread-based multi-channel photothermal biosensor for simultaneous detection of multiple microRNAs. Biosens Bioelectron 200:113913. https://doi.org/10.1016/j.bios.2021.113913

136. Sumantakul S, Harley WE, Remcho VT (2023) Laser patterned nitrocellulose-based microfluidic devices: Applications in fluid manipulation and immunoassay. Sens Actuators B Chem 389:133867. https://doi.org/10.1016/j.snb.2023.133867

137. Bikkarolla SK, McNamee SE, McGregor S, Vance P, McGhee H, Marlow EL, McLaughlin J (2020) A lateral flow immunoassay with self-sufficient microfluidic system for enhanced detection of thyroid-stimulating hormone. AIP Adv 10:125316. https://doi.org/10.1063/5.0026047

138. Park SB, Shin JH (2022) Pressed Lateral Flow Assay Strips for Flow Delay-Induced Signal Enhancement in Lateral Flow Assay Strips. BioChip J. https://doi.org/10.1007/s13206-022-00085-w

139. Zadehkafi A, Siavashi M, Asiaei S, Bidgoli MR (2019) Simple geometrical modifications for substantial color intensity and detection limit enhancements in lateral-flow immunochromatographic assays. J Chromatogr B 1110–1111:1–8. https://doi.org/10.1016/j.jchromb.2019.01.019

140. Afriat R, Chalupowicz D, Eltzov E (2020) Development of a point-of-care technology for bacterial identification in milk. Talanta 219:121223. https://doi.org/10.1016/j.talanta.2020.121223

141. Tang R, Xie MY, Li M, Cao L, Feng S, Li Z, Xu F (2022) Nitrocellulose Membrane for Paper-based Biosensor. Appl Mater Today 26:101305. https://doi.org/10.1016/j.apmt.2021.101305

142. Castro RB de, de Souza ACA, Pavione N da RT, Badaró de Moraes JV, Ribeiro IC, Agripino J de M, Bressan GC, Vasconcellos R de S, Silva-Júnior A, Fietto JLR (2022) Urea, salts, and Tween 20 influence on adsorption of IgG and Leishmania rNTPDase2 to nitrocellulose. Anal Biochem 646:114648. https://doi.org/10.1016/j.ab.2022.114648

143. Perju A, Baeumner AJ, Wongkaew N (2022) Freestanding 3D-interconnected carbon nanofibers as high-performance transducers in miniaturized

electrochemical sensors. Microchim Acta 189:424. https://doi.org/10.1007/s00604-022-05492-2

144. Pimentel ES, Brito-Pereira R, Marques-Almeida T, Ribeiro C, Vaz F, Lanceros-Mendez S, Cardoso VF (2020) Tailoring Electrospun Poly(l-lactic acid) Nanofibers as Substrates for Microfluidic Applications. ACS Appl Mater Interfaces 12:60–69. https://doi.org/10.1021/acsami.9b12461

145. Brito-Pereira R, Macedo AS, Tubio CR, Lanceros-Méndez S, Cardoso VF (2021) Fluorinated Polymer Membranes as Advanced Substrates for Portable Analytical Systems and Their Proof of Concept for Colorimetric Bioassays. ACS Appl Mater Interfaces 13:18065–18076. https://doi.org/10.1021/acsami.1c00227

146. Brito-Pereira R, Macedo AS, Ribeiro C, Cardoso VF, Lanceros-Méndez S (2022) Natural based reusable materials for microfluidic substrates: The silk road towards sustainable portable analytical systems. Appl Mater Today 28:101507. https://doi.org/10.1016/j.apmt.2022.101507

147. Mao X, Du T-E, Wang Y, Meng L (2015) Disposable dry-reagent cotton thread-based point-of-care diagnosis devices for protein and nucleic acid test. Biosens Bioelectron 65:390–396. https://doi.org/10.1016/j.bios.2014.10.053

148. Jang I, Kang H, Song S, Dandy DS, Geiss BJ, Henry CS (2021) Flow control in a laminate capillary-driven microfluidic device. Analyst 146:1932–1939. https://doi.org/10.1039/D0AN02279A

149. Arango Y, Temiz Y, Gökçe O, Delamarche E (2020) Electro-actuated valves and self-vented channels enable programmable flow control and monitoring in capillary-driven microfluidics. Sci Adv 6:eaay8305. https://doi.org/10.1126/sciadv.aay8305

150. Bhuiyan NH, Hong JH, Uddin MJ, Shim JS (2022) Artificial Intelligence-Controlled Microfluidic Device for Fluid Automation and Bubble Removal of Immunoassay Operated by a Smartphone. Anal Chem 94:3872–3880. https://doi.org/10.1021/acs.analchem.1c04827

151. Shen H, Li Q, Song W, Jiang X (2023) Microfluidic on-chip valve and pump for applications in immunoassays. Lab Chip 23:341–348. https://doi.org/10.1039/D2LC01042A

152. Azizian P, Casals-Terré J, Ricart J, Cabot JM (2023) Diffusion-free valve for preprogrammed immunoassay with capillary microfluidics. Microsyst Nanoeng 9:1–13. https://doi.org/10.1038/s41378-023-00568-2

153. Strohmaier-Nguyen D, Horn C, Baeumner AJ (2024) NT-proBNP detection with a one-step magnetic lateral flow channel assay. Anal Bioanal Chem 416:2411–2422. https://doi.org/10.1007/s00216-024-05223-x

154. Strohmaier-Nguyen D, Horn C, Baeumner AJ (2024) Membrane-Free Lateral Flow Assay with the Active Control of Fluid Transport for Ultrasensitive Cardiac Biomarker Detection. Anal Chem 96:7014–7021. https://doi.org/10.1021/acs.analchem.4c00142

155. Hemmig E, Temiz Y, Gökçe O, Lovchik RD, Delamarche E (2020) Transposing Lateral Flow Immunoassays to Capillary-Driven Microfluidics Using Self-Coalescence Modules and Capillary-Assembled Receptor Carriers. Anal Chem 92:940–946. https://doi.org/10.1021/acs.analchem.9b03792

156. Kim J, Hong K, Kim H, Seo J, Jeong J, Bae PK, Shin YB, Lee JH, Oh HJ, Chung S (2020) Microfluidic immunoassay for point-of-care testing using simple fluid vent control. Sens Actuators B Chem 316:128094. https://doi.org/10.1016/j.snb.2020.128094

157. Cui F, Rhee M, Singh A, Tripathi A (2015) Microfluidic Sample Preparation for Medical Diagnostics. Annu Rev Biomed Eng 17:267–286. https://doi.org/10.1146/annurev-bioeng-071114-040538

158. Anderson NL, Anderson NG (2002) The human plasma proteome: history, character, and diagnostic prospects. Mol Cell Proteomics MCP 1:845–867. https://doi.org/10.1074/mcp.r200007-mcp200

159. Shrirao AB, Schloss RS, Fritz Z, Shrirao MV, Rosen R, Yarmush ML (2021) Autofluorescence of blood and its application in biomedical and clinical research. Biotechnol Bioeng 118:4550–4576. https://doi.org/10.1002/bit.27933

160. Wang Y, Nunna BB, Talukder N, Etienne EE, Lee ES (2021) Blood Plasma Self-Separation Technologies during the Self-Driven Flow in Microfluidic Platforms. Bioengineering 8:94. https://doi.org/10.3390/bioengineering8070094

161. Maurya A, Murallidharan JS, Sharma A, Agarwal A (2022) Microfluidics geometries involved in effective blood plasma separation. Microfluid Nanofluidics 26:73. https://doi.org/10.1007/s10404-022-02578-4

162. Maria MS, Chandra TS, Sen AK (2017) Capillary flow-driven blood plasma separation and on-chip analyte detection in microfluidic devices. Microfluid Nanofluidics 21:72. https://doi.org/10.1007/s10404-017-1907-6

163. Tripathi S, Kumar YVBV, Prabhakar A, Joshi SS, Agrawal A (2015) Passive blood plasma separation at the microscale: a review of design principles and microdevices. J Micromechanics Microengineering 25:083001. https://doi.org/10.1088/0960-1317/25/8/083001

164. Shi Y, Guo J, Guo J (2023) Alphalisa immunoassay enabled centrifugal microfluidic system for “one-step” detection of pepsinogen in whole blood. Sens Actuators B Chem 376:133048. https://doi.org/10.1016/j.snb.2022.133048

165. Lee KK, Kim M-O, Choi S (2019) A whole blood sample-to-answer polymer lab-on-a-chip with superhydrophilic surface toward point-of-care technology. J Pharm Biomed Anal 162:28–33. https://doi.org/10.1016/j.jpba.2018.09.007

166. Qiu X, Jiang H, Zhang X, Li K, Ge S, Xia N, Mauk MG (2020) A plasma separator with a multifunctional deformable chamber equipped with a porous membrane for point-of-care diagnostics. Analyst 145:6138–6147. https://doi.org/10.1039/D0AN01014F

167. Bakhtiaridoost S, Habibiyan H, Ghafoorifard H (2023) A microfluidic device to separate high-quality plasma from undiluted whole blood sample using an enhanced gravitational sedimentation mechanism. Anal Chim Acta 1239:340641. https://doi.org/10.1016/j.aca.2022.340641

168. Liu SC, Yoo PB, Garg N, Lee AP, Rasheed S (2021) A microfluidic device for blood plasma separation and fluorescence detection of biomarkers using acoustic microstreaming. Sens Actuators Phys 317:112482. https://doi.org/10.1016/j.sna.2020.112482

169. Lenz KD, Jakhar S, Chen JW, Anderson AS, Purcell DC, Ishak MO, Harris JF, Akhadov LE, Kubicek-Sutherland JZ, Nath P, Mukundan H (2021) A centrifugal microfluidic cross-flow filtration platform to separate serum from whole blood for the detection of amphiphilic biomarkers. Sci Rep 11:5287. https://doi.org/10.1038/s41598-021-84353-z

170. Vemulapati S, Erickson D (2018) H.E.R.M.E.S: rapid blood-plasma separation at the point-of-need. Lab Chip 18:3285–3292. https://doi.org/10.1039/C8LC00939B

171. Kim J, Yoon J, Byun J-Y, Kim H, Han S, Kim J, Lee JH, Jo H-S, Chung S (2021) Nano-Interstice Driven Powerless Blood Plasma Extraction in a Membrane Filter Integrated Microfluidic Device. Sensors 21:1366. https://doi.org/10.3390/s21041366

172. Strohmaier-Nguyen D, Horn C, Baeumner AJ (2024) Sample-to-answer lateral flow assay with integrated plasma separation and NT-proBNP detection. Anal Bioanal Chem 416:3107–3115. https://doi.org/10.1007/s00216-024-05271-3

173. Jung C, Kim M-G (2022) Direct Use of a Saliva-Collected Cotton Swab in Lateral Flow Immunoassay for the Detection of Cotinine. Biosensors 12:214. https://doi.org/10.3390/bios12040214

174. Jajack A, Stamper I, Gomez E, Brothers M, Begtrup G, Heikenfeld J (2019) Continuous, quantifiable, and simple osmotic preconcentration and sensing within microfluidic devices. PLOS ONE 14:e0210286. https://doi.org/10.1371/journal.pone.0210286

175. Cuevas-Córdoba B, Santiago-García J (2014) Saliva: a fluid of study for OMICS. Omics J Integr Biol 18:87–97. https://doi.org/10.1089/omi.2013.0064

176. inne.io. In: Minilab. https://www.inne.io/en/product/minilab. Accessed 25 Dec 2023

177. Vinoth R, Sangavi P, Nakagawa T, Jayaraman M, Mohan AMV (2023) All-in-one microfluidic device with an integrated porous filtration membrane for on-site detection of multiple salivary biomarkers. Sens Actuators B Chem 379:133214. https://doi.org/10.1016/j.snb.2022.133214

178. Lee K, Yoon T, Yang H, Cha S, Cheon Y-P, Kashefi-Kheyrabadi L, Jung H-I (2020) All-in-one platform for salivary cotinine detection integrated with a microfluidic channel and an electrochemical biosensor. Lab Chip 20:320–331. https://doi.org/10.1039/C9LC01024F

179. Cai Y, Niu J-C, Liu Y-Q, Du X-L, Wu Z-Y (2020) Online sample clean-up and enrichment of proteins from salty media with dynamic double gradients on a paper fluidic channel. Anal Chim Acta 1100:149–155. https://doi.org/10.1016/j.aca.2019.11.048

180. Zhang Y, Liu X, Wang L, Yang H, Zhang X, Zhu C, Wang W, Yan L, Li B (2020) Improvement in Detection Limit for Lateral Flow Assay of Biomacromolecules by Test-Zone Pre-enrichment. Sci Rep 10:9604. https://doi.org/10.1038/s41598-020-66456-1

181. Drexelius A, Hoellrich A, Jajack A, Gomez E, Brothers M, Hussain S, Kim S, Heikenfeld J (2020) Analysis of pressure-driven membrane preconcentration for point-of-care assays. Biomicrofluidics 14:054101. https://doi.org/10.1063/5.0013987

182. Luppa PB, Bietenbeck A, Beaudoin C, Giannetti A (2016) Clinically relevant analytical techniques, organizational concepts for application and future perspectives of point-of-care testing. Biotechnol Adv 34:139–160. https://doi.org/10.1016/j.biotechadv.2016.01.003

183. Park J (2022) Lateral Flow Immunoassay Reader Technologies for Quantitative Point-of-Care Testing. Sensors 22:7398. https://doi.org/10.3390/s22197398

184. Hu J, Cui X, Gong Y, Xu X, Gao B, Wen T, Lu TJ, Xu F (2016) Portable microfluidic and smartphone-based devices for monitoring of cardiovascular diseases at the point of care. Biotechnol Adv 34:305–320. https://doi.org/10.1016/j.biotechadv.2016.02.008

185. Taylor P (2023) Statista. In: Stat. Forecast Number Mob. Users Worldw. 2020-2025. https://www.statista.com/statistics/218984/number-of-global-mobile-users-since-2010/. Accessed 5 Apr 2024

186. Nayak S, Blumenfeld NR, Laksanasopin T, Sia SK (2017) Point-of-Care Diagnostics: Recent Developments in a Connected Age. Anal Chem 89:102–123. https://doi.org/10.1021/acs.analchem.6b04630

187. Quesada-González D, Merkoçi A (2017) Mobile phone-based biosensing: An emerging "diagnostic and communication" technology. Biosens Bioelectron 92:549–562. https://doi.org/10.1016/j.bios.2016.10.062

188. Xu D, Huang X, Guo J, Ma X (2018) Automatic smartphone-based microfluidic biosensor system at the point of care. Biosens Bioelectron 110:78–88. https://doi.org/10.1016/j.bios.2018.03.018

189. Bui TH, Thangavel B, Sharipov M, Chen K, Shin JH (2023) Smartphone-Based Portable Bio-Chemical Sensors: Exploring Recent Advancements. Chemosensors 11:468. https://doi.org/10.3390/chemosensors11090468

190. Ulloa-Gomez AM, Agredo A, Lucas A, Somvanshi SB, Stanciu L (2023) Smartphone-based colorimetric detection of cardiac troponin T via label-free aptasensing. Biosens Bioelectron 222:114938. https://doi.org/10.1016/j.bios.2022.114938

191. Ruppert C, Phogat N, Laufer S, Kohl M, Deigner H-P (2019) A smartphone readout system for gold nanoparticle-based lateral flow assays: application to monitoring of digoxigenin. Mikrochim Acta 186:119. https://doi.org/10.1007/s00604-018-3195-6

192. Man Y, Ban M, Li A, Jin X, Du Y, Pan L (2021) A microfluidic colorimetric biosensor for in-field detection of Salmonella in fresh-cut vegetables using thiolated polystyrene microspheres, hose-based microvalve and smartphone imaging APP. Food Chem 354:129578. https://doi.org/10.1016/j.foodchem.2021.129578

193. Man Y, Li A, Li B, Liu J, Pan L (2019) A microfluidic colorimetric immunoassay for sensitive detection of altenariol monomethyl ether by UV spectroscopy and smart phone imaging. Anal Chim Acta 1092:75–84. https://doi.org/10.1016/j.aca.2019.09.039

194. Huang L, Ding L, Zhou J, Chen S, Chen F, Zhao C, Xu J, Hu W, Ji J, Xu H, Liu GL (2021) One-step rapid quantification of SARS-CoV-2 virus particles via low-cost nanoplasmonic sensors in generic microplate reader and point-of-care device. Biosens Bioelectron 171:112685. https://doi.org/10.1016/j.bios.2020.112685

195. Qin W, Wang K, Xiao K, Hou Y, Lu W, Xu H, Wo Y, Feng S, Cui D (2017) Carcinoembryonic antigen detection with "Handing"-controlled fluorescence spectroscopy using a color matrix for point-of-care applications. Biosens Bioelectron 90:508–515. https://doi.org/10.1016/j.bios.2016.10.052

196. Huttunen A, Aikio S, Kurkinen M, Mäkinen J-T, Mitikka R, Kivimäki L, Harjumaa M, Takalo-Mattila J, Liedert C, Hiltunen J, Hakalahti L (2020) Portable Low-Cost

Fluorescence Reader for LFA Measurements. IEEE Sens J 20:10275–10282. https://doi.org/10.1109/JSEN.2020.2992894

197. Alonso O, Franch N, Canals J, Arias-Alpízar K, de la Serna E, Baldrich E, Diéguez A (2020) An internet of things-based intensity and time-resolved fluorescence reader for point-of-care testing. Biosens Bioelectron 154:112074. https://doi.org/10.1016/j.bios.2020.112074

198. Rong Z, Xiao R, Peng Y, Zhang A, Wei H, Ma Q, Wang D, Wang Q, Bai Z, Wang F, Sun M, Wang S (2021) Integrated fluorescent lateral flow assay platform for point-of-care diagnosis of infectious diseases by using a multichannel test cartridge. Sens Actuators B Chem 329:129193. https://doi.org/10.1016/j.snb.2020.129193

199. Gong Y, Zheng Y, Jin B, You M, Wang J, Li X, Lin M, Xu F, Li F (2019) A portable and universal upconversion nanoparticle-based lateral flow assay platform for point-of-care testing. Talanta 201:126–133. https://doi.org/10.1016/j.talanta.2019.03.105

200. Su Y, Lin B, Zhang K, Zhan T, Li J, Zhang C (2023) A fluorescence point-of-care testing system for sample-to-answer detection of immunoglobulin E. Microchem J 192:108907. https://doi.org/10.1016/j.microc.2023.108907

201. Ireta-Muñoz LA, Morales-Narváez E (2020) Smartphone and Paper-Based Fluorescence Reader: A Do It Yourself Approach. Biosensors 10:60. https://doi.org/10.3390/bios10060060

202. Rong Z, Wang Q, Sun N, Jia X, Wang K, Xiao R, Wang S (2019) Smartphone-based fluorescent lateral flow immunoassay platform for highly sensitive point-of-care detection of *Zika virus* nonstructural protein 1. Anal Chim Acta 1055:140–147. https://doi.org/10.1016/j.aca.2018.12.043

203. Nguyen VD, Nguyen HQ, Bui KH, Ko YS, Park BJ, Seo TS (2022) A handheld-type total integrated capillary electrophoresis system for SARS-CoV-2 diagnostics: Power, fluorescence detection, and data analysis by smartphone. Biosens Bioelectron 195:113632. https://doi.org/10.1016/j.bios.2021.113632

204. Miao G, Jiang X, Yang D, Fu Q, Zhang L, Ge S, Ye X, Xia N, Qian S, Qiu X (2022) A hand-held, real-time, AI-assisted capillary convection PCR system for point-of-care diagnosis of African swine fever virus. Sens Actuators B Chem 358:131476. https://doi.org/10.1016/j.snb.2022.131476

205. Yin H, Tong Z, Shen C, Xu X, Ma H, Wu Z, Qi Y, Mao H (2022) Micro-PCR chip-based multifunctional ultrafast SARS-CoV-2 detection platform. Lab Chip 22:2671–2681. https://doi.org/10.1039/D2LC00101B

206. Nguyen HV, Nguyen VD, Liu F, Seo TS (2020) An Integrated Smartphone-Based Genetic Analyzer for Qualitative and Quantitative Pathogen Detection. ACS Omega 5:22208–22214. https://doi.org/10.1021/acsomega.0c02317

207. Liao S-C, Peng J, Mauk MG, Awasthi S, Song J, Friedman H, Bau HH, Liu C (2016) Smart cup: A minimally-instrumented, smartphone-based point-of-care molecular diagnostic device. Sens Actuators B Chem 229:232–238. https://doi.org/10.1016/j.snb.2016.01.073

208. Liu C, Mauk MG, Hart R, Qiu X, Bau HH (2011) A self-heating cartridge for molecular diagnostics. Lab Chip 11:2686–2692. https://doi.org/10.1039/C1LC20345B

209. Qiu X, Zhang S, Xiang F, Wu D, Guo M, Ge S, Li K, Ye X, Xia N, Qian S (2017) Instrument-free point-of-care molecular diagnosis of H1N1 based on microfluidic convective PCR. Sens Actuators B Chem 243:738–744. https://doi.org/10.1016/j.snb.2016.12.058

210. Srivastav S, Dankov A, Adanalic M, Grzeschik R, Tran V, Pagel-Wieder S, Gessler F, Spreitzer I, Scholz T, Schnierle B, Anastasiou OE, Dittmer U, Schlücker S (2021) Rapid and Sensitive SERS-Based Lateral Flow Test for SARS-CoV2-Specific IgM/IgG Antibodies. Anal Chem 93:12391–12399. https://doi.org/10.1021/acs.analchem.1c02305

211. Tran V, Walkenfort B, König M, Salehi M, Schlücker S (2019) Rapid, Quantitative, and Ultrasensitive Point-of-Care Testing: A Portable SERS Reader for Lateral Flow Assays in Clinical Chemistry. Angew Chem Int Ed Engl 58:442–446. https://doi.org/10.1002/anie.201810917

212. Xiao R, Lu L, Rong Z, Wang C, Peng Y, Wang F, Wang J, Sun M, Dong J, Wang D, Wang L, Sun N, Wang S (2020) Portable and multiplexed lateral flow immunoassay reader based on SERS for highly sensitive point-of-care testing. Biosens Bioelectron 168:112524. https://doi.org/10.1016/j.bios.2020.112524

213. Wang W, Li Y, Nie A, Fan G-C, Han H (2021) A portable SERS reader coupled with catalytic hairpin assembly for sensitive microRNA-21 lateral flow sensing. Analyst 146:848–854. https://doi.org/10.1039/D0AN02177F

214. Bandodkar AJ, Imani S, Nuñez-Flores R, Kumar R, Wang C, Vinu Mohan AM, Wang J, Mercier PP (2018) Re-usable electrochemical glucose sensors integrated into a smartphone platform. Biosens Bioelectron 101:181–187. https://doi.org/10.1016/j.bios.2017.10.019

215. Sun AC, Hall DA (2019) Point-of-Care Smartphone-based Electrochemical Biosensing. Electroanalysis 31:2–16. https://doi.org/10.1002/elan.201800474

216. Madrid RE, Ashur Ramallo F, Barraza DE, Chaile RE (2022) Smartphone-Based Biosensor Devices for Healthcare: Technologies, Trends, and Adoption by End-Users. Bioengineering 9:101. https://doi.org/10.3390/bioengineering9030101

217. Guo J (2017) Smartphone-Powered Electrochemical Dongle for Point-of-Care Monitoring of Blood β-Ketone. Anal Chem 89:8609–8613. https://doi.org/10.1021/acs.analchem.7b02531

218. Shin Low S, Pan Y, Ji D, Li Y, Lu Y, He Y, Chen Q, Liu Q (2020) Smartphone-based portable electrochemical biosensing system for detection of circulating microRNA-21 in saliva as a proof-of-concept. Sens Actuators B Chem 308:127718. https://doi.org/10.1016/j.snb.2020.127718

219. Aymerich J, Márquez A, Terés L, Muñoz-Berbel X, Jiménez C, Domínguez C, Serra-Graells F, Dei M (2018) Cost-effective smartphone-based reconfigurable electrochemical instrument for alcohol determination in whole blood samples. Biosens Bioelectron 117:736–742. https://doi.org/10.1016/j.bios.2018.06.044

220. Guo J (2016) Uric Acid Monitoring with a Smartphone as the Electrochemical Analyzer. Anal Chem 88:11986–11989. https://doi.org/10.1021/acs.analchem.6b04345

221. Shi Z, Dai C, Deng P, Wu Y, Liu G, An Z, Liang H, Zhang F, Lu Y, Liu Q (2023) Smartphone-based portable photoelectrochemical biosensing system for point-of-care detection of urine creatinine and albumin. Lab Chip 23:3424–3432. https://doi.org/10.1039/D3LC00238A

222. Wei M, Rao H, Niu Z, Xue X, Luo M, Zhang X, Huang H, Xue Z, Lu X (2021) Breaking the time and space limitation of point-of-care testing strategies: Photothermometric sensors based on different photothermal agents and materials. Coord Chem Rev 447:214149. https://doi.org/10.1016/j.ccr.2021.214149

223. Cheng N, Song Y, Shi Q, Du D, Liu D, Luo Y, Xu W, Lin Y (2019) Au@Pd Nanopopcorn and Aptamer Nanoflower Assisted Lateral Flow Strip for Thermal Detection of Exosomes. Anal Chem 91:13986–13993. https://doi.org/10.1021/acs.analchem.9b03562

224. Thapa D, Samadi N, Tabatabaei N (2021) Handheld Thermo-Photonic Device for Rapid, Low-Cost, and On-Site Detection and Quantification of Anti-SARS-CoV-2 Antibody. Ieee Sens J 21:18504. https://doi.org/10.1109/JSEN.2021.3089016

225. Mohammed MI, Haswell S, Gibson I (2015) Lab-on-a-chip or Chip-in-a-lab: Challenges of Commercialization Lost in Translation. Procedia Technol 20:54–59. https://doi.org/10.1016/j.protcy.2015.07.010

226. Annabestani M, Esmaeili-Dokht P, Fardmanesh M (2020) A novel, low cost, and accessible method for rapid fabrication of the modifiable microfluidic devices. Sci Rep 10:16513. https://doi.org/10.1038/s41598-020-73535-w

227. Assaifan AK, Al habis N, Ahmad I, Alshehri NA, Alharbi HF (2020) Scaling-up medical technologies using flexographic printing. Talanta 219:121236. https://doi.org/10.1016/j.talanta.2020.121236

228. Nishat S, Jafry AT, Martinez AW, Awan FR (2021) Paper-based microfluidics: Simplified fabrication and assay methods. Sens Actuators B Chem 336:129681. https://doi.org/10.1016/j.snb.2021.129681

229. Carrell C, Kava A, Nguyen M, Menger R, Munshi Z, Call Z, Nussbaum M, Henry C (2019) Beyond the lateral flow assay: A review of paper-based microfluidics. Microelectron Eng 206:45–54. https://doi.org/10.1016/j.mee.2018.12.002

230. Qin X, Liu J, Zhang Z, Li J, Yuan L, Zhang Z, Chen L (2021) Microfluidic paper-based chips in rapid detection: Current status, challenges, and perspectives. TrAC Trends Anal Chem 143:116371. https://doi.org/10.1016/j.trac.2021.116371

231. Raj M K, Chakraborty S (2020) PDMS microfluidics: A mini review. J Appl Polym Sci 137:48958. https://doi.org/10.1002/app.48958

232. Tsao C-W (2016) Polymer Microfluidics: Simple, Low-Cost Fabrication Process Bridging Academic Lab Research to Commercialized Production. Micromachines 7:225. https://doi.org/10.3390/mi7120225

233. Mukherjee P, Nebuloni F, Gao H, Zhou J, Papautsky I (2019) Rapid Prototyping of Soft Lithography Masters for Microfluidic Devices Using Dry Film Photoresist in a Non-Cleanroom Setting. Micromachines 10:192. https://doi.org/10.3390/mi10030192

234. Hiltunen J, Liedert C, Hiltunen M, Huttunen O-H, Hiitola-Keinänen J, Aikio S, Harjanne M, Kurkinen M, Hakalahti L, Lee LP (2018) Roll-to-roll fabrication of integrated PDMS–paper microfluidics for nucleic acid amplification. Lab Chip 18:1552–1559. https://doi.org/10.1039/C8LC00269J

235. Olmos CM, Vaca A, Rosero G, Peñaherrera A, Perez C, de Sá Carneiro I, Vizuete K, Arroyo CR, Debut A, Pérez MS, Cumbal L, Lerner B (2019) Epoxy resin mold and PDMS microfluidic devices through photopolymer flexographic printing plate. Sens Actuators B Chem 288:742–748. https://doi.org/10.1016/j.snb.2019.03.062

236. Guckenberger DJ, Groot TE de, Wan AMD, Beebe DJ, Young EWK (2015) Micromilling: a method for ultra-rapid prototyping of plastic microfluidic devices. Lab Chip 15:2364–2378. https://doi.org/10.1039/C5LC00234F

237. Waddell EA (2006) Laser ablation as a fabrication technique for microfluidic devices. Methods Mol Biol Clifton NJ 321:27–38. https://doi.org/10.1385/1-59259-997-4:27

238. Matellan C, del Río Hernández AE (2018) Cost-effective rapid prototyping and assembly of poly(methyl methacrylate) microfluidic devices. Sci Rep 8:6971. https://doi.org/10.1038/s41598-018-25202-4

239. Bhattacharjee N, Urrios A, Kang S, Folch A (2016) The upcoming 3D-printing revolution in microfluidics. Lab Chip 16:1720–1742. https://doi.org/10.1039/C6LC00163G

240. Yazdi AA, Popma A, Wong W, Nguyen T, Pan Y, Xu J (2016) 3D printing: an emerging tool for novel microfluidics and lab-on-a-chip applications. Microfluid Nanofluidics 20:50. https://doi.org/10.1007/s10404-016-1715-4

241. Ho CMB, Ng SH, Li KHH, Yoon Y-J (2015) 3D printed microfluidics for biological applications. Lab Chip 15:3627–3637. https://doi.org/10.1039/C5LC00685F

242. Waheed S, Cabot JM, Macdonald NP, Lewis T, Guijt RM, Paull B, Breadmore MC (2016) 3D printed microfluidic devices: enablers and barriers. Lab Chip 16:1993–2013. https://doi.org/10.1039/C6LC00284F

243. Mehta V, Rath SN (2021) 3D printed microfluidic devices: a review focused on four fundamental manufacturing approaches and implications on the field of healthcare. Bio-Des Manuf 4:311–343. https://doi.org/10.1007/s42242-020-00112-5

244. Singh S, Singh G, Prakash C, Ramakrishna S (2020) Current status and future directions of fused filament fabrication. J Manuf Process 55:288–306. https://doi.org/10.1016/j.jmapro.2020.04.049

245. Scott SM, Ali Z (2021) Fabrication Methods for Microfluidic Devices: An Overview. Micromachines 12:319. https://doi.org/10.3390/mi12030319

246. Peng L, Deng Y, Yi P, Lai X (2013) Micro hot embossing of thermoplastic polymers: a review. J Micromechanics Microengineering 24:013001. https://doi.org/10.1088/0960-1317/24/1/013001

247. Cecchini M, Signori F, Pingue P, Bronco S, Ciardelli F, Beltram F (2008) High-Resolution Poly(ethylene terephthalate) (PET) Hot Embossing at Low Temperature: Thermal, Mechanical, and Optical Analysis of Nanopatterned Films. Langmuir 24:12581–12586. https://doi.org/10.1021/la801706q

248. Deshmukh SS, Kar T, Goswami A (2023) Investigation and multi-objective optimization of replication accuracy of microfluidic chip fabricated through induction-aided hot embossing. J Braz Soc Mech Sci Eng 45:1–31. https://doi.org/10.1007/s40430-023-04538-7

249. Mortelmans T, Kazazis D, Werder J, Kristiansen PM, Ekinci Y (2022) Injection Molding of Thermoplastics for Low-Cost Nanofluidic Devices. ACS Appl Nano Mater 5:17758–17766. https://doi.org/10.1021/acsanm.2c03731

250. Lee UN, Su X, Guckenberger DJ, Dostie AM, Zhang T, Berthier E, Theberge AB (2018) Fundamentals of rapid injection molding for microfluidic cell-based assays. Lab Chip 18:496–504. https://doi.org/10.1039/C7LC01052D

251. Kim Y, Song J, Lee Y, Cho S, Kim S, Lee S-R, Park S, Shin Y, Jeon NL (2021) High-throughput injection molded microfluidic device for single-cell analysis of spatiotemporal dynamics. Lab Chip 21:3150–3158. https://doi.org/10.1039/D0LC01245A

252. Toren P, Smolka M, Haase A, Palfinger U, Nees D, Ruttloff S, Kuna L, Schaude C, Jauk S, Rumpler M, Hierschlager B, Katzmayr I, Sonnleitner M, Thesen MW, Lohse M, Horn M, Weigel W, Strbac M, Bijelic G, Hemanth S, Okulova N, Kafka J, Kostler S, Stadlober B, Hesse J (2020) High-throughput roll-to-roll production of polymer biochips for multiplexed DNA detection in point-of-care diagnostics. Lab Chip 20:4106–4117. https://doi.org/10.1039/D0LC00751J

253. Wang Y, Weng C, Fei Z, Sun H, Jiang B (2024) Enhancing structural replication of microfluidic chips: Parameter optimization and mold insert modification. Polym Eng Sci. https://doi.org/10.1002/pen.26675

254. Boutiette AL, Toothaker C, Corless B, Boukaftane C, Howell C (2020) 3D printing direct to industrial roll-to-roll casting for fast prototyping of scalable microfluidic systems. PLOS ONE 15:e0244324. https://doi.org/10.1371/journal.pone.0244324

255. Liedert C, Rannaste L, Kokkonen A, Huttunen O-H, Liedert R, Hiltunen J, Hakalahti L (2020) Roll-to-Roll Manufacturing of Integrated Immunodetection Sensors. ACS Sens 5:2010–2017. https://doi.org/10.1021/acssensors.0c00404

256. Vig AL, Mäkelä T, Majander P, Lambertini V, Ahopelto J, Kristensen A (2011) Roll-to-roll fabricated lab-on-a-chip devices. J Micromechanics Microengineering 21:035006. https://doi.org/10.1088/0960-1317/21/3/035006

257. Liu J, Kong X, Wang H, Zhang Y, Fan Y (2020) Roll-to-roll wax transfer for rapid and batch fabrication of paper-based microfluidics. Microfluid Nanofluidics 24:1–7. https://doi.org/10.1007/s10404-019-2310-2

258. Hoang T, Truong H, Han J, Lee S, Lee J, Parajuli S, Lee J, Cho G (2023) Room temperature roll-to-roll additive manufacturing of polydimethylsiloxane-based centrifugal microfluidic device for on-site isolation of ribonucleic acid from whole blood. Mater Today Bio 23:100838. https://doi.org/10.1016/j.mtbio.2023.100838

259. Dincer C, Bruch R, Kling A, Dittrich PS, Urban GA (2017) Multiplexed Point-of-Care Testing – xPOCT. Trends Biotechnol 35:728–742. https://doi.org/10.1016/j.tibtech.2017.03.013

260. Mohammed MI, Haswell S, Gibson I (2015) Lab-on-a-chip or Chip-in-a-lab: Challenges of Commercialization Lost in Translation. Procedia Technol 20:54–59. https://doi.org/10.1016/j.protcy.2015.07.010

3 Membrane-free lateral flow assay with active control of fluid transport for ultrasensitive cardiac biomarker detection

Abstract

Membrane-based lateral flow immunoassays (LFA) have been employed as early point-of-care (POC) testing tools in clinical settings. However, the varying membrane properties, uncontrollable sample transport in LFAs, visual readout and required large sample volumes have been major limiting factors in realizing needed sensitivity and desirable precise quantification. Addressing these challenges, we designed a membrane-free system in which the desirable 3D structure of the detection zone is imitated, used a small pump for fluid flow and fluorescence as read-out, all while maintaining a one-step assay protocol. A hydrogel-like protein-polyelectrolyte complex (PPC) within a polyelectrolyte multilayer (PEM) was developed as the test line by complexing polystreptavidin (pSA) with polydiallyldimethylammonium chloride (PDDA) which in turn was layered with polyacrylic acid (PAA) resulting in a superior 3D streptavidin-rich test line. Since the remainder of the microchannel remains material-free good flow control is achieved and with 20 µL total volume, 7.5 less sample volumes can be used in comparison to conventional LFAs. High sensitivity with desirable reproducibility and a 20-minute total assay time were achieved for the detection of NT-proBNP in plasma with a dynamic range of 60 pg·mL^{-1} – 9000 pg·mL^{-1} and a limit of detection of 56 pg·mL^{-1} using probe antibody-modified fluorescence nanoparticles. While instrument-free visual detection is no longer possible, the developed lateral flow channel platform has the potential to dramatically expand the LFA applicability, as it overcomes the limitations of membrane-based immunoassays, ultimately improving the accuracy and reducing the sample volume, so that finger prick analyses can easily be done in a one-step assay for analytes present at very low concentrations.

Graphical Abstract

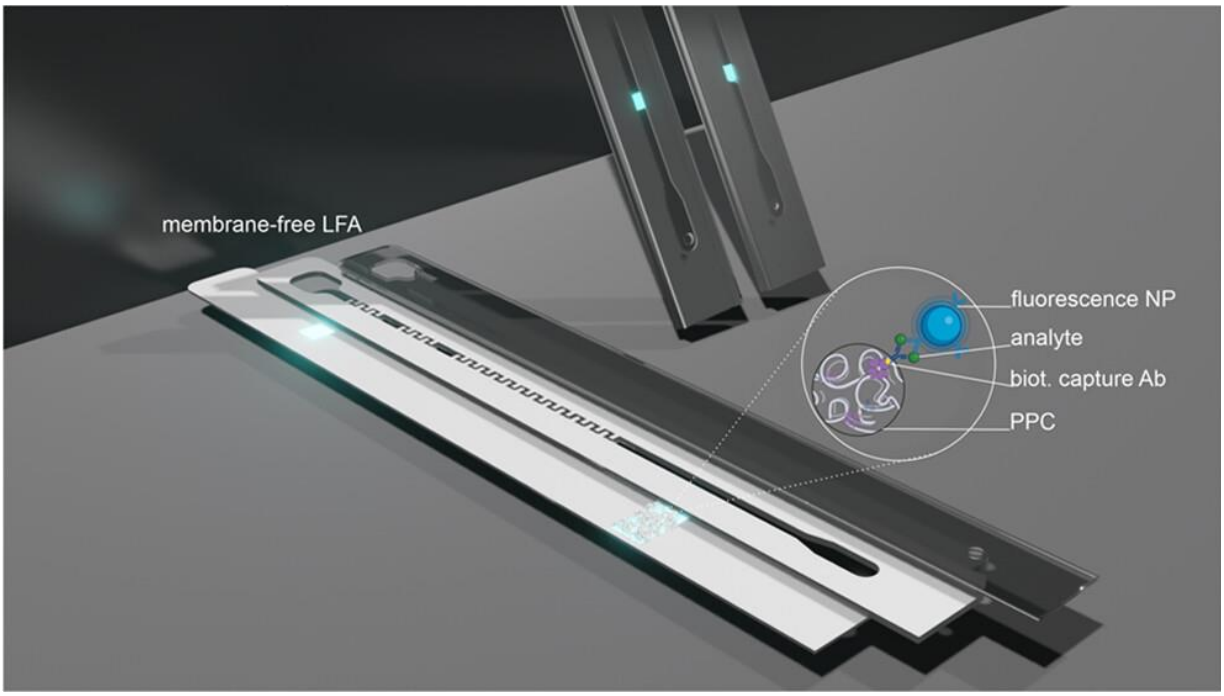

This chapter has been published.

Strohmaier-Nguyen, D., Horn, C., & Baeumner, A. J. (2024). Membrane-Free Lateral Flow Assay with the Active Control of Fluid Transport for Ultrasensitive Cardiac Biomarker Detection. *Analytical Chemistry*, *96*(18), 7014-7021.
https://doi.org/10.1021/acs.analchem.4c00142

Author contributions: AJB, CH and DSN developed the concept for this work. DSN planned the experiments, did the experimental work and wrote the first draft of the manuscript. AJB revised the manuscript and is corresponding author.

3.1 Introduction

Recently, with the continuous process in point-of-care testing (POCT), fast and ultra-sensitive detection is accomplished by lateral flow immunoassays (LFAs) [1, 2]. The simple, affordable, and user-friendly setup makes the LFA a relevant and efficient diagnostic tool where high-tech infrastructure may not be met. The fundamental part of the LFA is the porous membrane that enables passive sample migration through capillary forces and straightforward immobilization of proteins necessary for detection such as antibodies and streptavidin [3, 4]. However, the LFA also bears some major drawbacks and limitations such as variation of flow rate and analysis time due to varying pore structure and sample viscosity, obstruction of pores by matrix components, reasonably high sample volume due to its inherent absorbing properties, and inconsistency in the dispersion of the labeled sample to the membrane due to batch-to-batch variations of the membrane [5, 6]. In addition, as the LFA performance strongly depends on the properties of the membrane material, a change of the production line by the supplier results in changes in the membrane properties due to modifications of production parameters such as drying temperature and line speed, requiring re-optimization of an already finalized assay. In addition, Mosley et al. demonstrated that the membrane and analyte interaction hinders the forward binding event of the antibody, negatively affecting the sensor performance [7]. To address these challenges, number of researchers explored replacing the conventional membrane with other material [8, 9] or shifted its focus towards polymer-based channel systems, eliminating the need for membrane materials [10], thereby improving the assay sensitivity by one order of magnitude [11]. To replace the membrane, the transport of the fluid and immobilization of biorecognition elements must be reassessed. Fluid can be managed passively, utilizing capillary forces, or actively, necessitating external forces [12]. Regarding the substrate for immobilization, several polymers such as polyethylene terephthalate (PET), poly(methyl methacrylate) (PMMA) and cyclic olefin copolymer (COC) were used in biosensors due to their low cost [13] with planar (2D) or three dimensional (3D) immobilization strategies [14]. 2D approaches typically employ adsorption or covalent immobilization where the density and amount of the biorecognition molecules is limited to the active sites on the polymer surface itself [15].

In some instances, the polymers' hydrophobicity can lead to partial denaturing of proteins so that tethers or spacers need to be employed [16]. In contrast, 3D immobilization in a polymer matrix such as a hydrogel by encapsulation, copolymerization, electrostatic capture or covalent linking enables higher immobilization rates within a protective protein surrounding [17]. Here, the intrinsic swelling behavior of the hydrogel requires an additional washing step to prevent non-specific signals [18], and the overall chemistry involved may be more complex than for simple adsorptive strategies. To overcome these limitations, recent studies have demonstrated high efficiency of protein immobilization using polyelectrolyte multilayers (PEM) as the immobilization matrix [19]. To accomplish this, polyelectrolytes with opposite charges are alternately deposited onto the desired substrate through dip coating, spraying, spinning, and microfluidics [20] demonstrating high functionality of proteins within such layers such as the immobilization of a polyelectrolyte-protein complex (PPC), where the lysozyme retained all of its enzymatic activity [21]. Here, we studied and developed a novel, membrane-free LFA concept with 3D streptavidin multilayers as the detection zone and fluorescence nanoparticles as labels. An external pump was employed to control the immunoreaction, while fluorescence microscopy was utilized for POCT detection and quantification of NT-proBNP. This biomarker is associated with heart failure (HF) [22], which stands as the cardiovascular disorder with the highest mortality, morbidity, and healthcare costs [23]. NT-proBNP is considered the gold standard biomarker, attributed to its longer half-life of 120 minutes, in contrast to BNP with a half-life of 20 minutes. This leads to roughly six times higher concentrations of NT-proBNP in serum, making it more easily detectable [24]. With a minimal sample volume of just 15 µL, a rapid detection time of only 20 minutes, and the ability to integrate a pump and fluorescence detection into a compact and portable support device, this innovative concept successfully addresses the limitations associated with membrane-based lateral flow assays. Additionally, it offers a convenient alternative for finger-prick testing, suitable for both home use and low-resource settings.

3.2 Material and Methods

The biotinylated capture antibody (polyclonal NT-proBNP sheep-IgG-biotin, cAb), antigen (NT-proBNP (1-76) amid) in buffer or human serum, probe antibody (monoclonal NT-proBNP mouse-IgG), probe antibody–modified fluorescence nanoparticles (Ab-fluorescence NPs), and polystreptavidin (pSA) were provided by Roche Diagnostics GmbH (Mannheim, Germany). Hydrochloric acid (HCl, 0.1 M, 1 M), sodium chloride (NaCl, p.a.), bovine serum albumin (BSA, >96 %), poly(diallyldimethylammonium chloride) (PDDA, M_w 200,000 – 350,000, 20 wt. % in H_2O), poly(acrylic acid, sodium salt) solution (average M_w 15,000, 35 wt. % in H_2O), ethylenediaminetetraacetic acid (EDTA, ≥ 98.5 %), sodium hydroxide (NaOH, 1 M), poly(ethylene glycol)-block-poly(propylene glycol)-block-poly(ethylene glycol) (Synperonic® PE/P84), sodium azide, Tween 20 (>97 %) and biotinylated Rhodamine 6G (Rh-6G, 0.05 mg·mL^{-1}) were supplied from Sigma-Aldrich (www.sigmaaldrich.com). Sucrose was purchased from Serva (www.serva.de). NT-proBNP hs cobas 232 was provided by Roche Diagnostics (Mannheim, Germany).

The LFA consists of the substrate and spacer Melinex®329 (175 µm and 250 µm) which was purchased from Dupont Teijin Films (www.dupontteijinfilms.com), the cover foil Hostaphan RN 100 was purchased from Mitsubishi Polyester Film (www.m-petfilm.de) and double-sided adhesive tape was supplied from Henkel-Adhesives (www.henkel-adhesives.com).

HEPES-buffered saline (HBS) consisted of 50 mM HEPES, 150 mM NaCl, 3 mM EDTA, and 0.05 % (w/v) Tween 20 and was adjusted to pH 7.4. HEPES dispensing buffer was prepared with 50 mM HEPES, 1 % (w/v) albumin, 1 % (w/v) sucrose, 0.15 % (w/v) synperonic PE/P84, and 0.024 % (w/v) sodium azide and was adjusted to pH 7.4.

For particle characterization, the Zetasizer Ultra Pro (www.malvernpanalytical.com) was used. All drying procedures were done with the drying cabinet at 50 °C (FED 400 E2, www.binder-world.com). For plasma treatment, the plasma oven (www.gs-technologie.de) was used.

3.2.1 Pretreatment of substrate and blocking of non-specific adsorption

First, the substrate (MELINEX®329 175 µm) was pre-treated with oxygen plasma for 2 min, 100 W to increase the hydrophilicity and thus, enhance the polyelectrolyte multilayer attachment. For blocking non-specific adsorption, a thin polyacrylic acid (PAA) layer was used. Therefore, the base of the microfluidic sensor was dip-coated with PAA (0.2 % (w/v), 150 mM NaCl, pH 7.4) for 60 seconds, washed with distilled water, and dried at 50 °C and was then utilized for polyelectrolyte streptavidin multilayer deposition.

3.2.2 Polyelectrolyte-protein complex (PPC) fabrication

For the fabrication of the PPCs, a modified procedure of vander Straeten et al. is utilized.[21] PPCs were fabricated by mixing polydiallyldimethylammonium chloride (PDDA) with polystreptavidin (pSA). First, a PDDA solution was prepared in 150 mM NaCl and polystreptavidin was dissolved in water to reach an end concentration of 0.5 % (w/v) and 10 mg·mL^{-1}, respectively, and were adjusted to pH 7.4. Then, 500 µL PDDA was mixed with 500 µL pSA to generate the functionalized particles. The PPCs were stored at 4 °C until further use.

3.2.3 Fluidic-assisted PPC multilayer lane assembly and antibody dispensing

PPC multilayer lanes were deposited onto the base of the microfluidic using a fluidic immobilization channel. To assemble the polyelectrolyte multilayer (PEM) the PPC solution and polyacrylic acid (PAA) solution were alternate deposited onto the base by filling the immobilization channel by solely capillary forces. PAA was dissolved in 150 mM NaCl to a concentration of 0.5 % (w/v) and was adjusted to pH 4.55. The fluidic deposition channel with double-sided adhesive tape was bonded onto the PET substrate and was used as a shaping lane mold. By using a stop-flow approach, the channel was filled with the PPC solution and was deposited for 60 seconds. After the deposition time, the capillary was emptied and filled with the PAA solution for 60 seconds. This alternate coating process was repeated for a given number of cycles for the preparation of the PEMs. Afterwards, the channel mold was relieved from the substrate and the (PPC/PAA) multilayer was dried at 50 °C for 5 min. In the next step, 1.5 µL of each antibody was

dispensed onto the PET substrate and were dried at 40 °C for 3 minutes. The substrate with the streptavidin lane and probe antibodies was then adhered to the spacer and cover foil to finish the membrane-free LFA. The ready-to-use LFAs were stored at 4 °C until further use. Details of the fabrication process were provided in the Supporting Information (SI).

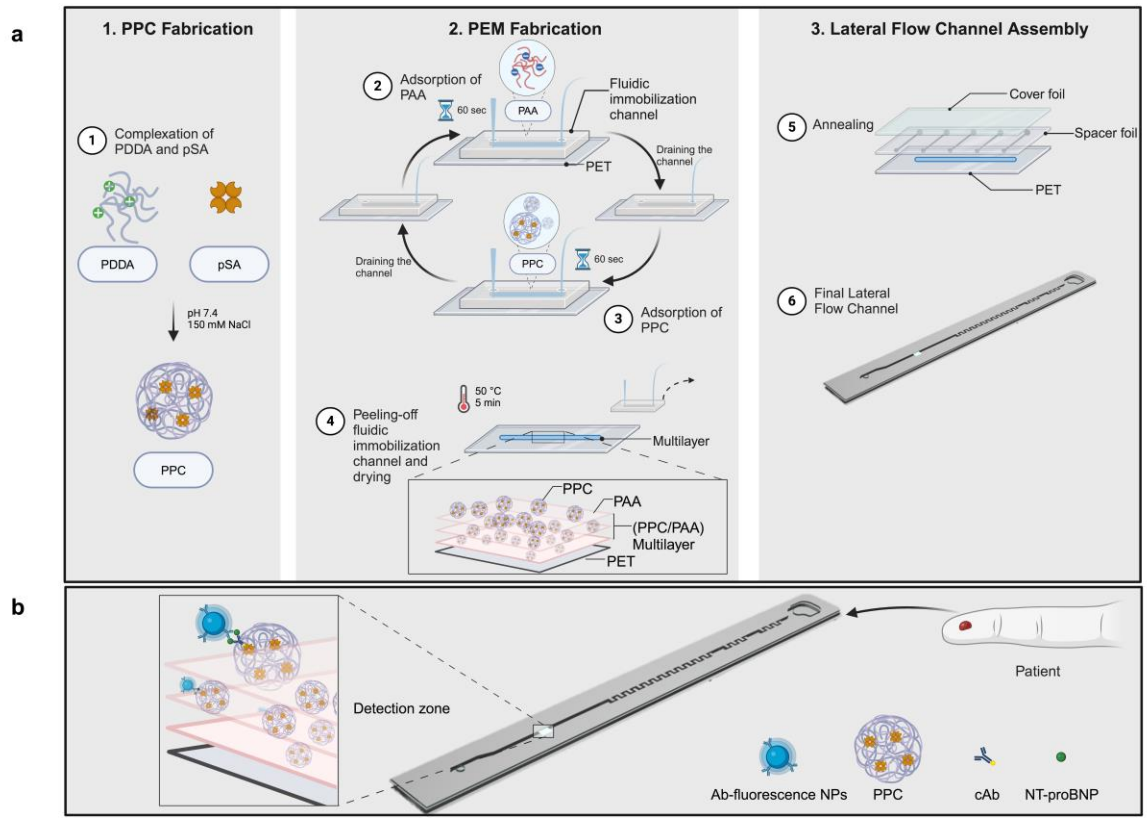

Figure 1: Schematic (not to scale) illustration of the membrane-free POCT device. Fabrication of the detection zone consists of two steps (a): Fabrication of the protein-polyelectrolyte complex (PPC) by complexation of pSA and PDDA at pH 7.5, 150 mM NaCl (1) and subsequently, layer-by-layer deposition of poly acrylic acid (PAA) and PPCs on the PET substrate of the sensor (2-4). The sensor was then annealed with the spacer and cover foil (5). The final lateral flow channel (6). Schematic (not to scale) illustration of the sensing principle (b). Ab-fluorescence NPs – probe antibody–modified fluorescence nanoparticles, cAb - biotinylated capture antibody. Adapted from "PDMS Microfluidic Chip Fabrication", by BioRender.com (2023). Retrieved from https://app.biorender.com/biorender-templates

3.2.4 Biofunctionality of PPCs

To investigate the biofunctionality of polystreptavidin within the prepared PPCs in the multilayer, the streptavidin multilayer was tested with the biotinylated Rhodamine 6G (Rh-6G, λ_{ex} = 525 nm, λ_{em} = 548 nm). Rh-6G was pre- pared in a 0.05 mg·mL^{-1} stock solution with distilled water. 20 µL Rh-6G solution were injected into the LFA and were actively transported over the streptavidin multilayer for 5 minutes. The unbound solution was removed, and the streptavidin multilayer was then analyzed with the fluorescence microscopy.

3.2.5 Assay equipment

The customized fluid control equipment and fluorescence microscopy were provided by Roche Diagnostics GmbH (Mannheim, Germany) (Figure S2). Details of the fluid control and fluorescence microscopy were provided in the SI.

3.2.6 Performance of the bioassay

A sandwich immunoassay with both buffer and plasma samples were carried out to investigate the assay performance of the bioassay. The analyte target was N-terminal prohormone of brain natriuretic peptide (NT-proBNP), which is a biomarker for heart failure. NT-proBNP biomarker samples were prepared in HBS buffer and human plasma through dilution of a stock solution to produce concentrations of 7.5, 15, 30, 60, 125, 250, 500, 1000, 2000, 4000, 6000 and 9000 pg·mL^{-1}, for analysis. The immunoassay was performed at room temperature. For the calculation of the limit of detection (LOD) the logistic fit parameter for the lower curve asymptote A and the standard deviation of the blank SD (blank):

$$LOD = A + 3.3 * SD(blank) \quad (1)$$

3.3 Results and Discussion

Main goal of this study was the design of a POCT device that does not require membranes and can hence function with very small sample volumes (finger-prick sampling) while maintaining the simplicity of use and sensitivity afforded by current

LFAs (Figure 1). The detection is accomplished using fluorescent immunobeads as described previously by Lutz et al. [25]. The immobilization of the biorecognition elements in a test line was achieved by designing protein-polyelectrolyte complexes (PPC) consisting of polystreptavidin - poly(diallyldimethylammonium chloride) composite microparticles, which were then integrated into a charged polymer multilayer. Fluid transport and the overall assay protocol were finally optimized for a sensitive detection of NT-proBNP (Figure S3).

3.3.1 Characterization of PPCs

PPCs were studied to develop a novel, sensitive POCT immunoassay. More specifically, we utilized the cationic polydiallyldimethylammonium chloride (PDDA) and the negatively charged polystreptavidin (pSA) for the synthesis of biofunctional microparticles. The characteristics of the protein-polyelectrolyte complex, especially the size and the charge of the complex depend on the nature and intensity of the polyelectrolyte protein interactions and on the environment [26]. Hence, we explored the impact of the polyelectrolyte-to-protein ratio and the pH on the complexation process. The latter has a major effect on the ionization of the materials used. Whereas PDDA, as a strong cationic polyelectrolyte, has a positive charge over a wide pH range (pH 2-13) and is stable to pH shifts, the amphoteric polystreptavidin with the isoelectric point (IEP) of 5 – 6 [27] is notably influenced by the pH of its environment. To ensure complexation of PDDA and pSA, both materials were mixed in different ratios at pH 7.4 and 150 mM NaCl (Figure S4). This pH level is slightly higher than pSA's isoelectric point (IEP), ensuring the overall negative charge of pSA, which in turn facilitates the electrostatic complexation with PDDA. Considering the physiological environment of the envisioned assay, pH of 7.4 and ionic strength of 150 mM NaCl were hence kept constant in all subsequent experiments. Directly after the mixing process, highly turbid samples were obtained immediately. DLS analysis and zeta potential measurements proved the complexation process [28]. The size and polydispersity index (PdI) of the resulting composite particles were dependent on the PDDA:pSA ratio (Figure S4a). In particular, an excess of pSA led to the attainment of maximum size with a minimal PdI, indicative of an intricate mesh-like network wherein streptavidin serves as a bridge connecting two or more PDDA chains. In this context, there are segments on the PDDA

chain without attached streptavidin. These unbound portions generate electrostatic repulsion, effectively preventing aggregation and complete collapse [29]. However, an excess of PDDA led to the formation of small particles characterized by relatively high PdI values. This suggested that the limited amount of streptavidin is bound in a densely compacted manner, effectively covered and regulated by PDDA. The high PdI can be explained by the fact that some parts of the PDDA stick out at the surface, like a core corona structure [30]. Regarding the zeta potential of the resulting composite material, it is evident that it naturally becomes increasingly positive as the PDDA:pSA ratio rises (Figure S4b). In this context, it is likely that PDDA completely envelops the particles. All of these were used in subsequent studies of the novel LFA concept.

3.3.2 Formation of the 3D test line and assessing the biofunctionality of the embedded PPCs

On the PET substrate, the 3D test line was generated in a layer-by-layer approach of the composite PPCs and polyacrylic acid (PAA). The PET substrate underwent oxygen plasma treatment to enhance its hydrophilic properties, a crucial step for facilitating the adhesion of bioactive coatings. Specifically, the plasma treatment induces increased surface roughness, thereby expanding the number of available attachment sites [31]. In general, a simple dip coating process in which the substrate is alternate dipped into the polyelectrolyte solutions is used to generate multilayers. The average dip coating time of each layer is 15 min in order to guarantee the PAA adsorption and charge overcompensation in the multilayer assembly [20]. Moreover, a washing step is necessary between each layer deposition to wash away unbound protein or PAA, resulting in a time-consuming and material-wasting procedure. Here, for the layer-by-layer process, a fluidic immobilization channel was used as lane shaping mold that was attached to the PET foil [32]. First, the positively charged PPCs were deposited onto the negatively charged PET substrate by capillary-driven filling of the channel. Subsequently, the anionic PAA was applied through the same process. By alternating these two steps, multilayers of 2 to 12 layers were created. It was determined that the deposition time of PAA and PPCs affected the multilayer performance. The deposition is hereby solely dependent on the Brownian diffusion to the bottom layer of the multilayer. Through the utilization of a material-efficient fluidic-assisted stop-flow

multilayer deposition method, we achieved a more economical and time-efficient procedure, eliminating the need for a washing step [33, 34]. Due to the geometry of the immobilization channel, the (PPC/PAA) multilayer assembly was completed within only 8 minutes. To assess the biofunctionality of pSA when inside the PPC/PAA multilayer lane, the binding efficiency of a biotinylated Rhodamine 6G (Rh-6G, λ_{ex} = 525 nm, λ_{em} = 548 nm) to pSA within the multilayer was investigated. Subsequently, the immobilization channel was removed and the actual LFA assembled (Figure 1). The 20 µL Rh-6G solution was transported to the test line and incubated for 10 min. After that the channel was emptied to remove unbound dye molecules and then the fluorescence quantified using a fluorescence microscopy and ImageJ. Binding of the dye by streptavidin within the multilayer was investigated depending on the PDDA:pSA ratio (Figure S5). The lowest fluorescence signals were found at low and high PDDA concentrations. At low PDDA concentrations large PPCs with low positive charges were generated which represented a loose network. It is assumed that this may encourage streptavidin leaching as it is insufficiently bound by PDDA. In addition, the particles only show a slightly positive charge (Figure S4b), which results in reduced electrostatic interactions with PAA during the multilayer deposition process. Conversely, an excess of PDDA can lead to a competition between PDDA and PPCs for the available electrostatic binding sites with PAA during the multilayer formation, resulting in a reduced amount of streptavidin within the multilayer. Overall, the maximum fluorescence intensity was found at PDDA:pSA ratio of 0.5 and 1 suggesting that the highest amount of streptavidin could be securely immobilized within the multilayer. Due to economic reasons, the PDDA:pSA ratio of 0.5 was used for further experiments.

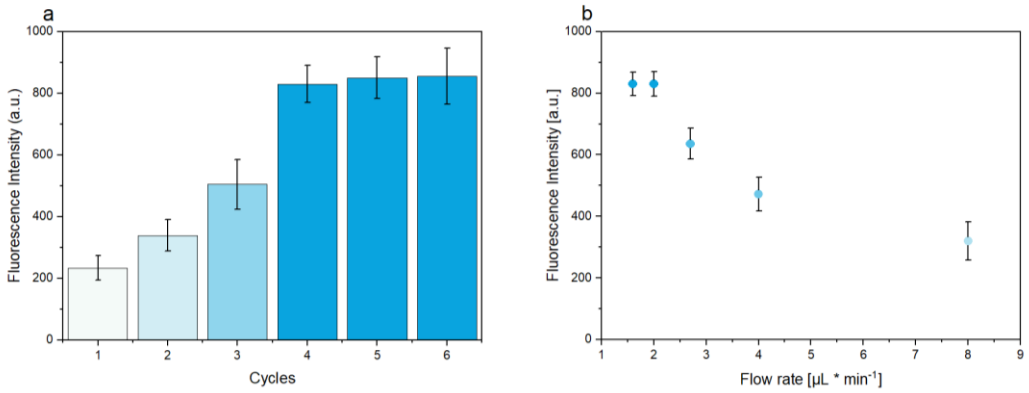

Figure 2: Plot of fluorescence intensity of the bioassay using a constant antigen concentration of 1 ng·mL⁻¹ in buffer against the number of layer-by-layer cycles (a). Plot of the fluorescence intensity of the bioassay using a constant antigen concentration of 1 ng·mL⁻¹ in buffer against the flow rate (b). Error bars represent mean values ±1σ and were calculated based on three parallel measurements on three different LFAs (n = 3).

3.3.3 Development and optimization of the novel LFA concept

After the initial proof-of-principle multilayer formation, we further optimized its performance in an antibody-based sandwich LFA. First, the number of $(PPC/PAA)_x$ layers was investigated using a sandwich assay of biotinylated capture antibodies (cAb), fluorescent reporter antibodies (Ab-fluorescence NPs) and NT-proBNP as analyte (Figure 2a). It was found that fluorescence signals increased significantly up to the first $(PPC/PAA)_4$ multilayers, which suggests that the immobilized pSA concentration increased initially with the number of layers [35]. Additional layers did not lead to further signal increase. Furthermore, the need for the composite PPC in contrast to mere polystreptavidin in the multilayer build-up was studied (Figure S6). It was found that even high concentration of pSA (15 mg·mL^{-1}) yielded in only low fluorescence signals. It is assumed that the strong and homogeneous positive charge of the PPCs leads to a stronger interaction with the PAA polyelectrolyte layers, potentially leading to an increased concentration of streptavidin within the multilayer. These findings were in accordance with the work of vander Straeten et al. who showed higher immobilization rate of the complexed protein than the pure protein itself in the multilayer [21]. Secondly, the impact of the flow rate on the assay was assessed. As the flow rate has influence on the immunoreaction and on the rehydration characteristics of dried

reagents, we initially dried biotinylated cAbs and Ab-fluorescence NPs on the PET substrate. The 20 µL sample volume was transported with a flow rate of 8, 4, 2.7, 2 and 1.6 $\mu L \cdot min^{-1}$. It was found that high flow rates resulted in low fluorescence signals (Figure 2b) most likely due to less efficient capturing of the immune sandwich and insufficient rehydration of the dried reagents. In contrast, at flow rates ≤ 2 $\mu L \cdot min^{-1}$ high fluorescence signals were obtained reaching a plateau. Therefore, a flow rate of 2 $\mu L \cdot min^{-1}$ was chosen for further experiments. Decreasing non-specific binding of sample matrix components onto the PET substrate was studied using BSA as a commonly used blocking agent in bioassays [36] and PAA, a highly hydrophilic polyelectrolyte (Figure S7) [37]. First, the channel was filled with 40 µL of the blocking solution, containing either BSA or PAA and then incubated for 10 min. After draining the channel, the LFAs were dried in an oven at 50 °C. Subsequently, an immunoassay was performed by applying 20 µL of the sample to the assay. High non-specific signals were found when no blocking was performed and when BSA acted as blocking agent. In the case of no blocking, it can be assumed that plasma proteins deposit on the channel surface which then further promote non-specific binding of the fluorescence nanoparticles. Similarly, when the channel surface is blocked with BSA, it is assumed that BSA molecules will adsorb on the channel surface and interact with the fluorescence latex beads. In contrary, when the hydrophilic PAA is used as a blocking agent, non-specific signals could be significantly decreased. Therefore, the channel surface was treated with PAA for subsequent experiments. Eventually, the concentration of the cAb and Ab-fluorescence NPs were optimized with respect to the strongest fluorescence intensity for a constant analyte concentration (Figure S8). For the maximum fluorescence signal, the cAb was prepared at a concentration of 2.5 $\mu g \cdot mL^{-1}$ and the Ab-fluorescence NPs were prepared at a concentration of 2 % (w/v) in the HEPES dispensing buffer.

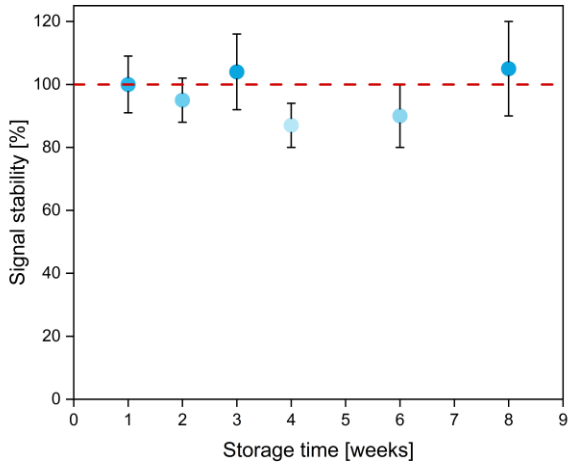

Figure 3: Stability of the fluorescence signal of the bioassay using a constant antigen concentration of 1 ng·mL⁻¹ over 8 weeks. The LFA were stored in an airtight capsule with a drying agent at 4 °C. Error bars represent mean values ±1σ and were calculated based on three parallel measurements on three different LFAs (n = 3).

3.3.4 Investigating storage stability of the novel LFA approach

The overall stability of the assembled LFA was investigated. While the antibodies and polystyrene Ab-fluorescence NPs are known to be stable when stored in dry stage through a fleece-based system [2], their storage within a non-fleece POCT immunoassay is not yet known. Antibodies have been successfully stored in dry stage on a plastic support within a sugar-based matrix and showed stable functionality over long time period [38]. Thus, the capture antibodies and polystyrene Ab-fluorescence NPs were dried in a sucrose matrix supporting the stability maintenance of both reagents in the dried state. Over a period of 8 weeks, no loss in activity could be observed (Figure 3). In addition, we assume that complexation of streptavidin and the incorporation of the PPCs in a multilayer also contributed to stable and reproducible signal values. This effect is linked to the additional hydrated state of the assemble, having a protective effect on the immobilized protein [21]. The signal's overall variability can be attributed to variations in multilayer formation, as the manual fabrication process may lead to differences in multilayer thickness, impacting the immobilized streptavidin concentration. We assume that an automated process for building up the multilayer would result in a more constant multilayer thickness, potentially reducing signal

variability. The elevated relative errors, approximately 20 %, could be justified by handling inaccuracies and the limited number of replicates in the handmade LFAs utilized.

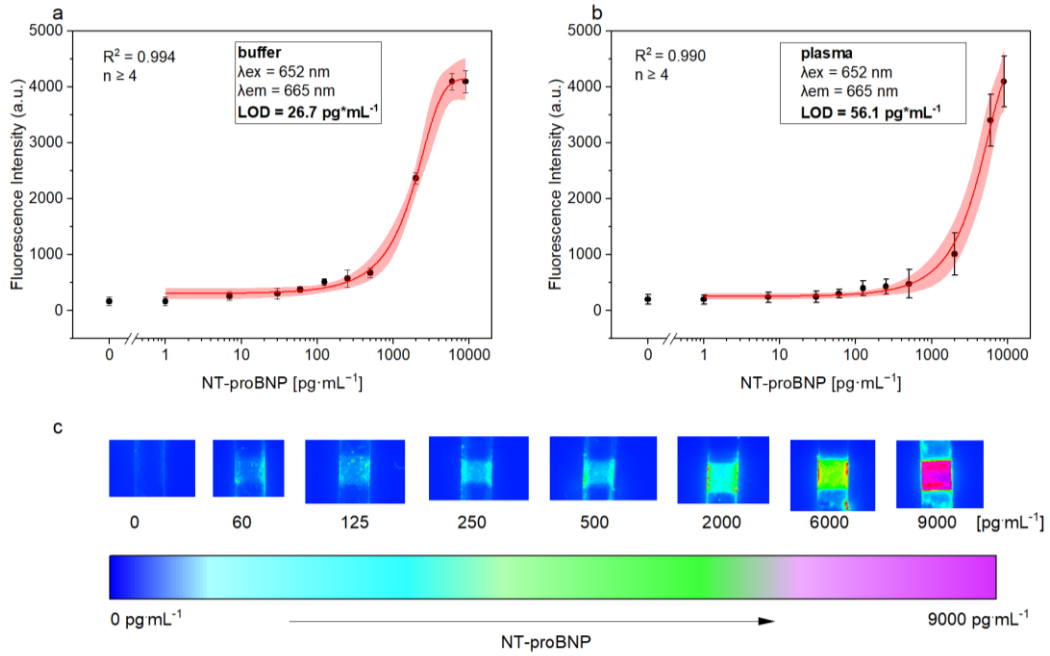

Figure 4: Plot of fluorescence intensity against logarithm of antigen concentration in spiked HBS buffer (a) and in spiked human serum samples (b) with logistic fit (red line), confidence interval 95 % (shaded red curve) and corresponding parameters. Fluorescence images of the detection zone illustrating the antigen concentration (c). Standard deviation was calculated based on 6 parallel measurements on 6 different LFAs, while outliers were removed after Q-test (confidence interval 95 %). Error bars represent mean values ±1σ (n ≥ 4).

3.3.5 Detection of NT-proBNP quantification in buffer and serum with the novel LFA system

To demonstrate the applicability of the LFA in a complex biological matrix, the bioassay was performed with both buffer and human serum samples that were spiked with different amounts of NT-proBNP (Figure 4). In the plot of the fluorescence intensities against logarithm NT-proBNP concentration, the typical sigmoidal curve for sandwich immunoassays is obtained. Based on the logistic fit for the assay with spiked buffer a LOD of 27 pg·mL^{-1} was calculated. The assay with human plasma showed a LOD of 56 pg·mL^{-1}. The slight decrease of the LOD is attributed to the higher blank value due to

the higher background signal originating from non-specific binding of the nanoparticles and autofluorescence of the plasma [39]. Additionally, we observed irreversible adsorption of the sample and antibodies on the channel sides when the sensor was not bonded appropriately, due to manual inaccuracies in the fabrication process. This led to increased variability in the signal, particularly noticeable when the analyte was present in low concentrations. This is also reflected by the mean coefficient of variation (CV) of the assay with buffer and plasma that were calculated to be 14 % and 19 %, respectively. The dynamic range of both assays are similar and extend as expected for an immunoassay over nearly two orders of magnitude. Most importantly, the new LFA compared very well to the current commercial LFA, the optical NT-proBNP cardiac POCT-system (hs cobas 232) from Roche Diagnostics, which showed a LOD of 60 $pg \cdot mL^{-1}$ and a dynamic range of 60 – 9000 $pg \cdot mL^{-1}$.[40] A NT-proBNP value of greater than 100 $pg \cdot mL^{-1}$ is abnormal in patients and is used to assess the severity of heart failure. Thus, this study shows that the membrane-free LFA can be used for the diagnosis and prognosis of heart failure and furthermore that no membrane is needed to achieve the same assay performance as the hs cobas 232 NT-proBNP. In addition, only 20 µL of plasma are needed for the new LFA, which suggests that it can in fact be used as a POCT assay with samples derived from a finger prick sampling.

Table 1. Determination of NT-proBNP.

NT-proBNP amount spiked (pg·mL^{-1})	CV	
	buffer (%)	*plasma (%)*
60	18	22
125	16	21
250	19	19
500	13	22
2000	11	21
6000	8	14
9000	9	11

Note: 20 µL of sample volume was used for each test. Samples were run in sextuplicates and the mean is reported. (n=6)

3.4 Conclusion

In summary, we introduce an innovative membrane-free and pump-driven fluorescence lateral flow assay (LFA) ready to meet the demands of one-step POCT applications. By utilizing composite polystreptavidin-polyelectrolyte multilayers as the detection zone and adopting a dry-storage approach for antibodies and fluorescence labels in our platform, the test not only simplifies assembly and reduces production costs but also achieves high sensitivity. Furthermore, our platform overcomes the typical limitations of traditional membrane-based LFAs, such as variations in membrane fabrication, limited control over immunoreactions, and the need for large sample volumes. Healthcare of the future will require reliable tests that can be conducted without the need for medical personnel, while still offering the quantitative and highly sensitive features of standard laboratory tests. The membrane-based LFA concept currently dominating the market can provide rapid answers with reasonable limits of detection but without reliable quantification and not at often-needed low analyte concentrations. The developed test homes in on the need for less sample volume and on a quantitative, sensitive and reliable measurement at the POCT. The design allows the usage of a 7.5-fold less volume of sample when compared to the conventional LFA format to achieve

the same assay performance, without sampling trough the vein and the need for intricate washing procedures. This allows straightforward testing without trained personnel and significantly improves patient comfort, especially when a finger-prick sample volume is sufficient. Active sample transport delivers the precise control necessary for immunoreaction and when combined with a fluorescence imaging system, enables highly sensitive detection, even if instrument-free visual detection is no longer possible. With the goal of increasing the simplification of the developed LFA, future improvements may include the introduction of a handheld device that combines a fluorescence detection camera, a pump system, and relevant software/apps for automated analysis that can be easily installed into POCT devices. With the ongoing trend of miniaturization and the rise of Internet of medical things (IoMT) the hardware has become cheap and allows straightforward testing and decision-making at home and in resource-limited settings [41]. Moreover, we will focus on expanding the variety of analytical targets that can be detected and quantified using the developed multilayer platform. Multiplexing can be readily achieved by establishing separate channels where precise control of the sample is maintained for each analyte. In addition, future work will seek to implement a blood-plasma separation mechanism to promote the practical applications in low-resource areas. Hence, this work may provide a new strategy to produce sensitive quantitation of HF biomarkers. We therefore, demonstrated that our membrane-free platform provides the quantitative and highly sensitive characteristics for the HF biomarker NT-proBNP.

3.5 References

1. Di Nardo F, Chiarello M, Cavalera S, Baggiani C, Anfossi L (2021) Ten Years of Lateral Flow Immunoassay Technique Applications: Trends, Challenges and Future Perspectives. Sensors 21:5185. https://doi.org/10.3390/s21155185

2. Koczula KM, Gallotta A (2016) Lateral flow assays. Essays Biochem 60:111–120. https://doi.org/10.1042/EBC20150012

3. Yuzon MaK, Kim J-H, Kim S (2019) A Novel Paper-plastic Microfluidic Hybrid Chip Integrated with a Lateral Flow Immunoassay for Dengue Nonstructural Protein 1 Antigen Detection. BioChip J 13:277–287. https://doi.org/10.1007/s13206-019-3305-5

4. Park M, Kang B-H, Jeong K-H (2018) Paper-Based Biochip Assays and Recent Developments: A Review. BioChip J 12:1–10. https://doi.org/10.1007/s13206-017-2101-3

5. Posthuma-Trumpie GA, Korf J, Van Amerongen A (2009) Lateral flow (immuno)assay: its strengths, weaknesses, opportunities and threats. A literature survey. Anal Bioanal Chem 393:569–582. https://doi.org/10.1007/s00216-008-2287-2

6. Gubala V, Harris LF, Ricco AJ, Tan MX, Williams DE (2012) Point of Care Diagnostics: Status and Future. Anal Chem 84:487–515. https://doi.org/10.1021/ac2030199

7. Mosley GL, Nguyen P, Wu BM, Kamei DT (2016) Development of quantitative radioactive methodologies on paper to determine important lateral-flow immunoassay parameters. Lab Chip 16:2871–2881. https://doi.org/10.1039/C6LC00518G

8. Natarajan S, Jayaraj J, Prazeres DMF (2021) A Cellulose Paper-Based Fluorescent Lateral Flow Immunoassay for the Quantitative Detection of Cardiac Troponin I. Biosensors 11:49. https://doi.org/10.3390/bios11020049

9. Su Y, Lin B, Zhang K, Zhan T, Li J, Zhang C (2023) A fluorescence point-of-care testing system for sample-to-answer detection of immunoglobulin E. Microchem J 192:108907. https://doi.org/10.1016/j.microc.2023.108907

10. Hemmig E, Temiz Y, Gökçe O, Lovchik RD, Delamarche E (2020) Transposing Lateral Flow Immunoassays to Capillary-Driven Microfluidics Using Self-Coalescence Modules and Capillary-Assembled Receptor Carriers. Anal Chem 92:940–946. https://doi.org/10.1021/acs.analchem.9b03792

11. Kim J, Hong K, Kim H, Seo J, Jeong J, Bae PK, Shin YB, Lee JH, Oh HJ, Chung S (2020) Microfluidic immunoassay for point-of-care testing using simple fluid vent

control. Sens Actuators B Chem 316:128094. https://doi.org/10.1016/j.snb.2020.128094

12. Iakovlev AP, Erofeev AS, Gorelkin PV (2022) Novel Pumping Methods for Microfluidic Devices: A Comprehensive Review. Biosensors 12:956. https://doi.org/10.3390/bios12110956

13. Tsao C-W (2016) Polymer Microfluidics: Simple, Low-Cost Fabrication Process Bridging Academic Lab Research to Commercialized Production. Micromachines 7:. https://doi.org/10.3390/mi7120225

14. Kim D, Herr AE (2013) Protein immobilization techniques for microfluidic assays. Biomicrofluidics 7:041501. https://doi.org/10.1063/1.4816934

15. Salva ML, Rocca M, Niemeyer CM, Delamarche E (2021) Methods for immobilizing receptors in microfluidic devices: A review. Micro Nano Eng 11:100085. https://doi.org/10.1016/j.mne.2021.100085

16. Koutsopoulos S, Patzsch K, Bosker WTE, Norde W (2007) Adsorption of trypsin on hydrophilic and hydrophobic surfaces. Langmuir ACS J Surf Colloids 23:2000–2006. https://doi.org/10.1021/la062238s

17. Bilal M, Rasheed T, Zhao Y, Iqbal HMN (2019) Agarose-chitosan hydrogel-immobilized horseradish peroxidase with sustainable bio-catalytic and dye degradation properties. Int J Biol Macromol 124:742–749. https://doi.org/10.1016/j.ijbiomac.2018.11.220

18. Gopal A, Herr AE (2019) Multiplexed in-gel microfluidic immunoassays: characterizing protein target loss during reprobing of benzophenone-modified hydrogels. Sci Rep 9:15389. https://doi.org/10.1038/s41598-019-51849-8

19. Vander Straeten A, Lefèvre D, Demoustier-Champagne S, Dupont-Gillain C (2020) Protein-based polyelectrolyte multilayers. Adv Colloid Interface Sci 280:102161. https://doi.org/10.1016/j.cis.2020.102161

20. Richardson JJ, Björnmalm M, Caruso F (2015) Multilayer assembly. Technology-driven layer-by-layer assembly of nanofilms. Science 348:aaa2491. https://doi.org/10.1126/science.aaa2491

21. Vander Straeten A, Bratek-Skicki A, Germain L, D'Haese C, Eloy P, Fustin C-A, Dupont-Gillain C (2017) Protein-polyelectrolyte complexes to improve the biological activity of proteins in layer-by-layer assemblies. Nanoscale 9:17186–17192. https://doi.org/10.1039/c7nr04345g

22. Panagopoulou V, Deftereos S, Kossyvakis C, Raisakis K, Giannopoulos G, Bouras G, Pyrgakis V, Cleman MW (2013) NTproBNP: an important biomarker in cardiac diseases. Curr Top Med Chem 13:82–94. https://doi.org/10.2174/1568026611313020002

23. Cardiovascular diseases (CVDs). https://www.who.int/news-room/fact-sheets/detail/cardiovascular-diseases-(cvds). Accessed 10 Jul 2023

24. Weber M, Mitrovic V, Hamm C (2006) B-type natriuretic peptide and N-terminal pro-B-type natriuretic peptide – Diagnostic role in stable coronary artery disease. Exp Clin Cardiol 11:99–101

25. Lutz S, Lopez-Calle E, Espindola P, Boehm C, Brueckner T, Spinke J, Marcinowski M, Keller T, Tgetgel A, Herbert N, Fischer T, Beiersdorf E (2017) A fully integrated microfluidic platform for highly sensitive analysis of immunochemical parameters. The Analyst 142:4206–4214. https://doi.org/10.1039/C7AN00547D

26. Cooper CL, Dubin PL, Kayitmazer AB, Turksen S (2005) Polyelectrolyte–protein complexes. Curr Opin Colloid Interface Sci 10:52–78. https://doi.org/10.1016/j.cocis.2005.05.007

27. Bergman L, Rosenholm J, Öst A-B, Duchanoy A, Kankaanpää P, Heino J, Lindén M (2008) On the Complexity of Electrostatic Suspension Stabilization of Functionalized Silica Nanoparticles for Biotargeting and Imaging Applications. J Nanomater 2008:e712514. https://doi.org/10.1155/2008/712514

28. Nita LE, Chiriac AP, Stoleru E, Diaconu A, Tudorachi N (2016) Tailorable polyelectrolyte protein complex based on poly(aspartic acid) and bovine serum albumin. Des Monomers Polym 19:596–606. https://doi.org/10.1080/15685551.2016.1187436

29. Cousin F, Gummel J, Ung D, Boué F (2005) Polyelectrolyte-protein complexes: structure and conformation of each specie revealed by SANS. Langmuir ACS J Surf Colloids 21:9675–9688. https://doi.org/10.1021/la0510174

30. Cousin F, Gummel J, Combet S, Boué F (2011) The model Lysozyme-PSSNa system for electrostatic complexation: Similarities and differences with complex coacervation. Adv Colloid Interface Sci 167:71–84. https://doi.org/10.1016/j.cis.2011.05.007

31. Junkar I, Vesel A, Cvelbar U, Mozetič M, Strnad S (2009) Influence of oxygen and nitrogen plasma treatment on polyethylene terephthalate (PET) polymers. Vacuum 84:83–85. https://doi.org/10.1016/j.vacuum.2009.04.011

32. Madaboosi N, Uhlig K, Jäger MS, Möhwald H, Duschl C, Volodkin DV (2012) Microfluidics as A Tool to Understand the Build-Up Mechanism of Exponential-Like Growing Films. Macromol Rapid Commun 33:1775–1779. https://doi.org/10.1002/marc.201200353

33. Delamarche E, Bernard A, Schmid H, Bietsch A, Michel B, Biebuyck H (1998) Microfluidic Networks for Chemical Patterning of Substrates: Design and Application to Bioassays. J Am Chem Soc 120:500–508. https://doi.org/10.1021/ja973071f

34. Minnikanti S, Gangopadhyay A, Reyes D (2014) Polyelectrolyte Multilayers in Microfluidic Systems for Biological Applications. Polymers 6:2100–2115. https://doi.org/10.3390/polym6082100

35. Salloum DS, Schlenoff JB (2004) Protein Adsorption Modalities on Polyelectrolyte Multilayers. Biomacromolecules 5:1089–1096. https://doi.org/10.1021/bm034522t

36. Xiao Y, Isaacs SN (2012) Enzyme-linked immunosorbent assay (ELISA) and blocking with bovine serum albumin (BSA)–not all BSAs are alike. J Immunol Methods 384:148–151. https://doi.org/10.1016/j.jim.2012.06.009

37. Lai X, Gao G, Watanabe J, Liu H, Shen H (2017) Hydrophilic Polyelectrolyte Multilayers Improve the ELISA System: Antibody Enrichment and Blocking Free. Polymers 9:51. https://doi.org/10.3390/polym9020051

38. Beck F, Horn C, Baeumner AJ (2022) Dry-reagent microfluidic biosensor for simple detection of NT-proBNP via Ag nanoparticles. Anal Chim Acta 1191:339375. https://doi.org/10.1016/j.aca.2021.339375

39. Wang Y, Zhu J, Chen X (2020) Autofluorescence spectroscopy of blood plasma with multivariate analysis methods for the diagnosis of pulmonary tuberculosis. Optik 224:165446. https://doi.org/10.1016/j.ijleo.2020.165446

40. cobas h 232 POC System. In: Diagnostics. https://diagnostics.roche.com/ch/de/article-listing/cobas-h-232-system.html. Accessed 29 Dec 2023

41. Jain S, Nehra M, Kumar R, Dilbaghi N, Hu TonyY, Kumar S, Kaushik A, Li C (2021) Internet of medical things (IoMT)-integrated biosensors for point-of-care testing of infectious diseases. Biosens Bioelectron 179:113074. https://doi.org/10.1016/j.bios.2021.113074

3.6 Supporting Information

3.6.1 Lateral flow immunoassay materials and fabrication

LFAs were built up from four components: 1) a PET foil as substrate, 2) a spacer with laser cut capillaries, 3) a cover foil with sample port and outlet port and 4) pressure sensitive double sided adhesive tape. The spacer (MELINEX®329 250µm) was coated with double sided adhesive tape on both sides and then capillaries (dimension: 90 mm x 1.5 mm x 0.28 mm) were cut with the laser MicroLine 6000 P (www.lpkf.com) at a frequency of 30 kHz and 3 W. The second laser-cutting step was used to generate the sample inlet and outlet in the cover foil. The spacer and cover foil were then stuck together as depicted in the ESM (Figure S1) and finally joined on top of the base, orthogonal to the streptavidin multilayer, to get the ready to use microfluidic sensor. The fluidic immobilization channel (dimension: 90 mm x 1.5 mm x 0.28 mm) for the deposition of the streptavidin multilayer was similarly prepared with the exception that it only consists of the spacer and the cover foil

3.6.2 Principle of the LFA

Upon adding the sample, the dried antibodies dissolve, initiating the immunoreaction. The pump regulates the sample flow, directing it through the mixing area, thereby enhancing the diffusion-based formation of the immunocomplex. The immunocomplex, owing to robust biotin-streptavidin binding, gets captured in the detection zone, allowing analysis of the fluorescence signal using a fluorescence microscope.

3.6.3 Assay equipment

The fluid control consisted of a metal housing that houses 1) a LFA mold, 2) an Arduino Due board, 3) and a miniaturized vacuum pump. The fluid control system was linked to a computer via USB and managed using an Arduino code. To initiate the immunoassay fhe fluid control was mounted on top of the outlet port of the LFA. All fluorescence images were acquired using a fluorescence microscope, LINOS lens (www.excelitas.com), HTC camera with a Sony CCD sensor ICX285AL (www.sony.com), XENON XBO R 100W/45 OFR lamp (www.osram.com), 633nm excitation filter and 685nm detection filter (www.semrock.com). The fluorescence images were taken with

an exposure time of 25 ms. Image processing and data analyses were carried out with ImageJ and Origin 2021.

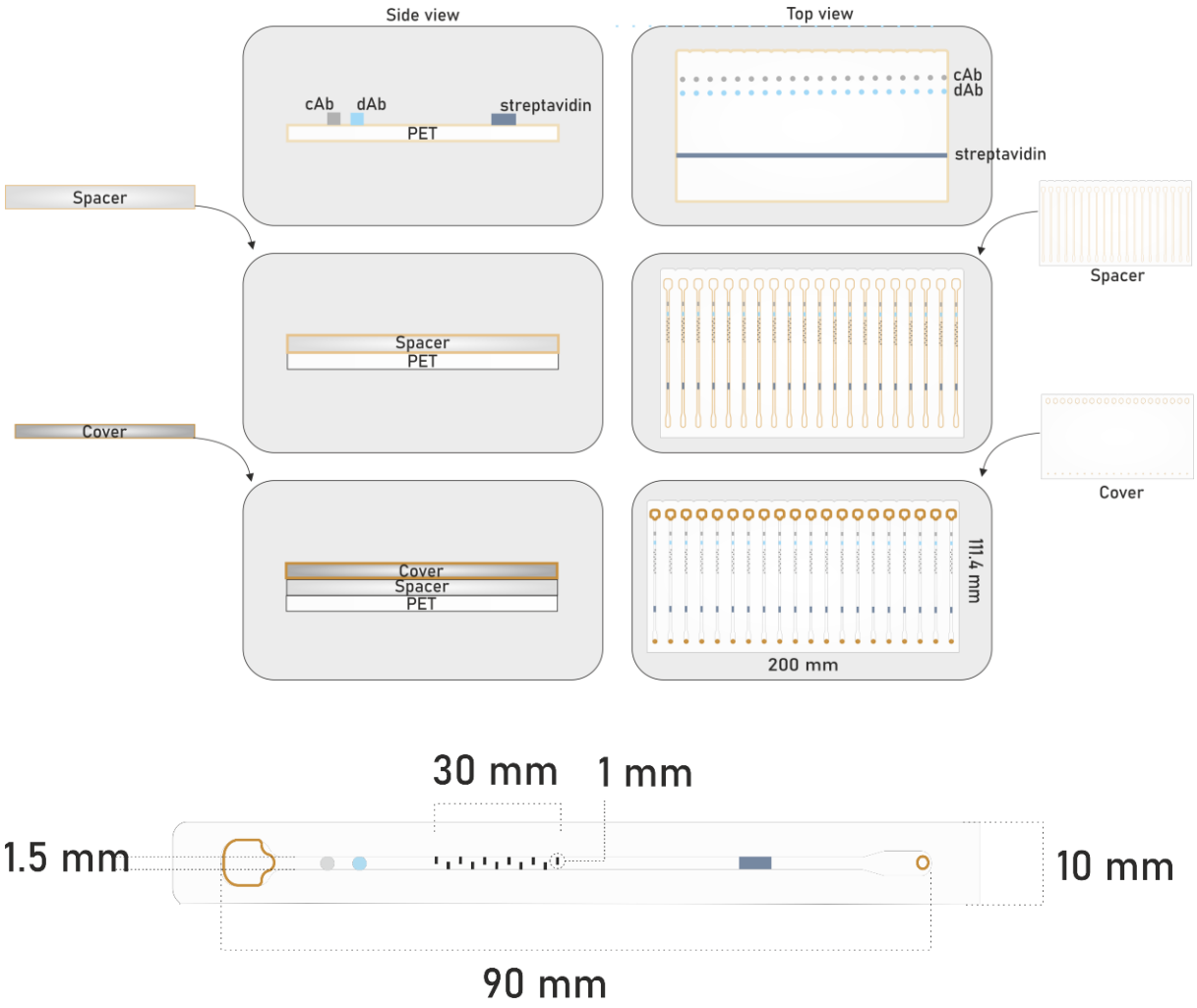

Figure S1: Buildup of the LFA in the side view (left) and in the top view (right). Single LFA with corresponding dimensions (bottom). cAb – capture antibody and dAb – detection antibody.

a) b)

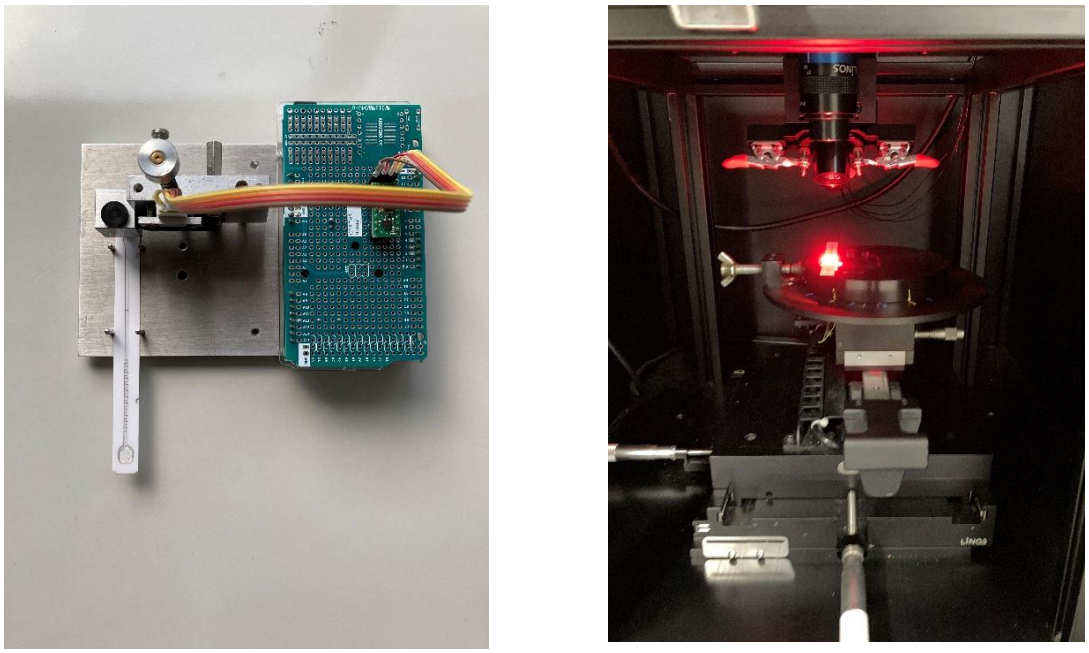

Figure S2: Photographs of the assay equipment. Fluid control system (a) and fluorescence microscopy (b).

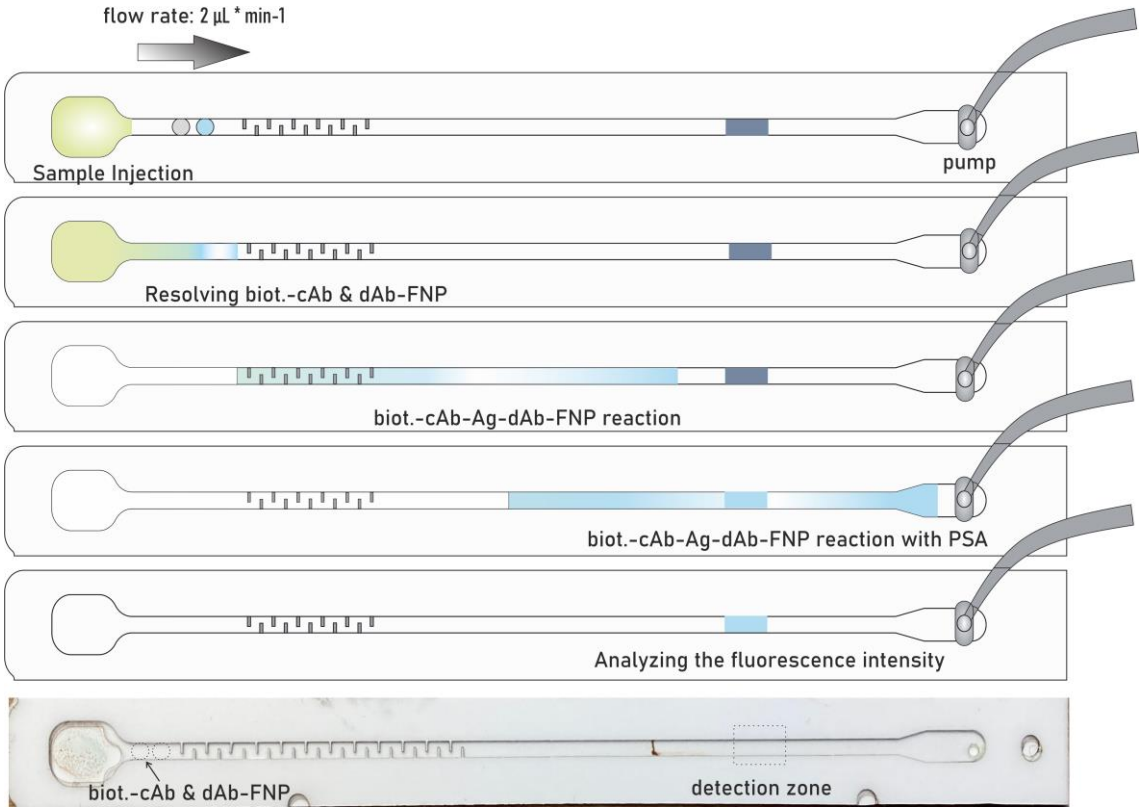

Figure S3: Schematic (not to scale) illustration of the active sample transport by the pump and process of the immunoreaction.

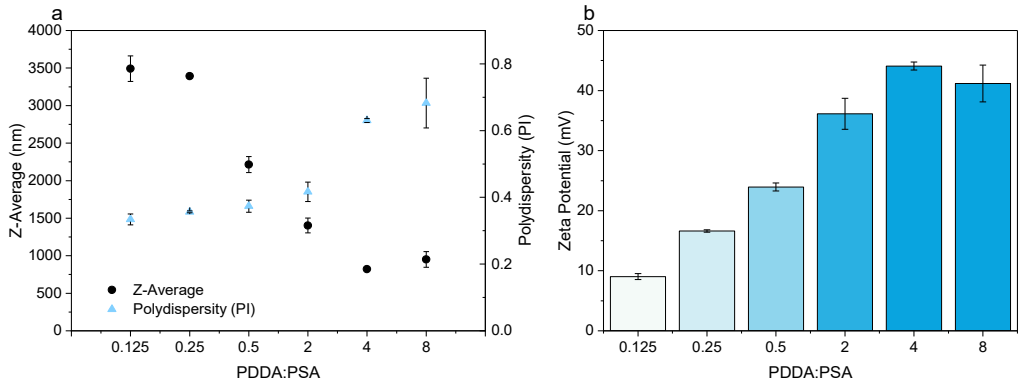

Figure S4: Characterization of the PDDA:PSA particles at pH 7.4 and 150 mM NaCl and the effect of the PDDA:PSA ratio on the size (a) and on the zeta potential of the PDDA:PSA complex (b). Error bars represent mean values ±1σ. (n = 3)

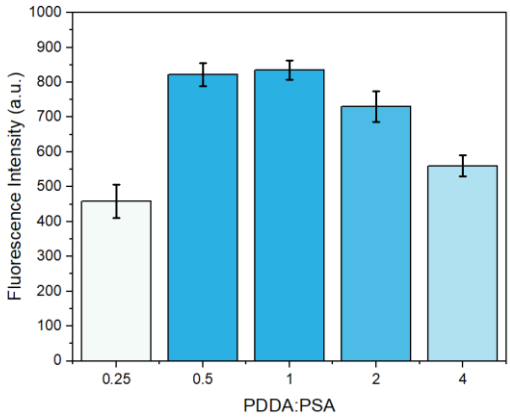

Figure S5: Optimization of PDDA:PSA ratio in the complexation process. Plot of fluorescence intensity of a constant Rhodamine 6G concentration (0.05 mg·mL^{-1}) against the PDDA:PSA ratio. Error bars represent mean values ±1σ and were calculated based on three parallel measurements (n = 3)

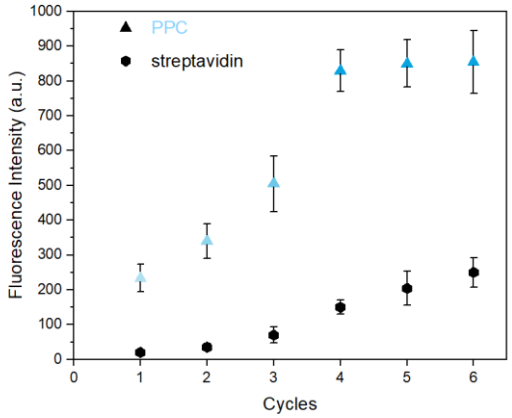

Figure S6: Plot of the fluorescence intensity of a constant Rhodamine 6G concentration (0.05 mg·mL^{-1}) against the number of layer-by-layer cycles of $(PPC/PAA)_x$ and (streptavidin (15 mg·mL^{-1})/$PAA)_x$. Error bars represent mean values ±1σ and were calculated based on three parallel measurements on three different LFAs (n = 3)

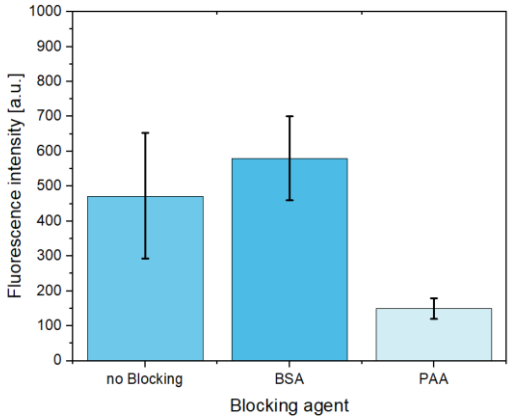

Figure S7: Plot of fluorescence intensity of the bioassay using a constant antigen concentration of 1 ng·mL^{-1} in buffer against different blocking agents. Error bars represent mean values ±1σ (n = 3)

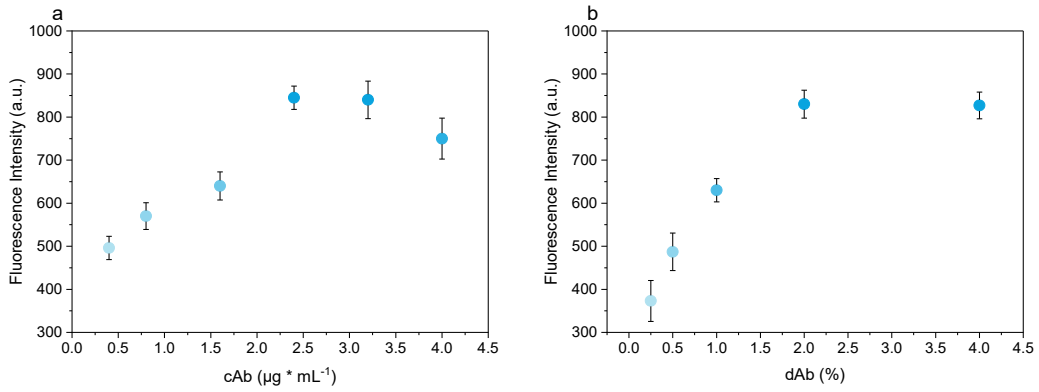

Figure S8: Optimization of cAb and dAb. Plot of the fluorescence intensity of the bioassay using a constant antigen concentration of 1 ng·mL⁻¹ in buffer against the cAb concentration used in the bioassay (a). Plot of the fluorescence intensity of the bioassay using a constant antigen concentration of 1 ng·mL⁻¹ in buffer against the dAb concentration used in the bioassay (b). Error bars represent mean values ±1σ (n = 3).

4 NT-proBNP Detection with a One-Step Magnetic Lateral Flow Channel Assay

Abstract

Point-of-care sensors targeting blood marker analysis must be designed to function with very small volumes since acquiring a blood sample through a simple, mostly pain-free finger prick dramatically limits the sample size and comforts the patient. Therefore, we explored the potential of converting a conventional lateral flow assay (LFA) for a significant biomarker into a self-contained and compact polymer channel-based LFA to minimize the sample volume, while maintaining the analytical merits. Our primary objective was to eliminate the use of sample-absorbing fleece and membrane materials commonly present in LFAs. Simultaneously, we concentrated on developing a ready-to-deploy one-step LFA format, characterized by dried reagents, facilitating automation and precise sample transport through a pump control system. We targeted the detection of the heart failure biomarker NT-proBNP in only 15 µL human whole blood and therefore implemented strategies that ensure highly sensitive detection. The biosensor combines streptavidin-functionalized magnetic beads (MNPs) as a 3D detection zone and fluorescence nanoparticles as signal labels in a sandwich-based immunoassay. Compared to the currently commercialized LFA, our biosensor demonstrates comparable analytical performance with only a tenth of the sample volume. With a detection limit of 43.1 pg·mL^{-1} and a mean error of 18 % ($n \geq 3$), the biosensor offers high sensitivity and accuracy. The integration of all-dried long-term stable reagents further enhances the convenience and stability of the biosensor. This lateral flow channel platform represents a promising advancement in point-of-care diagnostics for heart failure biomarkers, offering a user-friendly and sensitive platform for rapid and reliable testing with low finger-prick blood sample volumes.

Keywords: magnetic bead, lateral flow assay, immunoassay, cardiac, one-step, point-of-care

Graphical Abstract

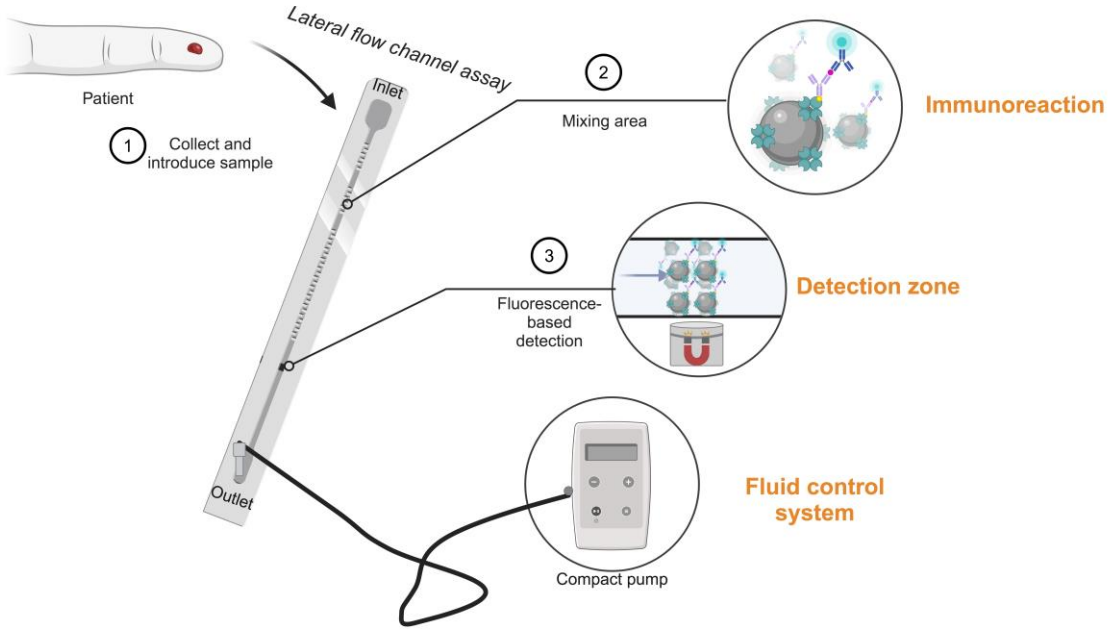

This chapter has been published.

Strohmaier-Nguyen, D., Horn, C. & Baeumner, A.J. NT-proBNP detection with a one-step magnetic lateral flow channel assay. *Anal Bioanal Chem* 416, 2411–2422 (2024). https://doi.org/10.1007/s00216-024-05223-x

Author contributions: AJB, CH and DSN developed the concept for this work. DSN planned the experiments, did the experimental work and wrote the first draft of the manuscript. AJB revised the manuscript and is corresponding author

4.1 Introduction

According to the World Health Organization (WHO) cardiovascular diseases (CVDs) remain the most frequent cause of death globally [1]. Among all cardiovascular disorders of the heart and blood vessels, heart failure (HF) leads to the highest rate of mortality, morbidity and health care costs [2]. HF represents the condition when the heart insufficiently provide blood and oxygen to the body organs and thus cannot meet the demands of the organs [3]. It describes a progressive condition and is grouped into four stages based on the magnitude and progression of the disease. HF starts with cardiovascular risk factors for left ventricular systolic followed by structural and functional changes of the cardiac system such as left ventricular hypertrophy and eventually leads to observable HF, dysfunction and death [4]. Therefore, detection and intervention in early phases can prevent or decelerate disease progression and is of primary importance for the patient.

N-terminal prohormone of BNP (NT-proBNP) is one of the major biomarkers in HF due to its significance in diagnosis and treatment [5–7]. Abnormal levels of NT-proBNP are released in response to myocyte enlargement following left ventricle hypertrophy [8]. Early detection and monitoring of NT-proBNP level can diagnose and prevent the risk of LVH, LVSD, and HF and thus, can protect the cardiovascular function and clarify the treatment strategy for the physician [9, 10]. The age-independent NT-proBNP value of 300 pg·mL^{-1} is recommended as cut-off value for HF diagnosis, which had a sensitivity of 99 % and a specificity of 68 % [11]. Fast and reliable diagnosis of HF has been accomplished by commercially viable lateral flow assays (LFAs) in point-of-care testing (POCT). For example, the cobas h 232 NT-proBNP from Roche Diagnostics GmbH provides a sensitive platform that detects NT-proBNP in 150 µL whole blood with a detection limit of 60 pg·mL^{-1} and a detection range of 60 – 9000 pg·mL^{-1} [12]. In general, the LFAs consist of fleece-fiber and membrane components, often employed as the drying substrate for probe-specific antibodies and the sample transport [13]. Both come with an innate high analyte and sample adsorption capacity, resulting in a notable requirement for sample volume, a relatively substantial dead volume, and an impairment of the sensor performance [14]. Therefore, the requirement of relatively large blood sample volume, attributed to sample-adsorbing materials like fleece and

membrane, compromises the test's performance and patient convenience. In addition, it necessitates the presence of skilled personnel to obtain blood from veins in a clinical setting, increasing the risk of complications and infection and reducing patient comfort and safety. Hence, the field of POCT is characterized by intense competition, driving a continuous demand for the rapid, cost-effective development of precise tests with low sample volumes. Developing POCT into minimally invasive finger-prick blood tests has presented challenges due to technological limitations. The primary hurdle in working with finger-prick volumes is that the target analyte for detection exists in lower concentrations compared to venous blood samples, which poses a difficulty in accurately detecting such minimal analyte levels. Predominantly, the challenge of maintaining assay performance has impeded the widespread commercial operation. However, this aspiration must remain a priority driven by the potential to offer techniques enabling ultrasensitive detection with just finger-prick volumes that reduce the invasiveness and simplify the sample processing. As a result, this comforts the patient and enables diagnostics through lay personnel, thereby expanding medical care into rural areas and homecare.

Microfluidic platforms, in POCT, have gained a lot of attention due to their benefits, including the ability to work with small volumes of samples and reagents, seamless integration of multiple components, and fast reaction kinetics [15–17]. In addition, it is commonly acknowledged that microfluidic channels offer superior surface area to volume ratios [18, 19]. However, it should be noted that the detection area is often restricted to the miniaturized geometric structure of the channel, where the antibodies or other recognition molecules are fixed. Thus, due to the slow diffusion in the laminar flow only a limited part of the sample can be captured, reducing the sensor’s performance [20]. To enhance the surface area and reduce the diffusion distance for binding, particles labeled with recognition elements can be introduced into the channels. This significantly reduces the diffusion distance and increases the surface area available for binding relative to the sample volume in the detection zone, increasing the assay signal [20, 21]. Especially, the inclusion of magnetic nanoparticles in LFAs and microfluidic systems plays a crucial role in performing biochemical assays for healthcare and diagnosis [20, 22–25]. MNPs contribute to the enhancement of various

biosensing applications due to their distinctive superparamagnetic properties since they can function as both mobile substrates and detection markers simultaneously [26, 27]. The simple bio-functionalization with a variety of molecules makes them an ideal option for capturing and signaling label in immunoassays [28–30]. Here, we developed a novel LFA concept using an external suction pump for sample transportation, and streptavidin functionalized magnetic particles (MNPs) for the POC detection and quantification of NT-proBNP in whole blood. Since the assay requires only 15 µL whole blood and the pump can be included in a simple, portable support device, this new concept offers an alternative to membrane-based LFAs as it requires less sample volume and can thus easily be used for finger-prick analyses.

4.1.1 Theory and operating principle

When particles move within a Newtonian flow of a microchannel, they are subjected to forces such as inertia lift and hydrodynamic drag [31]. The inertial lift force can be calculated by [32]:

$$F_l = \frac{\rho_f U_m^2 a^4}{D_h^2} f_L(Re_c, x_c) \qquad (1)$$

while ρ_f, μ_f, and U_m represent the density, dynamic viscosity, and mean flow velocity of the fluid transporting the particles, respectively. The diameter of the spherical microparticle is denoted by a, and D_h refers to the hydraulic diameter of the flow channel, which can be expressed as $D_h = \frac{2wh}{(w+h)}$ for a rectangular channel, where h is the height and w is the width of the channel. f_L represents the lift coefficient and is a function of the Reynolds number Re_c and the normalized cross-sectional position of the particle within the channel x_c. The hydrodynamic drag force can be expressed by the following [33]:

$$F_d = 3\pi\mu_f a(v_f - v_p) f_D \sim 3\pi\mu_f a(v_f - v_p) \qquad (2)$$

In this context, the velocities of the fluid and microparticles are represented by v_f and v_p, respectively. The coefficient for hydrodynamic drag force, denoted as f_D, is dependent on the hydraulic diameter of the channel and the diameter of the particles, as well as the distance between the particle and the closest channel wall. For low concentrations of ferrofluid, such as those studied in this study, f_D can be considered equal to 1, since the magneto-viscous effect can be disregarded [34].

The MNPs were captured from the sample by applying an external magnetic field, using a circular permanent magnet. In this case, the particles are exposed to the magnetophoresis force [35, 36]:

$$F_m = \frac{\Delta\lambda * V_p}{\mu_0} * (\nabla B) * B \qquad (3)$$

In the given equation, B represents the magnetic flux density, ∇B denotes the gradient of the externally applied magnetic field, μ_0 refers to free space permeability, and $\Delta\lambda$ represents the difference in susceptibility between the particle and the fluid. In general, the deflection process of the MNPs in the microchannel is the total of three forces: the magnetically induced force on the particle, F_m, the hydrodynamic drag force F_d, and the lift force F_l [37]:

$$F_{defl} = F_m + F_d + F_l \qquad (4)$$

In this study, streptavidin magnetic nanoparticles were utilized as mobile capturing particles for the detection of NT-proBNP in a sandwich-based fluorescence lateral flow channel assay (Figure 1). The MNPs were able to capture the analyte in a sandwich complex in undiluted blood samples through streptavidin-biotin interaction. The immunoassay utilizes a magnetic separation where the MNPs are pulled from the sample stream to the detection zone by a stationary external magnet, whereas the unbound sample solution flows further into the waste outlet. Subsequently, the

sandwich complex captured in the detection zone was quantitatively analyzed using fluorescence microscopy.

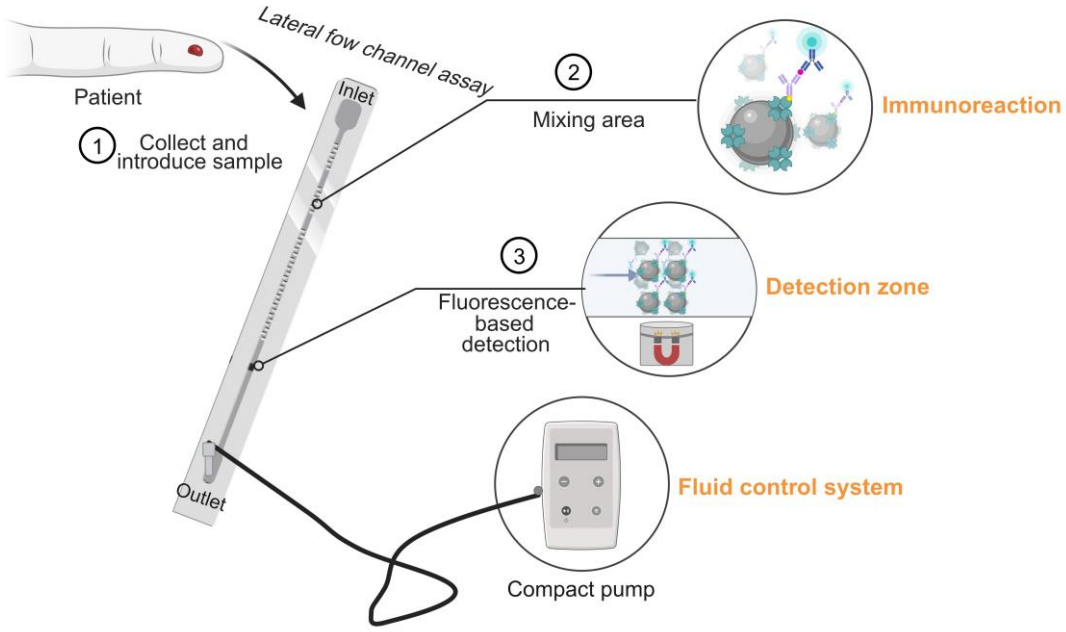

Figure 1: Schematic (not-to-scale) illustration of the sandwich-based fluorescence assay in a lateral flow channel with MNPs as capturing particles, an external magnet for fixing the MNPs in the detection zone, fluorescence nanoparticles as label and a fluid control system for sample transportation. Upon sample application (15 µL) at the inlet (1), the dried reagents undergo rehydration and subsequent transport through the mixing area, initiating the immunoreaction process (2). Positioned within the detection zone, an external magnet captures the MNP-immunosandwich complex (3), enabling the quantification of analyte-dependent fluorescence. Adapted from "Microfluidic Device", by BioRender.com (2023). Retrieved from https://app.biorender.com/biorender-templates

4.2 Materials and Methods

For the NT-proBNP immunoassay all reagents unless stated otherwise were provided by Roche Diagnostics GmbH (Mannheim, Germany) and Sigma-Aldrich. Mouse anti-human NT-proBNP antibodies were used as biotinylated capture antibody (capture Ab) and the detection antibody for the formation of the sandwich complex were identical to the antibodies in the 5th generation hs-BNP assay in the Elecsys®/cobas e^{TM} platform. NT-proBNP antibody-modified fluorescence nanoparticles (Ab-fluorescent NPs) were

used for fluorescence signal generation. For this reason, latex particles (200 nm, Thermo Fisher Scientific) were dyed with squaraine (λ_{ex} = 652 nm, λ_{em} = 665 nm) and coupled with the detection antibody via EDC and sulfo-NHS chemistry. For capturing the biotinylated sandwich complex, streptavidin-conjugated magnetic particles (MNPs) (diameter (d) = 0.3 µm, 3 µm; 10 % (w/v)) in combination of a round external magnet (r = 6 mm) were used.

HEPES-buffered saline (HBS) consisted of 50 mM HEPES, 150 mM NaCl, 3 mM EDTA and 0.05 % (w/v) Tween 20 and was adjusted to pH 7.4. The dispensing buffer was prepared with 50 mM HEPES, 1 % (w/v) BSA, 8 % (w/v) sucrose, 0.15 % (w/v) synperonic PE/P84 and 0.024 % (w/v) sodium azide and was adjusted to pH 7.4. The dextran dispensing buffer was prepared with 50 mM HEPES, 1 % (w/v) BSA, 8 % (w/v) dextran, 0.15 % (w/v) synperonic PE/P84 and 0.024 % (w/v) sodium azide and was adjusted to pH 7.4. HEPES blocking buffer was prepared with 50 mM HEPES, 2.5 % (w/v) BSA, 0.15 % (w/v) synperonic PE/P84 and was adjusted to pH 7.4.

4.2.1 Fabrication of lateral flow channel immunoassay and drying of reactive reagents

The LFA consists of a three-layer built-up: 1) The support foil (Melinex® 329 foil, 175 µm (Dupont Teijin Films, www.dupontteijinfilms.com)), 2) the spacer foil (Melinex®329 foil, 250 µm, with double-sided adhesive tape (Henkel Adhesives, www.henkel-adhesives.com) on both sides) and 3) the cover foil (Hostaphan RN 100, 125 µm (Mitsubishi Polyester Film, www.m-petfilm.de)) (see Supporting Information (SI) Figure S1). The capillary (dimension: 90 mm x 1.5 mm x 0.28 mm) were cut in the spacer foil and the inlet and outlet (r = 0.5 mm) were cut in the cover foil with the laser MicroLine 6000 P (www.lpkf.com) at a frequency of 30 kHz and 3W.

To prepare the ready-to-go, one-step immunoassay, the reactive reagents capture Ab and detection Ab-fluorescence NP were mixed with the dispensing buffer to give a 2.5 µg·mL^{-1} and 2 % (w/v) solution, respectively and a sucrose concentration of 6 % (w/v). For the MNPs the dispensing buffer was adjusted through replacing sucrose by additives such as trehalose, dextran, Tween 20, Tween 80, and polyethylene glycol. The drying and the additives' content were optimized with respect to prevention of aggregation and high assay signal. The MNPs were mixed with the adjusted dispensing

buffer to give a 2 % (w/v) MNP solution. Capture Abs, Ab-fluorescent NPs and MNPs were applied separately (2 µL each) onto the support of the immunoassay and dried in a drying cabinet at 50 °C for 10 min (FED 400 E2, www.binder-world.com). The support, spacer and cover foil were then bonded together as depicted in the SI (Figure S1).

4.2.2 Analysis of the capturing efficiency of the applied magnetic field

To investigate the capture efficiency of the small and large MNPs by the magnet, 200 µl of MNPs 2 % (w/v) in HEPES buffer were transported in different flow rates to the magnet in the detection zone of the lateral flow channel. The magnet is placed at a distance of 175 µm from the bottom wall of the channel and at a distance of 6.5 cm from the application zone to mitigate the impact of initial forces that may arise upon applying the sample to the sensor. After capturing the MNPs, the downstream sample was collected, and its transmittance was analyzed in the photometer.

4.2.3 Analysis of the biotin-binding capacity of the MNPs

A biotin-5-fluorescein working solution (1 µmol·L^{-1}) was prepared in HEPES buffer. 500 µl of the biotin-5-fluorescein working solution was mixed with 50 µl of MNPs (0.3 µm, 2 % (w/v)) and 50 µl of MNPs (3 µm, 2 % (w/v)) and incubated in the dark at room temperature for 15 min. Afterwards the MNPs were pelleted by centrifugation (5000 x g for 10 min) and the fluorescence of the supernatant was measured (λ_{ex} = 490 nm, λ_{em} = 524 nm). The biotin-binding capacity (pmol biotin/mg MNP) was then calculated from the difference of the fluorescence intensity in the presence and absence of the MNPs.

4.2.4 Sample preparation

Human blood samples were drawn by venipuncture from volunteers and provided by Roche Diagnostics GmbH in compliance with safety and ethical regulations. The hematocrit was obtained by micro-hematocrit capillary tubes. The blood samples were collected in EDTA-K3 vacutainer tubes and were used within a day.

4.2.5 NT-proBNP assay

A sandwich immunoassay with spiked samples was conducted to investigate the assay performance of the bioassay. For analysis, NT-proBNP biomarker samples were prepared in HBS buffer, human plasma, and human whole blood through dilution of a stock solution to produce concentrations of 7.5, 15, 30, 60, 125, 250, 500, 1000, 2000, 4000, 6000 and 9000 pg·mL^{-1}. A volume of 15 µL of the spiked sample was applied on the sample application area. The sample was transported with a flow rate of 2 µL/min by the external vent control. The immunoassay was performed at room temperature and fluorescence signals could be obtained after 10 min. For the calculation of the limit of detection (LOD) the logistic fit parameter for the lower curve asymptote A and the standard deviation of the blank SD (blank) was used:

$$LOD = A + 3.3 * SD(blank) \qquad (5)$$

The concentration of NT-proBNP in the sample is determined by correlating the fluorescence intensity to a calibration curve constructed using known concentration standards.

The functionality of the dried reagents was assessed by replicating the bioassay over a 8-week period. To conduct these measurements, the sucrose-based dispensing buffer was utilized to dry the capture Ab, Ab-fluorescent NPs and the dextran-based dispensing buffer was utilized to dry the MNPs for 10 min at 50 °C. The one-step LFA was stored at 4 °C in an airtight capsule.

4.2.6 Supporting instrumentation

For any of these applications, the microfluidic assay will require supporting instrumentation to control reagent and sample transport, along with fluorescence detection. The embodiment includes a customized fluid control equipment (suction pump system) that is controlled by a program code, provided by Roche Diagnostics GmbH (Mannheim, Germany). The fluid vent control was mounted on top of the outlet port. All fluorescence images were acquired using a fluorescence microscope, LINOS

lens (www.excelitas.com), HTC camera with a Sony CCD sensor ICX285AL (www.sony.com), XENON XBO R 100W/45 OFR lamp (www.osram.com), 633 nm excitation filter and 685 nm detection filter (www.semrock.com) and an image processing software provided by Roche Diagnostics (Mannheim, Germany). The fluorescence images were taken with an exposure time of 25 ms. Data was analyzed with Origin 2021.

4.3 Results and Discussion

Finger-prick blood tests hold significant promise as POCTs due to their convenience in sample collection and the minimal sample volume needed. This not only enhances patient comfort but also eliminates the need for trained personnel for venous blood withdrawal. The fleece-fibers in conjugate pads, commonly used as a drying matrix for probe-specific antibodies in traditional LFAs has an inherent high analyte and sample adsorptive capacity, which leads to a significant demand for sample volume, a relatively large dead volume and a reduction of the sensor performance. The same principle applies to membrane materials, which enable the sample transport and the immobilization of capture ligands for proteins. Considering the commercial application of a finger-prick blood test without sample-adsorbing components we studied the analyte capture efficiency and flow behavior of MNPs in a straight channel for a fluorescence-based immunoassay. The conjugate pad was replaced by dry-spotted Abs, whereas streptavidin magnetic nanoparticles and the pump system replaced the membrane's function.

4.3.1 Biotin-binding capacity

We examined the impact of different sizes and surface areas (sa) of MNPs on their ability to improve diffusion-limited interactions in polymer channel lateral flow assays. First, we compared the biotin-binding capacity for biotin-5-fluorescein between small MNPs (d = 0.3 µm, sa = 4.57 x 10^{-6} $m^2 \cdot mg^{-1}$) and large MNPs (d = 3 µm, sa = 3.81 x 10^{-8} $m^2 \cdot mg^{-1}$) (SI, Figure S2, dark blue). Interestingly, both MNPs provided similar biotin-binding capacity of 2600 µmol·g MNP^{-1} and 2400 µmol·g MNP^{-1}, respectively. Despite smaller MNPs having a larger surface area, they may exhibit a lower streptavidin coverage density compared to their larger counterparts, suggesting that, in this case, the

size of the MNPs does not affect the binding capacity. In addition, to account for the factor of steric hindrance of antibodies the fluorescence signal of the immunoassay in the LFA was investigated (Figure S2, light blue). Similar fluorescence signals were obtained for both MNPs for a given analyte concentration, using the same MNP concentration. These findings suggest that interestingly the size of the particles and surface area do not significantly affect factors such as biotin-binding capacity and steric hindrance during the immunoreaction.

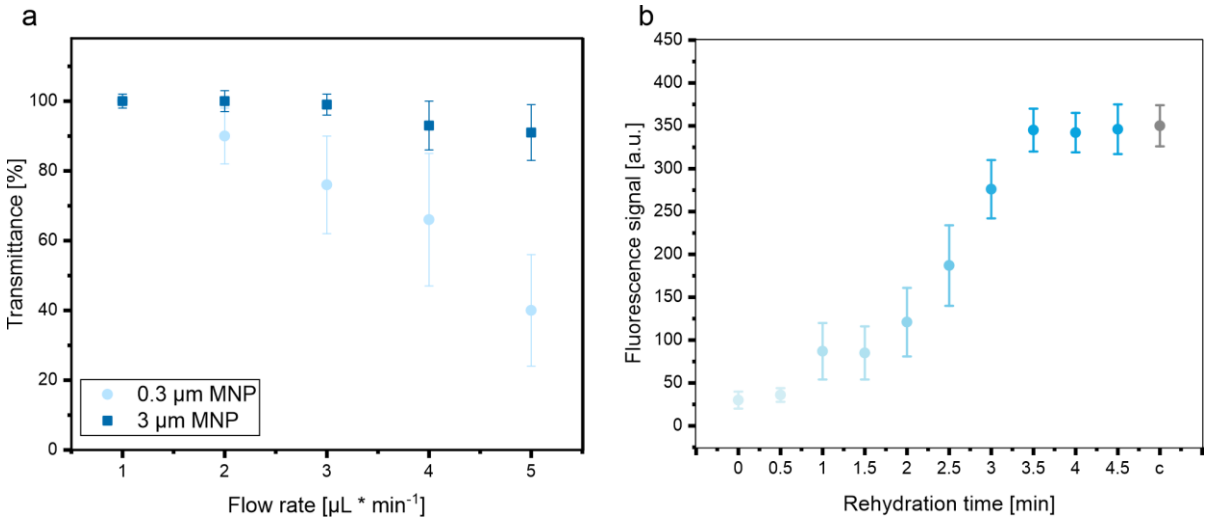

Figure 2: Optimization of the capture efficiency by the external magnetic field in the lateral flow channel in dependency of the particle size and flow rate. Plot of the transmittance of the sample against the flow rate and particle size (a). 200 µL of MNP (2 % (w/v) in HEPES buffer was transported with different flow rates through the channel and the transmittance of the sample was then analyzed in the photometer. Plot of the assay signal against the rehydration time of the dried reagents (b). Control - c - represents the assay signal with Ab-fluorescent NPs, capture Ab and MNPs in solution. Standard deviations were calculated based on three parallel measurements on three different lateral flow channels (n=3)

4.3.2 Capture efficiency by external magnet

The primary goals of the magnetophoretic capture process are to decrease the count of untrapped particles and to ensure that the flow rate is adequate for achieving optimal capture efficiency and collection quality during magnetic separation. The capture efficiency of the MNPs was determined by measuring the transmittance of the supernatant after the capture process in the lateral flow channel, taking into account the particle size and flow rate (Figure 2a). A 100 % transmittance of the supernatant is defined as the state where all MNPs have been captured by the magnet, resulting in a

maximum capture efficiency and a MNP-free supernatant. Conversely, if MNPs are not adequately captured by the magnet, the supernatant will contain MNPs, leading to a decrease in transmittance. As expected, for both MNPs the capture efficiency decreased with an increasing flow rate. Moreover, at the lowest flow rate both MNP samples demonstrated full capturing. Interestingly, at higher flow rates, differences between nanoparticles and microparticles were observed. The transmittance of the small MNPs strongly decreased with an increasing flow rate, while the transmittance of the large MNPs decreased only slightly. The optimal flow rate for the 0.3 µm particles (1 $\mu l \cdot ml^{-1}$) was generally lower than that for the 3 µm magnetic particles (3 $\mu l \cdot ml^{-1}$). The larger particles with greater susceptibility experienced a greater magnetic attraction and therefore endured higher flow velocities. This correlates to earlier findings indicating a dependency of particle size or magnetic core size of coated particles on flow behavior under flow conditions [35, 37]. As a result, the selection of larger MNPs for subsequent experiments was driven by the potential to apply a wider range of flow rates in the assay. Furthermore, we enhanced the slightly lower specific surface area of these larger MNPs and their increased steric hindrance by augmenting the particle count.

4.3.3 Development of a dry-reagent lateral flow channel immunoassay

The biotinylated polyclonal capture antibodies and monoclonal probe antibodies employed in this study were identical to the antibodies of Roche's 5th generation hs-BNP assay in the Elecsys®/cobas e™ platform. Hence, the antibodies' selectivity and specificity were presumed to be adequate without conducting additional tests. The initial experiments aimed to assess the viability of drying probe antibodies, probe antibodies labeled fluorescent NPs and MNPs. Since Lutz et al. demonstrated that the functionality of the antibodies could be effectively preserved after the drying and rehydration process [38], here only the effect of drying on MNPs was investigated. Nanoparticles are known to easily adsorb or aggregate irreversibly due to the reduced spacing and the compromised electrostatic repulsion between the nanoparticles during the drying process. This impairs the biological functionality of the particles [39–41]. Thus, to prevent aggregation and maintain long-term functionality, various additives such as polyethylene glycol (PEG), surfactants such as Tween 20 and Tween 80 and various sugars were included in the dispensing matrix (Figure S3). After drying 2 µL of

MNPs (2 % (w/v)) in the dispensing buffer on the PET support and rehydration with 15 µL of NT-proBNP-spiked HEPES ($c_{[analyte]}$ = 1 ng·mL^{-1}), we observed the formation of aggregates and significant irreversible adsorption of MNPs onto the PET support with all additives except of dextran. Drying the MNPs in only HEPES buffer (blank) diminished the signal to only 5 %. In all other drying buffers, the fluorescence signal dropped to only 55 % of the original signal. The drying of MNPs in the dextran-based matrix resulted in the most favorable fluorescence signals, indicated by a signal drop to only 92 % in comparison to the control. This observation suggests that dextran successfully prevented the irreversible adsorption of MNPs on the support and minimized aggregation, indicating its efficacy in maintaining the integrity of the MNPs during the drying process. Subsequently, the rehydration time of the dried reagents was assessed by exposing them to different durations of rehydration in the channel. Here, we determined the optimal condition with respect to the reagent's effective functionality and fluorescence signal in the immunoassay (Figure 2b). The most favorable signal was obtained by rehydrating the dried reagents with 15 µL NT-proBNP-spiked HEPES-buffer ($c_{[analyte]}$ = 1 ng·mL^{-1}) for 3 min. In fact, the fluorescence signal was minimally affected by drying when compared to the control, which represents Ab-fluorescent NPs, capture Abs, and MNPs in solution. This suggests that the rehydrated probe antibodies retain their biological function and that the Ab-fluorescent NPs do not form aggregates that would hinder their fluorescence quantification.

4.3.4 Optimization of analyte-capture antibody interactions

It is known that heterogeneous immunoassays can have lengthy detection times due to the duration required for analytes to reach surface-bound receptors [42–44]. Harnessing the advantage of MNPs, these were spotted in the beginning of the channel, hence allowing analyte-antibody interactions throughout the flow through the channel. This was compared to MPNs spotted in the detection zone to demonstrate the advantage of prolonged incubation and diffusional access between capture antibody and analyte (SI, Figure S4). The concentration of capture Abs, Ab-fluorescent NPs and MNPs strongly influenced the sensitivity of the immunoassay. For a 15 µl NT-proBNP-spiked HEPES buffer (1 ng·ml^{-1}) we found optimal concentrations of 2.5 µg·ml^{-1}, 2 % (w/v) and 3 µg, respectively (Figure 3a-c). It is worth noting that as the concentration of

MNPs increases, the fluorescence intensity also increases. This is due to the increased density of streptavidin recognition sites for the specific binding of the biotinylated sandwich complex, which leads to an improvement in the detection sensitivity. To further optimize the diffusional transport to the reactive sites, the duration for which the MNPs are in contact with the sample was modified by changing the flow rate as this influences capture efficiency, analyte-antibody interaction, and shear forces [45]. Thus, the fluorescence signal after the immunoreaction for a given analyte concentration at different flow rates were investigated (Figure 3d). First, 15 µl of NT-proBNP-spiked HEPES buffer (1 ng·ml^{-1}) was applied on the ready-to-go lateral flow channel, which subsequently initiated the rehydration of the dried reagents. The sample was transported with flow rates of 4, 3, 2 and 1 µL·min^{-1} and the fluorescence intensity was measured at the detection zone. It was found that lower flow rates resulted in overall more favorable conditions combining superior capture efficiency and increased interaction time. Furthermore, the rehydration ability of the dried reagents such as capture Abs, Ab-fluorescent NPs, MNPs was visually observed to be better at lower flow rates due to the longer rehydration times. In general, the highest fluorescence signal was obtained with the optimal flow rate of 2 µl·min^{-1}.

4.3.5 Performance of the lateral flow channel assay

Finally, the previously optimized conditions were transferred to generate dose-response curves for NT-proBNP in buffer and undiluted human blood. The spiked buffer measurements yielded a LOD of 26.7 pg·mL^{-1} with an error of only 11 % (n=4) (data not shown). In spiked human blood, a LOD of 43.1 pg·mL^{-1} and a mean standard deviation of 18 % (n=4) was obtained (Figure 4). As anticipated, the sensitivity and standard deviation were slightly affected due to the partial blocking of MNPs by adsorbed serum proteins and an increased background signal originating from these proteins. Notably, the mean error of the proposed assay is expected to benefit from enhanced fabrication processes when specifically tailored for large-scale production. In contrast to the established POCT assays presently employed in clinical environments, like the commercially accessible NT-proBNP tests developed by Roche Diagnostics [46], one of the key benefits of our assay is its ability to deliver similar results (detection range: 60 – 9000 pg·mL^{-1}) using a minimal sample volume of just 15 µL.

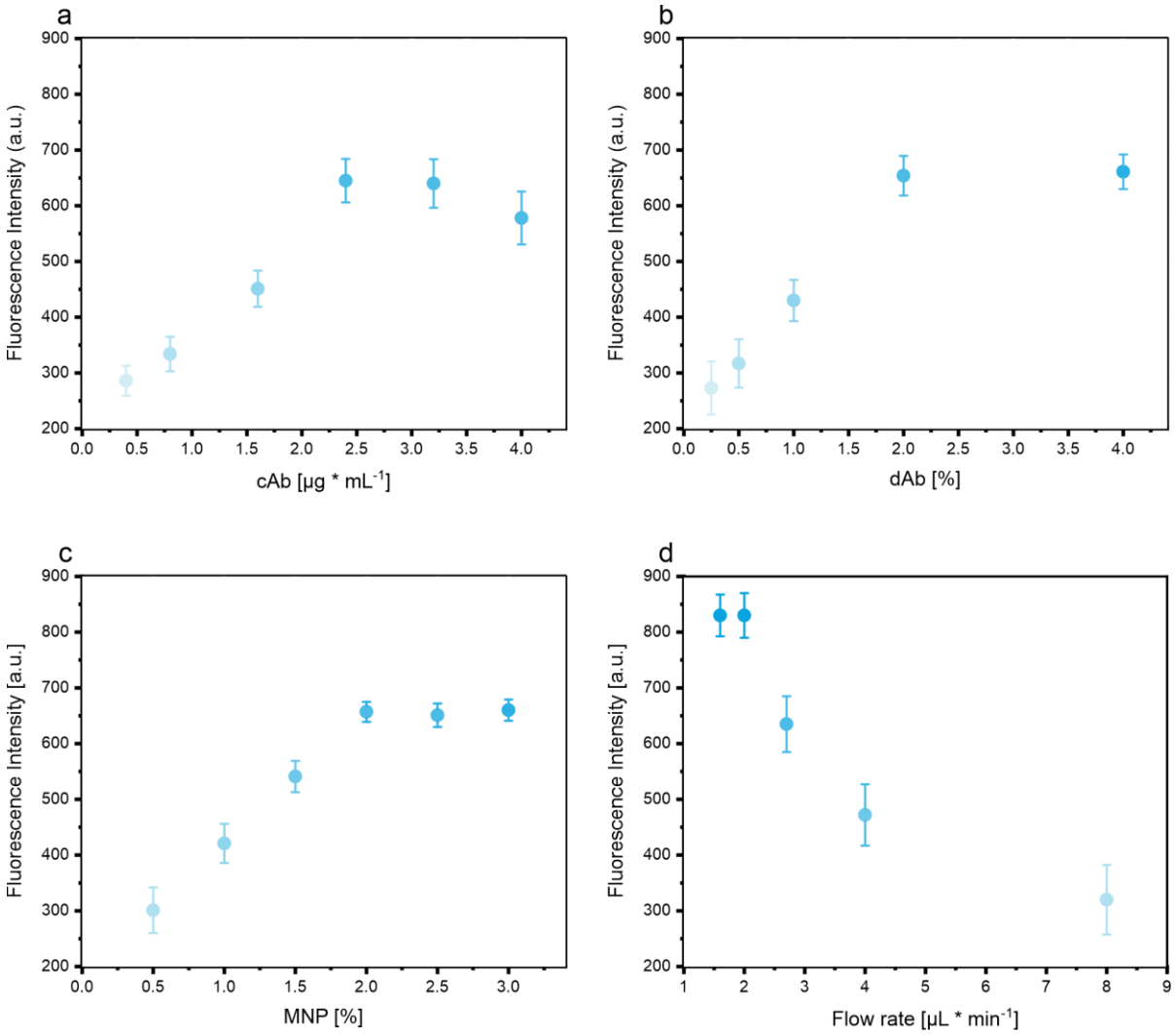

Figure 3: Optimization of the immunoassay by varying the concentration of the dried reagents and the flow rate. Plot of the assay signal against the capture antibody (cAb) concentration (a), plot of the assay signal against the Ab-fluorescent NP (dAb) concentration (b), plot of the assay signal against the MNP concentration (c), and plot of the assay signal against the flow rate (d). Error bars represent mean values ±1 σ (n=5)

This is a remarkable improvement compared to the Roche Cobas h 232 that requires up to 10 times more sample volume (15 µL vs. 150 µL). While experiments revealed that the limit of detection decreases with higher volume input, the primary objective was to showcase the viability of using small volumes. Specifically, our sensor can detect 0.076 fmol of NT-proBNP, whereas the Roche Cobas h 232 detects 1.06 fmol. To facilitate accurate addition of 15 µL by the patient, the implementation of capillary tubes, a conventional method for precise measurement of sample volumes, is also envisioned for the diagnostic test. This advancement not only preserves high sample volumes but also

simplifies the sampling process, making it more convenient for both medical assistants and patients. Additionally, the utilization of a bead-based immunoassay in this lateral flow channel overcomes the limitations associated with diffusion in traditional microfluidic sensors. By leveraging the unique properties of magnetic nanoparticles, the assay enables efficient and targeted analyte capture and enhancing sensitivity. Recently, a newly commercially available MNP-based NT-proBNP assay has been demonstrated, that is technologically the closest to our lateral flow channel assay [47]. This microfluidic chip enables NT-proBNP detection from 20 µL blood within 12 min with a range of 50 – 9000 pg·mL^{-1}. The assay demonstrated an average error of 4.1 % within the NT-proBNP range of 59 – 4559 pg·mL^{-1}, indicating its superior analytical precision. However, the testing protocol relies on additional washing steps, which in turn raises the complexity and expenses associated with the assay. Another similar MNP-based system is the well-established Cobas Elecsys® for the ultra-sensitive detection of NT-proBNP [48]. The platform provides a superior detection range of 5 – 35000 pg·mL^{-1} with only 15 µL sample and an assay time of 9 – 18 min. Nevertheless, this system operates within a laboratory setting, being costly, necessitating sample preparation, and unsuitable for point-of-care implementation. The materials utilized in LFAs, such as fleece-fiber and membrane materials, often exhibit variations and inconsistencies in fabrication processes. These variations can impact factors such as sample flow rate and the release of dried reagents, ultimately affecting sensor performance. Thus, the incorporation of a compact pump system for controlled and automated fluid transport in this assay provides a crucial advantage in terms of precise sample transportation. Despite the need for an additional handheld device, this controlled flow system ensures consistent and uniform sample movement, reducing the impact of sample variability and improving the reliability of results. This feature is particularly important in applications where accurate and reproducible measurements are paramount.

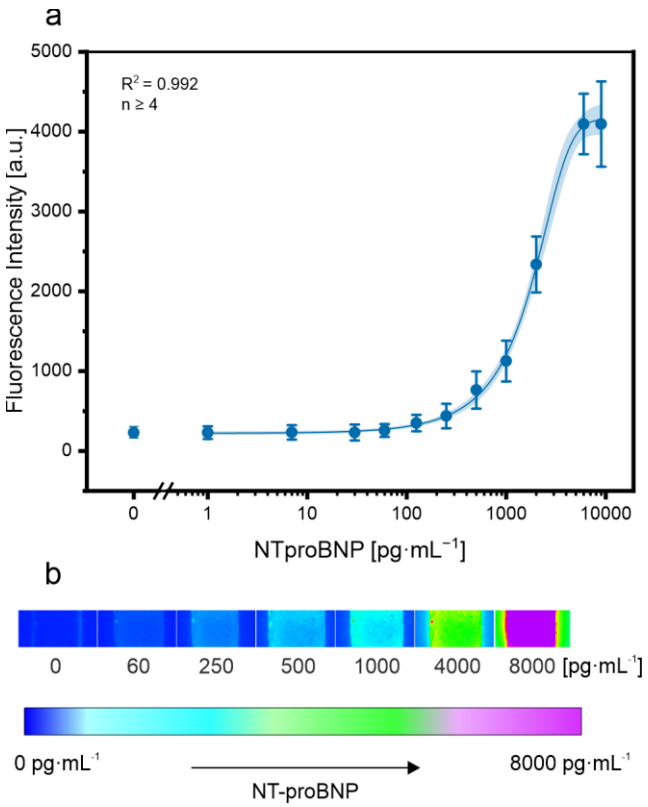

Figure 4: Dose response curve of NT-proBNP concentration in undiluted whole blood with logistic fit (blue line), 95 % confidence interval (shaded blue curve) (a) and fluorescence images representing NT-proBNP concentration (b). Standard deviations were calculated based on three parallel measurements using four flow channels, while outliers were removed after Q-test (confidence interval 95 %). Error bars represent mean values ± 1 σ (n = 3)

4.3.6 Signal stability

Furthermore, the signal stability of the one-step NT-proBNP immunoassay was assessed over a period of 8 weeks, using all the required reagents stored in a dry state. It is well-established that storing the reagents in the conjugate pad within a storage buffer, composed of stabilizers like trehalose or sucrose, preserves the biological activity of antibodies and ensures colloidal stability [49, 50]. In our assay, the reagents were dried on the sensor support, in direct contact to the PET surface. Within this hydrophobic environment, proteins might experience unfavorable conformational changes or irreversible adsorption, leading to compromised protein functionality and, consequently, hindering the overall sensor performance [51–53]. Moreover, it was crucial to enable fast rehydration and maintain the colloidal stability of the fluorescence-polystyrene nanoparticles and the MNPs. Particularly, MNPs have a tendency to create permanent aggregates when there is a transition in the medium

composition, for instance, from liquid to dry [54]. Thus, the study was essential for evaluating the storage stability of the utilized reagents after drying on the sensor surface. Therefore, the capture Abs and the fluorescence-NPs were dried in 6 % (w/v) sucrose and the MNPs were dried in 6 % (w/v) dextran at 50 °C for 10 min for the long-term storage. The LFA was stored airtight at 4 °C, and an immunoassay was performed weekly throughout the duration of the study (Figure 5). During the observation period, the fluorescence signal remains consistent with a mean relative error of 12 %. This finding holds significant importance as it validates the overall viability of storing the reagents in a dry state in ambient conditions. In addition to the small number of replicates the manual fabrication inaccuracies of the lateral flow channel assay have contributed to the overall high error bars.

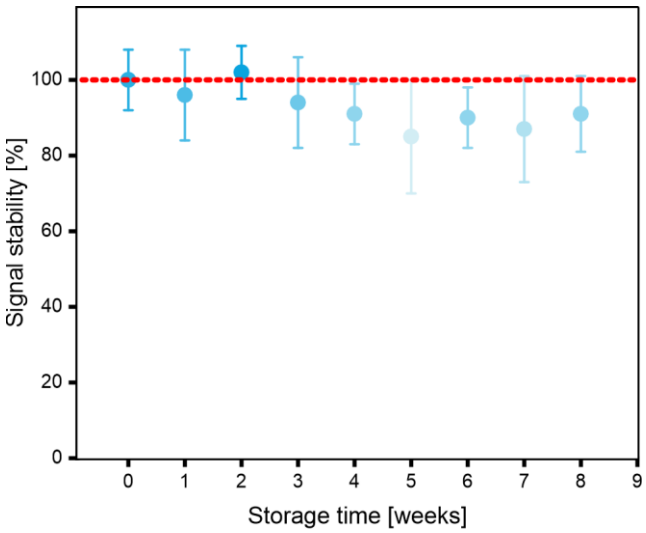

Figure 5: Performance stability of the bioassay with dried capture Abs, Ab-fluorescent NPs in 6 % (w/v) sucrose and MNPs in 6 % (w/v) dextran at 50 °C, stored at 4 °C over 8 weeks. Standard deviations were calculated based on three parallel measurements on three different LFAs, while outliers were removed after Q-test (confidence interval 95 %). Error bars represent mean values ±1 σ (n = 3). In all measurements, the immunoassay was performed in the lateral flow channel with a constant analyte concentration of 1 ng·mL^{-1}and signal stability means were normalized to the signal right after drying (storage time = 0)

4.4 Conclusion

In the future of medical care an increasing need for reliable tests performed without medical personnel yet providing the quantitative and highly sensitive characteristics of standard laboratory tests is predicted not necessarily limited to rural areas and

homecare. To fully support this need with POCTs, it is essential to switch from a venous blood draw to a small finger-prick blood sample. This change reduces invasiveness, ensures patient comfort and streamlines sample handling. Thus, future tests must be as easy-to-use as the one-step LFA, yet provide better analytical figures of merit, considering patient comfort. The test system proposed here suggests that through small associated hardware such analytical features are achievable. The combination of nanotechnology and active fluid control along with fluorescence detection has created new possibilities for achieving highly sensitive and reliable point-of-care diagnostics, even if instrument-free visual detection is here no longer possible. Yet, improved surface-to-volume ratios, enhanced reaction kinetics, precise fluid control, and amplified detection have collectively enabled a user-friendly, one-step automated POCT system. Future improvements encompass expanding the scope of detectable analytes, integrating multiplexing capabilities, and developing a cost-effective handheld and portable analytical device that combines fluorescence detection, flow control, and automated analysis. This will allow for easy and efficient testing for both clinical and home use.

4.5 References

1. Cardiovascular diseases. https://www.who.int/health-topics/cardiovascular-diseases. Accessed 10 Jul 2023

2. Cardiovascular diseases (CVDs). https://www.who.int/news-room/fact-sheets/detail/cardiovascular-diseases-(cvds). Accessed 10 Jul 2023

3. (2022) Heart Failure - What Is Heart Failure? | NHLBI, NIH. https://www.nhlbi.nih.gov/health/heart-failure. Accessed 10 Jul 2023

4. Song K-S, Nimse SB, Sonawane MD, Warkad SD, Kim T (2017) Ultra-Sensitive NT-proBNP Quantification for Early Detection of Risk Factors Leading to Heart Failure. Sensors 17:2116. https://doi.org/10.3390/s17092116

5. Corteville DCM, Bibbins-Domingo K, Wu AHB, Ali S, Schiller NB, Whooley MA (2007) N-terminal pro-B-type natriuretic peptide as a diagnostic test for ventricular dysfunction in patients with coronary disease: data from the heart and soul study. Arch Intern Med 167:483–489. https://doi.org/10.1001/archinte.167.5.483

6. Mukoyama M, Nakao K, Hosoda K, Suga S, Saito Y, Ogawa Y, Shirakami G, Jougasaki M, Obata K, Yasue H (1991) Brain natriuretic peptide as a novel cardiac hormone in humans. Evidence for an exquisite dual natriuretic peptide system, atrial natriuretic peptide and brain natriuretic peptide. J Clin Invest 87:1402–1412

7. Santaguida PL, Don-Wauchope AC, Oremus M, McKelvie R, Ali U, Hill SA, Balion C, Booth RA, Brown JA, Bustamam A, Sohel N, Raina P (2014) BNP and NT-proBNP as prognostic markers in persons with acute decompensated heart failure: a systematic review. Heart Fail Rev 19:453–470. https://doi.org/10.1007/s10741-014-9442-y

8. Daniels LB, Maisel AS (2007) Natriuretic peptides. J Am Coll Cardiol 50:2357–2368. https://doi.org/10.1016/j.jacc.2007.09.021

9. Kara K, Lehmann N, Neumann T, Kälsch H, Möhlenkamp S, Dykun I, Broecker-Preuss M, Pundt N, Moebus S, Jöckel K-H, Erbel R, Mahabadi AA (2015) NT-proBNP is superior to BNP for predicting first cardiovascular events in the general population: the Heinz Nixdorf Recall Study. Int J Cardiol 183:155–161. https://doi.org/10.1016/j.ijcard.2015.01.082

10. Taylor CJ, Roalfe AK, Iles R, Hobbs FDR (2014) The potential role of NT-proBNP in screening for and predicting prognosis in heart failure: a survival analysis. BMJ Open 4:e004675. https://doi.org/10.1136/bmjopen-2013-004675

11. Januzzi JL, Camargo CA, Anwaruddin S, Baggish AL, Chen AA, Krauser DG, Tung R, Cameron R, Nagurney JT, Chae CU, Lloyd-Jones DM, Brown DF, Foran-Melanson S, Sluss PM, Lee-Lewandrowski E, Lewandrowski KB (2005) The N-terminal Pro-

BNP investigation of dyspnea in the emergency department (PRIDE) study. Am J Cardiol 95:948–954. https://doi.org/10.1016/j.amjcard.2004.12.032

12. Roche Diagnostics. Roche Cardiac proBNP+. Mannheim (DE): Roche Diagnostics. 2018. https://assets.roche.com/f/173850/x/1bdc1c1d83/05533643190-can-en-v4.pdf. Accessed 10 Jul 2023

13. O'Farrell B (2008) Evolution in Lateral Flow–Based Immunoassay Systems. Lateral Flow Immunoass 1–33. https://doi.org/10.1007/978-1-59745-240-3_1

14. Atthoff B, Hilborn J (2007) Protein adsorption onto polyester surfaces: Is there a need for surface activation? J Biomed Mater Res B Appl Biomater 80B:121–130. https://doi.org/10.1002/jbm.b.30576

15. Jung W, Han J, Choi J-W, Ahn CH (2015) Point-of-care testing (POCT) diagnostic systems using microfluidic lab-on-a-chip technologies. Microelectron Eng 132:46–57. https://doi.org/10.1016/j.mee.2014.09.024

16. Sachdeva S, Davis RW, Saha AK (2021) Microfluidic Point-of-Care Testing: Commercial Landscape and Future Directions. Front Bioeng Biotechnol 8:

17. Vashist SK, Luppa PB, Yeo LY, Ozcan A, Luong JHT (2015) Emerging Technologies for Next-Generation Point-of-Care Testing. Trends Biotechnol 33:692–705. https://doi.org/10.1016/j.tibtech.2015.09.001

18. (2007) How to exploit the features of microfluidics technology. Lab Chip 8:20–22. https://doi.org/10.1039/B717986N

19. Nge PN, Rogers CI, Woolley AT (2013) Advances in Microfluidic Materials, Functions, Integration, and Applications. Chem Rev 113:2550–2583. https://doi.org/10.1021/cr300337x

20. Engels JF, Henderson CJ, Daly R, Renneberg R, Hall EAH (2018) A lateral flow channel immunoassay combining a particle binding zone geometry with nanoparticle labelling amplification. Sens Actuators B Chem 262:1–8. https://doi.org/10.1016/j.snb.2018.01.213

21. Buranda T, Huang J, Perez-Luna VH, Schreyer B, Sklar LA, Lopez GP (2002) Biomolecular Recognition on Well-Characterized Beads Packed in Microfluidic Channels. Anal Chem 74:1149–1156. https://doi.org/10.1021/ac0109624

22. Giouroudi I, Keplinger F (2013) Microfluidic Biosensing Systems Using Magnetic Nanoparticles. Int J Mol Sci 14:18535–18556. https://doi.org/10.3390/ijms140918535

23. Hejazian M, Li W, Nguyen N-T (2015) Lab on a chip for continuous-flow magnetic cell separation. Lab Chip 15:959–970. https://doi.org/10.1039/C4LC01422G

24. Lim CT, Zhang Y (2007) Bead-based microfluidic immunoassays: the next generation. Biosens Bioelectron 22:1197–1204. https://doi.org/10.1016/j.bios.2006.06.005

25. Zheng L, Cai G, Wang S, Liao M, Li Y, Lin J (2019) A microfluidic colorimetric biosensor for rapid detection of Escherichia coli O157:H7 using gold nanoparticle aggregation and smart phone imaging. Biosens Bioelectron 124–125:143–149. https://doi.org/10.1016/j.bios.2018.10.006

26. Kim J, Johnson M, Hill P, Gale BK (2009) Microfluidic sample preparation: cell lysis and nucleic acid purification. Integr Biol Quant Biosci Nano Macro 1:574–586. https://doi.org/10.1039/b905844c

27. Nabaei V, Chandrawati R, Heidari H (2018) Magnetic biosensors: Modelling and simulation. Biosens Bioelectron 103:69–86. https://doi.org/10.1016/j.bios.2017.12.023

28. Bilal M, Zhao Y, Rasheed T, Iqbal HMN (2018) Magnetic nanoparticles as versatile carriers for enzymes immobilization: A review. Int J Biol Macromol 120:2530–2544. https://doi.org/10.1016/j.ijbiomac.2018.09.025

29. Cardoso VF, Francesko A, Ribeiro C, Bañobre-López M, Martins P, Lanceros-Mendez S (2018) Advances in Magnetic Nanoparticles for Biomedical Applications. Adv Healthc Mater 7:1700845. https://doi.org/10.1002/adhm.201700845

30. Liu S, Yu B, Wang S, Shen Y, Cong H (2020) Preparation, surface functionalization and application of Fe3O4 magnetic nanoparticles. Adv Colloid Interface Sci 281:102165. https://doi.org/10.1016/j.cis.2020.102165

31. Zhang J, Yan S, Yuan D, Alici G, Nguyen N-T, Warkiani ME, Li W (2015) Fundamentals and applications of inertial microfluidics: a review. Lab Chip 16:10–34. https://doi.org/10.1039/C5LC01159K

32. Ho BP, Leal LG (1974) Inertial migration of rigid spheres in two-dimensional unidirectional flows. J Fluid Mech 65:365–400. https://doi.org/10.1017/S0022112074001431

33. Furlani EP (2006) Analysis of particle transport in a magnetophoretic microsystem. J Appl Phys 99:024912. https://doi.org/10.1063/1.2164531

34. Odenbach S, Thurm S (2002) Magnetoviscous Effects in Ferrofluids. In: Odenbach S (ed) Ferrofluids: Magnetically Controllable Fluids and Their Applications. Springer, Berlin, Heidelberg, pp 185–201

35. Lenshof A, Laurell T (2010) Continuous separation of cells and particles in microfluidic systems. Chem Soc Rev 39:1203–1217. https://doi.org/10.1039/B915999C

36. Nguyen N-T (2012) Micro-magnetofluidics: interactions between magnetism and fluid flow on the microscale. Microfluid Nanofluidics 12:1–16. https://doi.org/10.1007/s10404-011-0903-5

37. Pamme N, Manz A (2004) On-Chip Free-Flow Magnetophoresis: Continuous Flow Separation of Magnetic Particles and Agglomerates. Anal Chem 76:7250–7256. https://doi.org/10.1021/ac049183o

38. Lutz S, Lopez-Calle E, Espindola P, Boehm C, Brueckner T, Spinke J, Marcinowski M, Keller T, Tgetgel A, Herbert N, Fischer T, Beiersdorf E (2017) A fully integrated microfluidic platform for highly sensitive analysis of immunochemical parameters. The Analyst 142:4206–4214. https://doi.org/10.1039/C7AN00547D

39. Tang C, Prud'homme RK (2016) Targeted Theragnostic Nanoparticles Via Flash Nanoprecipitation: Principles of Material Selection. In: Vauthier C, Ponchel G (eds) Polymer Nanoparticles for Nanomedicines: A Guide for their Design, Preparation and Development. Springer International Publishing, Cham, pp 55–85

40. Trenkenschuh E (2021) Freeze-drying of nanoparticles: Impact of particle properties on formulation and process development. Text.PhDThesis, Ludwig-Maximilians-Universität München

41. Yokota H, Kadowaki M, Matsuura T, Imanaka H, Ishida N, Imamura K (2020) The Use of a Combination of a Sugar and Surfactant to Stabilize Au Nanoparticle Dispersion against Aggregation during Freeze-Drying. Langmuir 36:6698–6705. https://doi.org/10.1021/acs.langmuir.0c00695

42. Bange A, Halsall HB, Heineman WR (2005) Microfluidic immunosensor systems. Biosens Bioelectron 20:2488–2503. https://doi.org/10.1016/j.bios.2004.10.016

43. Hart R, Lec R, Noh H "Moses" (2010) Enhancement of heterogeneous immunoassays using AC electroosmosis. Sens Actuators B Chem 147:366–375. https://doi.org/10.1016/j.snb.2010.02.027

44. Tsai T-T, Huang T-H, Chen C-A, Ho NY-J, Chou Y-J, Chen C-F (2018) Development a stacking pad design for enhancing the sensitivity of lateral flow immunoassay. Sci Rep 8:17319. https://doi.org/10.1038/s41598-018-35694-9

45. Sasso LA, Johnston IH, Zheng M, Gupte RK, Ündar A, Zahn JD (2012) Automated microfluidic processing platform for multiplexed magnetic bead immunoassays. Microfluid Nanofluidics 13:603–612. https://doi.org/10.1007/s10404-012-0980-0

46. Bertsch T, Chapelle J-P, Dempfle C-E, Giannitsis E, Schwabs M, Zerback R (2010) Multicentre analytical evaluation of a new point-of-care system for the determination of cardiac and thromboembolic markers. Clin Lab 56:37–49

47. Larsson AO, Eriksson MB (2023) Validation of a Novel Point-of-Care Testing Device Designed for Assessment of NT-pro BNP. Fam Med Prim Care Open Access

48. Elecsys® NT-proBNP. In: Diagnostics. https://diagnostics.roche.com/ch/de/products/params/elecsys-nt-probnp.html. Accessed 29 Aug 2023

49. Beck F, Horn C, Baeumner AJ (2022) Dry-reagent microfluidic biosensor for simple detection of NT-proBNP via Ag nanoparticles. Anal Chim Acta 1191:339375. https://doi.org/10.1016/j.aca.2021.339375

50. Sukumaran A, Thomas T, Thomas R, Thomas RE, Paul JK, Vasudevan DM (2021) Development and Troubleshooting in Lateral Flow Immunochromatography Assays. Indian J Clin Biochem 36:208–212. https://doi.org/10.1007/s12291-020-00887-5

51. Koc Y, Mello AJ de, McHale G, I. Newton M, Roach P, J. Shirtcliffe N (2008) Nano-scale superhydrophobicity: suppression of protein adsorption and promotion of flow-induced detachment. Lab Chip 8:582–586. https://doi.org/10.1039/B716509A

52. Roach LS, Song H, Ismagilov RF (2005) Controlling Nonspecific Protein Adsorption in a Plug-Based Microfluidic System by Controlling Interfacial Chemistry Using Fluorous-Phase Surfactants. Anal Chem 77:785–796. https://doi.org/10.1021/ac049061w

53. von Stockert AR, Luongo A, Langhans M, Brandstetter T, Rühe J, Meckel T, Biesalski M (2021) Reducing Unspecific Protein Adsorption in Microfluidic Papers Using Fiber-Attached Polymer Hydrogels. Sensors 21:6348. https://doi.org/10.3390/s21196348

54. Gutiérrez L, Cueva L de la, Moros M, Mazarío E, Bernardo S de, Fuente JM de la, Morales MP, Salas G (2019) Aggregation effects on the magnetic properties of iron oxide colloids. Nanotechnology 30:112001. https://doi.org/10.1088/1361-6528/aafbff

4.6 Supporting Information

4.6.1 Fluid control system

The fluid control consisted of a metal housing that includes 1) a LFA mold, 2) an Arduino Due board, 3) and a miniaturized vacuum pump. The fluid control system was linked to a computer via USB and managed using an Arduino code. To initiate the immunoassay the fluid control was mounted on top of the outlet port of the LFA. The piezo effect- based micropump, mechanically positioned on the test strip using a suction cup. Specifically, two piezoceramics in a pump deform when a voltage is applied, allowing the transportation of liquid into a specific direction.

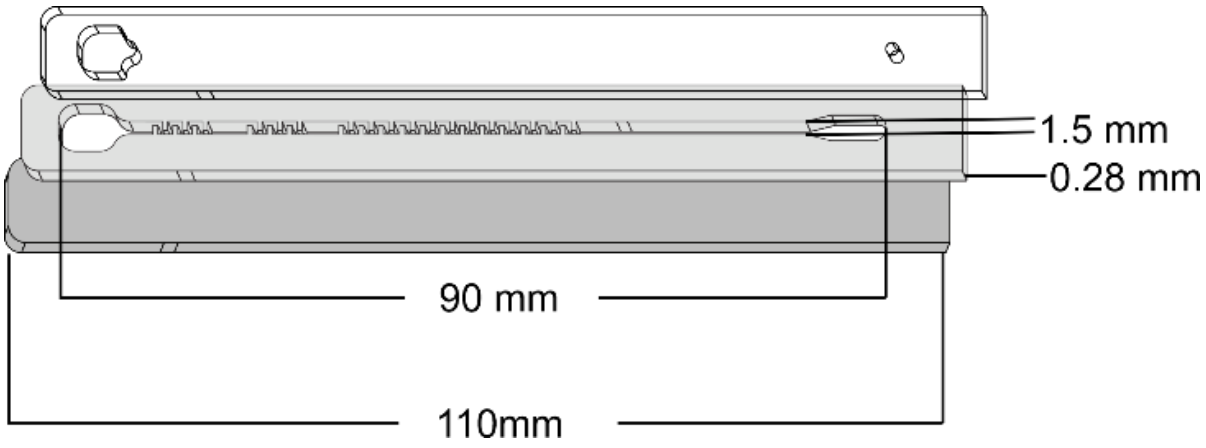

Figure S1: Schematic representation of the three-layered lateral flow channel with Melinex® 329 foil 175 µm as the support layer (dark grey), Melinex®329 foil 250 µm with double-sided adhesive tape as spacer foil (light grey) and Hostaphan RN 100, 125 µm as the cover foil (transparent)

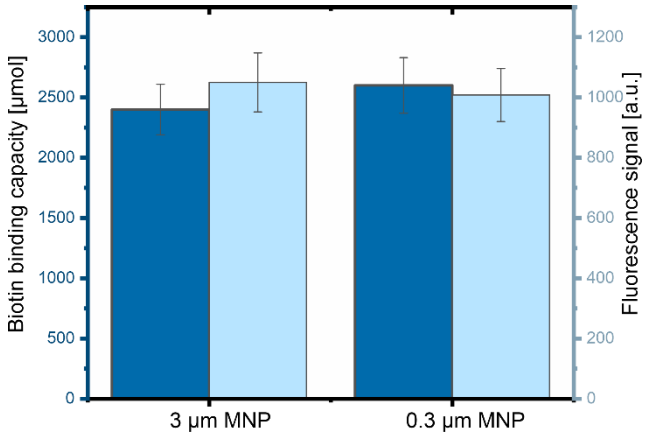

Figure S2: Biotin-binding capacity of large MNPs (3 µm, 2% (w/v)) and small MNPs (0.3 µm, 2 % (w/v)) (dark blue) and assay signal for constant MNP concentration (2 % (w/v)) for a given analyte concentration (c(analyte)=1 ng·mL^{-1}) (light blue). Standard deviations were calculated based on three parallel measurements on three different lateral flow channels (n=3)

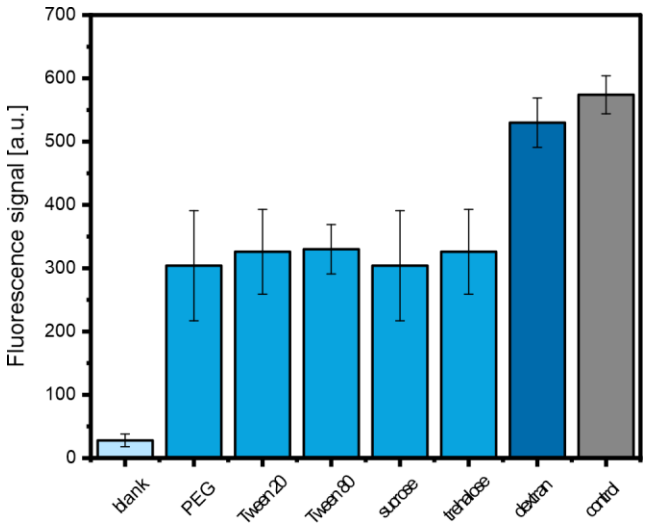

Figure S3: Optimization of drying MNPs with different additives in the dispensing buffer. Plot of the assay signal against the additives. Blank represents dried MNPs in HEPES buffer only, control represents MNPs not dried. 2 µL of MNPs (2 % (w/v) were dried in HEPES dispensing buffer on the sensor support at 50 °C for 10 min with the additives PEG 8000 (5 % (w/v)), Tween 20 (2 % (w/v), Tween 80 (2 % (w/v)), sucrose (20 % (w/v), trehalose (20 % (w/v), dextran (6 % (w/v), respectively. Rehydration was performed with 15 µL BNP-spiked HEPES buffer (1 ng·mL^{-1}) with

cAb (2.5 µg·mL^{-1}) and dAb-FNPs (2 % (w/v)) for 5 min. Standard deviations were calculated based on three parallel measurements on three different lateral flow channels (n=3)

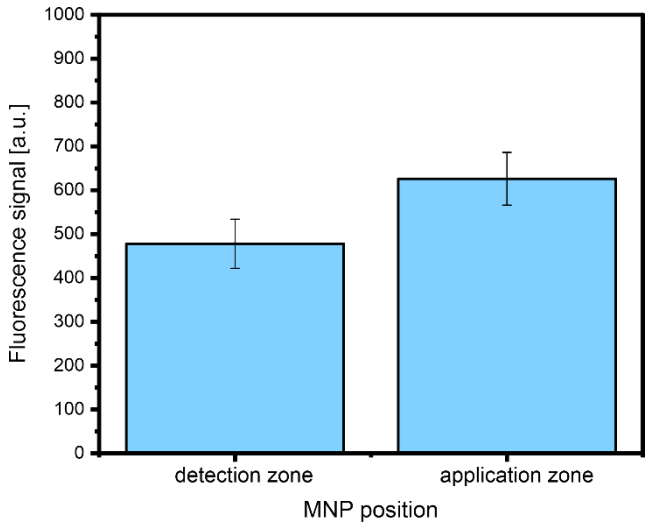

Figure S4: Influence of the deposition area of MNPs (2 % (w/v)) on the immunoreaction ($c_{[analyte]}$ = 1 ng·mL^{-1}, time = 10 min). MNPs deposited and dried in the detection zone have short immunoreaction time and low capture efficiency, resulting in low signal intensities. MNPs deposited upstream next to the sample application area have longer immunoreaction time and higher capture efficiency, resulting in higher signal intensities. Standard deviations were calculated based on three parallel measurements on three different lateral flow channels (n=3)

5 Sample-to-answer lateral flow assay with integrated plasma separation and NT-proBNP detection

Abstract

Through enabling whole blood detection in point-of-care testing (POCT) sedimentation-based plasma separation promises to enhance the functionality and extend the application range of lateral-flow assays (LFAs). To streamline the entire process from the introduction of the blood sample to the generation of quantitative immune-fluorescence results, we combined a simple plasma separation technique, an immunoreaction, and a micropump-driven external suction control system in a polymer channel-based LFA. Our primary objective was to eliminate the reliance on sample-absorbing separation membranes, the use of active separation forces commonly found in POCT, and ultimately allowing finger-prick testing. Combining the principle of agglutination of red blood cells with an on-device sedimentation-based separation, our device allows for the efficient and fast separation of plasma from a 25 µL blood volume within a mere 10 minutes and overcomes limitations such as clogging, analyte adsorption, and blood pre-dilution. To simplify this process, we stored the agglutination agent in a dried state on the test and incorporated a filter trench to initiate sedimentation-based separation. The separated plasma was then moved to the integrated mixing area, initiating the immunoreaction by rehydration of probe-specific fluorophore-conjugated antibodies. The biotinylated immune complex was subsequently trapped in the streptavidin-rich detection zone and quantitatively analyzed using a fluorescence microscope. Normalized to the centrifugation-based separation, our device demonstrated high separation efficiency of 96 % and a yield of 7.23 µL (=72 %). Furthermore, we elaborate on its user-friendly nature and demonstrate its proof-of-concept through an all-dried ready-to-go NT-proBNP lateral flow immunoassay with clinical blood samples.

Keywords:

Lateral flow assay, Blood plasma separation, Sedimentation, Point-of-care diagnostics, Sample-to-answer

Graphical Abstract

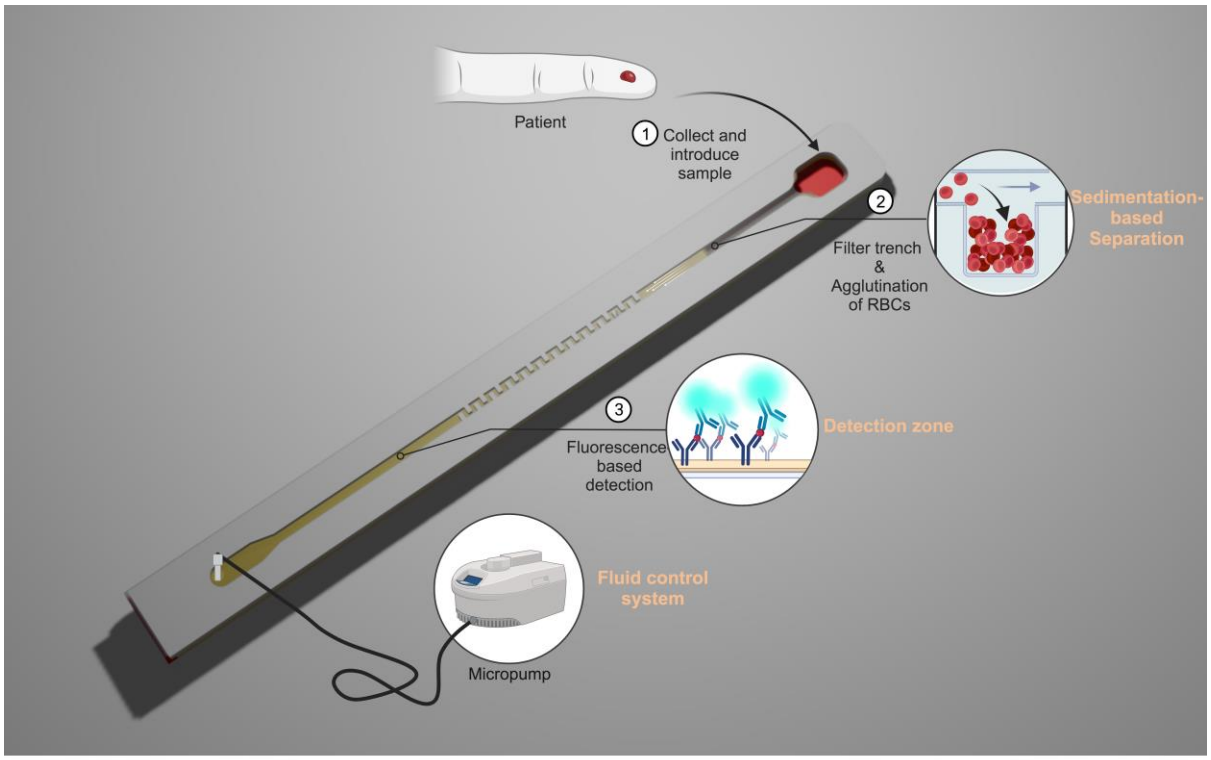

This chapter has been published.

Strohmaier-Nguyen, D., Horn, C. & Baeumner, A.J. Sample-to-answer lateral flow assay with integrated plasma separation and NT-proBNP detection. Anal Bioanal Chem 416, 3107–3115 (2024). https://doi.org/10.1007/s00216-024-05271-3

Author contributions: AJB, CH and DSN developed the concept for this work. DSN planned the experiments, did the experimental work and wrote the first draft of the manuscript. AJB revised the manuscript and is corresponding author.

5.1 Introduction

Medical professionals commonly employ blood tests as a primary diagnostic method to detect various conditions. This procedure entails examining a small blood sample for any deviations or abnormalities in the individual's biochemical profile, which may indicate the presence of a pathological disorder [1]. Whole blood is one of the most complex and relevant body fluids that is used in clinical analysis [2]. Its analysis typically requires costly bench-top instruments and skilled personnel, making it unsuitable in resource-limited surroundings [3]. Moreover, conventional blood tests are relatively complex and time cumbersome (>1 h) requiring large sample volumes [4, 5]. The utilization of POCT technology has exhibited the ability to scale down the size of laboratory instruments and assays, resulting in economically favored, reproducible, and faster detection systems. The success of POCT systems lies in the integrated separation mechanism in order to circumvent bulky bench-top centrifuges to generate human plasma, removing the necessity for sample handling, transport, and storage. The plasma extraction through a patented separation membrane such as “Asymmetric Polysulfone Membrane (APM), Fusion 5, and others” is the gold standard. Its well-defined pore size retains the blood cells in the membrane while the plasma can be further analyzed. Especially, in low-setting surroundings the separation membrane has been shown advantageous. Previous studies have indicated that the accuracy of testing results heavily relies on the quality of plasma, which can be negatively impacted by blood cell-related issues like hemolysis and leukolysis [6, 7]. The separation of blood cells is primarily aimed at achieving a reproducible detection read-out as the presence of red blood cells and their lysed fragments can obstruct the visibility of test and control lines, leading to inaccurate results [8]. Nonetheless, employing the separation membrane also brings about limitations, including blood clogging [9], potential interactions with analytes [10], as well as relatively high sample volumes, caused by the membrane’s high dead volume. This, in turn, might cause discomfort for the patient, as the blood needs to be drawn from a vein rather than through a finger prick. Therefore, recent studies have concentrated on plasma separation techniques suitable for small finger prick sample volumes [11–13], which can generally be categorized into active and passive methods

[14]. Active separation includes external fluid control forces, whereas, in passive separation, no external forces are required for the separation process, making the system more suitable for the POCT environment. Most of the reported separation techniques, however, come with three major disadvantages. Firstly, expensive and cumbersome bench-top instruments are required, hindering the application in low-resource settings [15]. Secondly, the device involves sophisticated geometric structures [16], posing a challenge in achieving consistent fabrication and hindering the scalability process [17]. Thirdly, these techniques exhibit limited efficiency in separating plasma from high hematocrit samples, necessitating off-chip dilution of whole blood before analysis, thereby introducing cost and complexity to the procedure and diluting the target analyte, which presents a challenge in precisely detecting such minimal levels of analytes, especially when working with small finger prick volumes [18–20]. Affordable technologies capable of achieving efficient blood-plasma separation at the point of need, while ensuring reliability and effectiveness, are in demand. Plasma separation by sedimentation has been used for decades and relies on the gravitational density disparities between plasma and blood cells (ρ_{RBCs}=1100 kg/m^3, ρ_{WBCS}= 1050–1090 kg/m^3 and ρ_{plasma}=1030 kg/m^3) [14]. Blood cells in whole blood tend to sediment based on their differing densities, allowing the plasma to remain on top as a result of this separation process [21]. Sedimentation offers advantages as it eliminates the need for expensive equipment and highly trained personnel. One major limitation of this process, however, is the time it takes for blood cells to settle toward the bottom. Scaling down the dimension and integrating the process into a microfluidic system shortens the sedimentation time as the blood cells are effectively separated within shorter distances. Dimov et al., for example, observed that the gravitational force acting on blood cells is considerably greater than that on plasma within a filter trench, which allows the plasma and blood cells to segregate into an upper and a lower layer [22]. However, the self-contained system exhibited an unstable separation rate, and it necessitated relatively low flow rates to achieve 100 % filtration efficiency. Such low flow rates are impractical when dealing with larger blood volumes. Yang et al. further developed the integration of gravitational separation mechanism in a microfluidic design [23]. The device requires a heater to create a vacuum or a low-pressure environment for fluid transportation, but

this introduces considerable variability and can be further affected by temperature fluctuations from the external environment. Additionally, only 2 µL of plasma could be separated from 10 µL whole blood. Therefore, we proceeded to explore the filter trench while considering the impact of an aggregation agent that facilitates the clustering of red blood cells during the sedimentation phase, thereby enhancing the sedimentation rate. Consequently, we designed a lateral flow channel assay including a sedimentation-based erythrocyte separator that separates red blood cells (RBCs) from plasma in only 10 min. A filter trench not only acts as a physical barrier for the blood cells but also enables the RBCs to sediment, leading to high separation efficiency with low-cost ingredients. By improving the filter trench depth and sedimentation time the separation efficiency can be increased. Eventually, the assessment of the practicality of utilizing our device for the separation of clinical blood samples in the context of an immunochemical test was conducted. By controlling the fluid movement via a micropump the separated plasma passes through the trench and is analyzed in a fluorescence sandwich-based immunoreaction.

5.2 Materials and Methods

The biotinylated capture antibody (polyclonal NT-proBNP sheep-IgG-biotin, cAb), antigen (NT-proBNP (1-76) amid) in whole blood, probe antibody (monoclonal NT-proBNP mouse-IgG), probe antibody–modified fluorescence nanoparticles (Ab-fluorescence NPs), albumin (97 %) and poly streptavidin (pSA) were provided by Roche Diagnostics GmbH (Mannheim, Germany). Hydrochloric acid (HCl, 0.1 M, 1 M), sodium chloride (NaCl, p.a.), bovine serum albumin (BSA, >96 %), poly(diallyldimethylammonium chloride) (PDDA, M_w 200,000 – 350,000, 20 wt. % in H_2O), poly(acrylic acid, sodium salt) solution (average M_w 15,000, 35 wt. % in H_2O), ethylenediaminetetraacetic acid (EDTA, ≥ 98.5 %), sodium hydroxide (NaOH, 1M), poly(ethylene glycol)-block-poly(propylene glycol)-block-poly(ethylene glycol) (Synperonic® PE/P84), sodium azide and Tween 20 (>97 %) were supplied from Sigma-Aldrich (www.sigmaaldrich.com). HetaSep™ (www.stemcell.com) was utilized as agglutination agent.

5.2.1 Lateral flow channel fabrication with filter trench

The lateral flow channel was composed of an inlet, a channel, a filter trench, a detection zone, and an outlet that was connected to the micropump (Figure S1). For the construction of the lateral flow channel a slightly modified procedure of Yang et al. was used [23]. The platform is built-up out of four layers: 1) the substrate (Melinex®329, 175 µm), 2) a capillary-given spacer (Melinex®329, 250 µm), both were purchased from Dupont Teijin Films (www.dupontteijinfilms.com), 3) the filter trench-given foam spacer was customized by ATP Adhesive Systems (atp-ag.com) and 4) the cover foil Hostaphan RN 100 was purchased from Mitsubishi Polyester Film (www.m-petfilm.de). The capillary-given spacer and the filter-trench-given spacer were coated with double-sided adhesive tape on both sides, which was supplied by Henkel-Adhesives (www.henkel-adhesives.com). The channel (dimension: 90 mm x 1.5 mm x 0.28 mm), filter trench (dimension: 10 mm x 1.5 mm x 3 mm), the inlet (dimension: 4.5 mm x 3 mm x 0.28 mm) and outlet (dimension: Ø 1.5 mm) were designed by using the CorelDraw 2016 software and were then engraved.

To create the all-in-one, single-step immunoassay, the bio-recognition line on the substrate (Melinex®329, 175 µm) was patterned perpendicular to the flow direction with 1 mm wide lines of a polyelectrolyte-poly streptavidin multilayer using the layer-by-layer approach before assembling the device. Briefly, poly streptavidin (500 µL, 10 mg·mL^{-1}) and polydiallyldimethylammonium chloride (500 µL, 0.5 % (w/v)) was mixed at pH 7.4 and 150 mM NaCl to produce PDDA-poly streptavidin complexes. To assemble the detection zone, the PDDA-poly streptavidin complexes and polyacrylic acid (0.5 % (w/v), pH 4.55, PAA) were alternately deposited for 60 seconds onto the plastic slide through a shape-giving mold. The repetition of this alternative coating procedure was carried out for four cycles to create the detection zone. Capture Abs at a concentration of 2.5 µg·mL^{-1} and the Ab-fluorescence NPs at a concentration of 2 % (w/v) were individually dispensed onto the immunoassay support, with 2 µL of each reagent. For the plasma separation, 6 µL of the aggregation agent was dispensed in the sample application zone. The dispensed reagents were then dried using a drying cabinet at a temperature of 50 °C for a duration of 10 minutes. Following the drying process, the

support, spacer, and cover foil were assembled as shown in Figure S1 of the Supporting Information (SI).

5.2.2 Human blood sample

Samples of human blood from healthy donors were provided from Roche Diagnostics (Mannheim, Germany) in vacutainers with 7.2 mg K2 Ethylene diamine tetraacetic acid (EDTA).

5.2.3 Quantification of the plasma purity

For the quantification of the plasma purity, we followed the procedure of Sneha Maria et al. with slight changes [25]. Briefly, the plasma purity was examined in the lateral flow channel by comparing the grey scale intensities of the plasma obtained by the proposed device (Ig_{trench}) and the plasma obtained from the centrifuge ($Ig_{centrifuge}$). As RBCs are darker in color than plasma, their presence in the sample can reduce the grayscale intensity of the channel. Hence, the plasma purity was expressed as followed:

$$purity_{plasma} = 100\ \% * \frac{I_{g\_trench}}{I_{g\_centrifuge}} \quad (1)$$

5.2.4 Quantification of the recovered plasma volume

The volumes of the plasma present in the channel and the volume of the plasma in whole blood after centrifuge were measured, by comparing the distance of transported plasma in the channel, and the following formula was applied:

$$volume_{plasma} = h_{channel} * w_{channel} * d_{plasma} \quad (2)$$

, where $h_{channel}$, $w_{channel,}$ and d_{plasma} represent the channel height, channel width, and traveled distance of plasma, respectively.

5.2.5 Performance of the bioassay

A sandwich immunoassay with spiked blood samples was carried out to investigate the assay performance of the lateral flow channel assay. The samples were prepared in human whole blood through dilution of an AG stock solution (0-9000 pg·mL^{-1}) for analysis. For the immunoassay 25 µL of the spiked sample were applied on the sample application area. The sample was immediately transported to the filter trench with a flow rate of 60 µL·min^{-1} by the external vent control. After the separation time of 10 min, the separated plasma was further transported to the outlet with a flow rate of 2 µL·min^{-1}, crossing the detection zone. The immunoassay was performed at room temperature and fluorescence signals could be obtained after 35 min. For the calculation of the limit of detection (LOD) the logistic fit parameter for the lower curve asymptote A and the standard deviation of the blank SD (blank):

$$LOD = A + 3.3 * SD(blank) \quad (3)$$

The concentration of the antigen in the sample is determined by correlating the fluorescence intensity to a calibration curve constructed using known antigen concentration standards.

5.2.6 Supporting instruments

The drying processes were carried out using a drying cabinet set at a temperature of 50 °C (FED 400 E2, www.binder-world.com). The fluid control equipment and software used in this study were custom-made and supplied by Roche Diagnostics GmbH (Mannheim, Germany) (Figure S2a). The fluorescence images were captured using a fluorescence microscope equipped with a LINOS lens (www.excelitas.com) and an HTC camera featuring a Sony CCD sensor ICX285AL (www.sony.com) (Figure S2b). Illumination was provided by a XENON XBO R 100W/45 OFR lamp (www.osram.com), and specific excitation and detection filters (633 nm excitation and 685 nm detection) were utilized (www.semrock.com). The imaging software used for data acquisition was provided by Roche Diagnostics (Mannheim, Germany). The fluorescence images were

taken with an exposure time of 25 ms. Image processing and data analysis were carried out with ImageJ and Origin 2021.

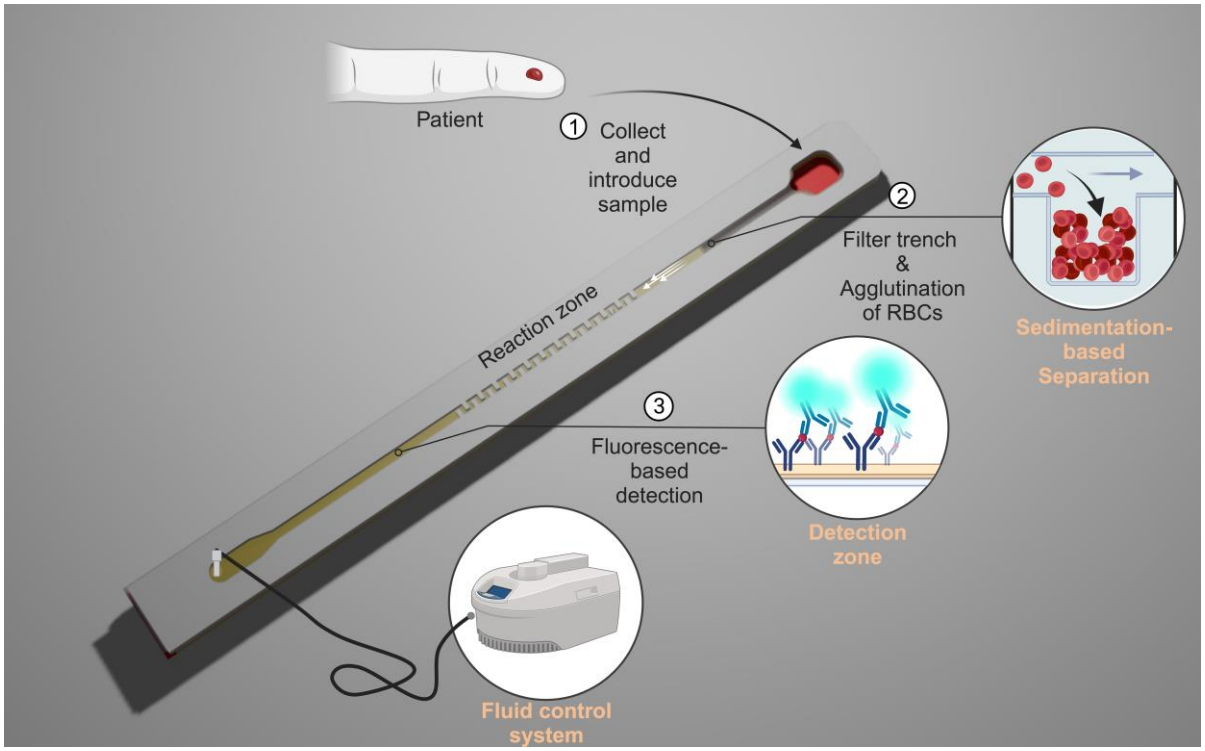

Figure 1: Schematic (not to scale) of the lateral flow channel assay with integrated plasma separation. After introducing the sample to the inlet (1), the sample is transported to the filter trench by the fluid control system. In the filter trench, the RBCs are aggregated and separated from the plasma through sedimentation (2). The separated plasma is then moved from the plasma separation module towards the reaction zone, reconstituting the probe antibodies and initiating the immunoreaction. In the detection zone, streptavidin is immobilized on the bottom of the channel for capturing the biotinylated sandwich complex (3). Adapted from "PDMS Microfluidic Chip Fabrication", by BioRender.com (2023). Retrieved from https://app.biorender.com/biorender-templates.

5.3 Results and Discussion

5.3.1 Design and operational principle behind the lateral flow channel assay device

The integrated blood-plasma separation biosensing system should exhibit reproducible functionality, fast and high separation efficiency, and compatibility with finger-prick sample volumes. Our setup enables sensitive analyte detection within ~20 minutes with

minimal user intervention. The proposed device includes the sample application port, the filter trench, the straight capillary channel with a mixing zone, the detection zone, and the outlet valve that is connected to the micropump (Figure 1). After applying the blood sample at the inlet, the micro pump controls the fluid movement, guiding the sample towards the filter trench. Within the filter trench, the agglutination agent prompts the red blood cells to aggregate. Subsequently, the sample was halted for a specified duration to ensure stable sedimentation of the blood cells. Finally, the microprocessor selectively activated the pump to sequentially move the sample from the plasma separation module towards the reaction zone, reconstituting the probe antibodies and initiating the immunoreaction. In the detection zone, streptavidin is immobilized on the bottom of the channel for capturing the biotinylated sandwich complex. Through the process of blood cell separation, we aim to minimize the impairment of the fluorescence signal and reduce any potential obstructions caused by the presence of hemoglobin in red blood cells. In our device, the separated plasma is further transported to the outlet and then the detection zone is fluorescently analyzed for quantitative signals (Figure S3).

5.3.2 Plasma separation efficiency

For the separation process to work efficiently, the time that blood cells remain in the trench must be long enough to cause sedimentation and entrapment within the trench. Therefore, the impact of various parameters including trench depth and separation time on the efficacy of plasma separation to enhance the effectiveness of the trench filter were studied (Figure 2a). Specifically, a volume of 25 µL undiluted whole blood was introduced into the platform and subsequently transported to the filter trench for varying durations of separation. The experimental results confirmed that longer sedimentation times led to an increase in the volume of obtained plasma. This outcome was in line with expectations, as the extended sedimentation period allowed the blood cells more time to settle, resulting in a greater volume of separated plasma. Additionally, increasing the depth of the trench also led to an increase in plasma volume. In fact, increasing the depth of the filter trench was found to enhance the sedimentation effect, as gravity had a significant impact on blood cells in the trench [22]. Insufficient or no separation of blood was observed in cases of shorter

sedimentation times (1-2 min) and shallow trenches (1-2 mm). For the sedimentation time of 10 min the trench depth of 2.5 mm and 3 mm yielded the highest plasma volumes, measuring 7.23 µL and 7.29 µL, respectively. This corresponds to a plasma yield of 72 % and 73 % compared to that achieved through centrifugal separation (= 10.05 µL). This suggests that increasing the trench depth at this dimension does not lead to an enhancement in plasma yield. The overall observed decrease in relative plasma volume can be attributed to the presence of minor volumes of plasma that remain in the filter as dead volume, which cannot be effectively separated. This phenomenon accounts for the reduced overall plasma volume obtained in the process. Additionally, it was noted that a minor fraction of whole blood experienced non-specific adsorption at the device inlet, resulting in a decrease in the overall plasma volume obtained. This also highlights the discrepancy in plasma volume between the proposed separation method and the centrifugal separation process. Given the relatively comparable obtained plasma volumes for both trench depths, the choice for further experimentation was at 2.5 mm due to the potential reduction in material costs associated with this specific trench depth. All-in-all, these findings contribute to the understanding of key factors influencing plasma separation in the proposed system and offer guidance for optimizing the design and operation parameters of the lateral flow channel.

5.3.3 Plasma purity

The evaluation of plasma purity was performed by analyzing the variation in grayscale intensity within a defined section of the channel containing the separated plasma [24]. This analysis aimed to assess the effectiveness of plasma purification in both the proposed approaches and the conventional centrifugation process. By comparing the grayscale intensities, we were able to quantify the level of impurities present in the obtained plasma and determine the efficiency of the separation methods. Due to the darker color of RBCs, the grayscale intensities in the presence of RBCs will be significantly lower compared to a sample without RBCs. The grayscale intensities of the separated plasma showed that the purity of the plasma obtained from the proposed approaches is similar to the plasma obtained using centrifugation (Figure 2b).

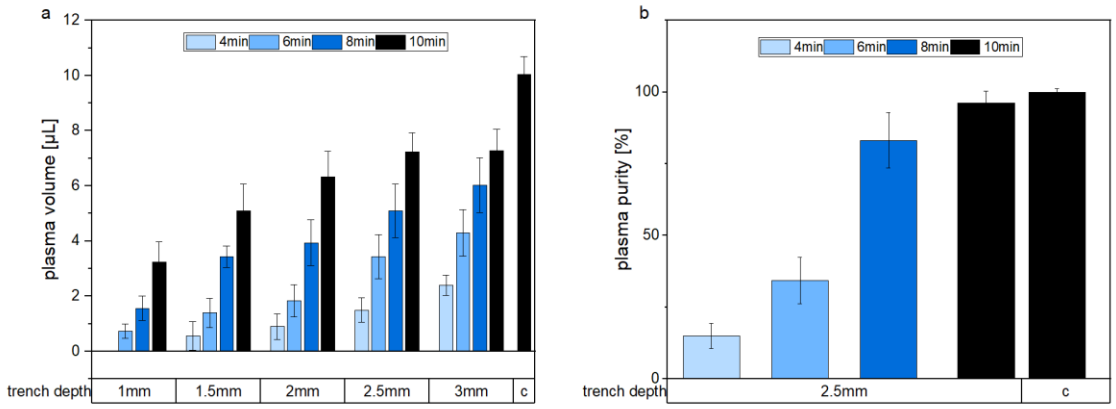

Figure 2: Optimization of the separated plasma volume (a) and optimization of the plasma purity (b) with respect to the trench depth and the time for separation. C - represents the plasma separation through centrifugation. The lateral flow channel was loaded with 25 µL of whole blood (hematocrit: 44 %), and the purity as well as the volume of plasma obtained was measured. Error bars representing the standard deviation (n=4).

Furthermore, since photometric absorption was not applicable with the tested volume, visual inspection of the separated plasma samples showed no visible signs of hemolysis, such as discoloration or the presence of red blood cell remnants [25]. This provided additional evidence supporting the absence of hemolysis during the plasma separation process, further ensuring the integrity and quality of the obtained plasma samples. However, it should be noted that platelets, which have lower sedimentation rates due to its smaller size (diameter ~ 2 µm) [26], may be present in the extracted plasma. It is worth mentioning that the presence of platelets does not notably interfere with the fluorescence read-out, consistent with existing findings [22, 27]. Nonetheless, should there be a requirement to identify platelets within the sample, a range of imaging techniques can be employed [28]. Overall, the findings demonstrate the effectiveness of the proposed approach in achieving high-quality plasma separation [11, 12, 23] and shows its potential for various biomedical applications.

Table 1 provides a comprehensive summary and comparison of the performance characteristics of the proposed device for blood separation in contrast to the conventional centrifuge-based method, highlighting its potential for practical and efficient blood separation applications. Included are key parameters such as separation efficiency, plasma volume yield, processing time, and equipment requirements, which

demonstrate that the proposed device achieved comparable performance. The device demonstrated high separation efficiency and yields a substantial volume of plasma with minimal loss. Additionally, the processing time was significantly reduced, offering a time-efficient alternative. Furthermore, the proposed device required minimal equipment, making it a cost-effective and accessible solution. However, it should be noted that the overall higher mean error in the separation efficiency and the separation yield may arise from variations in the manual fabrication of the test.

5.3.4 Combination of on-device plasma separation with analyte detection

Following the proof-of-principle and optimization of the blood separation, the proposed separation mechanism was implemented into a sandwich-based lateral flow assay. The platform was tested with real human blood samples, spiked with different concentrations of NT-proBNP (Figure 3). The 25 µL undiluted whole blood is introduced to the sensor and guided toward the filter trench. Along the way, the dry-spotted biotinylated capture Abs are resolubilized, initiating the immunoreaction. After 10 minutes of sedimentation time in the filter trench, the separated plasma is further transported to the dry-spotted Ab-fluorescence NPs, initiating the formation of the sandwich complex. The sample is then transported to the detection site where the channel's bottom is immobilized with streptavidin. Finally, the presence of the biotinylated sandwich complex can be detected at the detection zone, resulting in highly sensitive and specific detection of the target analyte. The immunoassay without blood separation and the proposed on-chip plasma separation showed similar curve shapes, suggesting comparable dynamic ranges. For the measurements with integrated blood separation, a limit of detection (LOD) of 365 pg·mL^{-1} with a mean error of 18 % was calculated in comparison to 283 pg·mL^{-1} and 14 % mean error for the centrifugation-based plasma preparation. Sample adsorption at the sample application zone and in the filter trench, resulting from manual fabrication variations are likely to be the reason for the higher LOD for our platform. But may also be caused by the lower plasma separation yield (Table 1). At the same time, the assay without blood separation demonstrated inferior signal responses in the analyte concentration range above 500 pg·mL^{-1} and below 9000 pg·mL^{-1}. Moreover, the biosensor would provide a LOD of 1680 pg·mL^{-1}, and a mean error of 26 %, hence, resulting in an about 5-fold higher LOD for whole blood

on-chip analysis. This discrepancy can be attributed to the adsorption of blood cells, particularly RBCs, onto the test line, leading to the absorption of the fluorescence signal due to their broad absorption spectra [30]. In addition, higher background signals were observed at low analyte concentrations (< 500 pg·mL^{-1}), resulting in the data points to not be statistically significantly different with the sample size of n=4 used.

Table 1. Comparison of performance characteristics of the separation techniques

	Separation technique			
	Filter trench		Centrifuge	
Performance characteristics	*mean*	*sd*	*mean*	*sd*
Plasma purity	96 %	6 %	Set to 100 %	2 %
Plasma Volume Obtained	7.23 µL	0.74 µL	10.05 µL	0.63 µL
Separation yield	72 %	7 %	Set to 100%	6 %
Time for Extraction	10 min		15 min	
Required equipment	Portable pump		Bench-top centrifuge	

Note: 25 µL undiluted whole blood (hct 44 %) was used for each test. Samples were run in triplicates and the mean and the standard deviation are reported. Results were normalized to the average volume of plasma and purity obtained from centrifugation (10.05 µL, 100 %) (n=3).

Still, the achieved LOD value and the statistically significant data falls within the threshold range used to evaluate heart failure severity and the risk of hospitalization [31]. The improved detection limit was expected due to the prevention of blood cell adsorption in the detection zone and the interaction with the read-out. Thus, the on-strip blood separation drastically improves the detection capabilities. Currently, commercially available NT-proBNP tests, such as the Cobas h 232 provided by Roche Diagnostics demonstrate superior temporal and analytical performance with a LOD of 60 pg·mL^{-1} and a detection time of only 12 minutes. This suggests that there is still potential for enhancement in our developed platform. Nonetheless, the assay showcase in this study presents a notable benefit by demanding a notably smaller blood volume (25 µL compared to 150 µL). This reduction is attributed to the diminished dead volume stemming from the unused filtration membrane and nitrocellulose membrane. This not only increases convenience for the patient but also allows for sample collection via a simple finger prick, eliminating the necessity for skilled personnel and significantly

cutting down costs for testing. As a result, our platform is well suited for home-testing and point-of-care applications in low-resource settings.

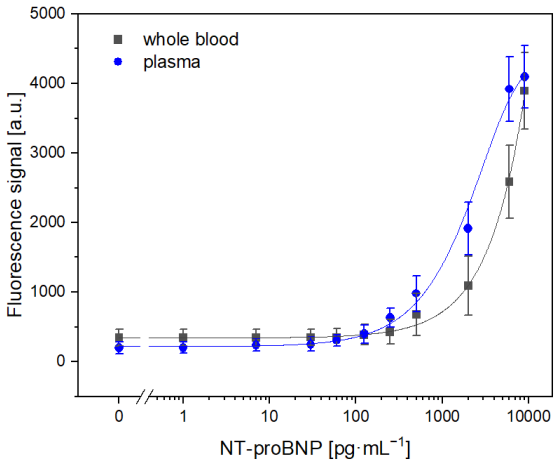

Figure 3: Plot of fluorescence intensity against logarithm of antigen concentration. Fluorescent read-out of the analyte in 25 µL whole blood with logistic fit (black line) and using the integrated plasma separation with logistic fit (blue line). Standard deviations were calculated based on four parallel measurements on four different LFAs, while outliers were removed after Q-test (confidence interval 95 %). Error bars represent mean values ±1σ (n ≥ 4).

5.4 Conclusion

In summary, we proposed a self-contained lateral flow channel assay with an integrated sedimentation-based separation of red blood cells from plasma, enabling sensitive quantification of the HF biomarker NT-proBNP in undiluted whole blood. The platform relies on the gravity-based sedimentation of agglutinated RBCs in a filter trench allowing for the subsequent immunoreaction to take place without blood cell interference and also demonstrates resilience against potential clogging that can arise in pore-based filtration mechanisms. The proposed biosensor is capable not only of handling small quantities of undiluted whole blood (25 µL), which improves the patients' comfort as the sample volume can be conveniently obtained via a finger prick, but also possesses a cost-effective production approach since no complex geometric µm-structures are required. This facilitates consistent manufacturing and seamless

scalability of production. Utilizing minimal hardware, including a portable pump and a fluorescence detection camera, the platform demonstrated the desired control over the flow rate and compatibility with a fluorescence immunoassay, while retaining the straightforward one-step detection feature found in conventional LFAs. Consequently, this uncomplicated plasma separation method can easily be applied to the POCT in clinical and home testing settings. Future enhancements will focus on further reducing sample volume requirements by avoiding analyte loss in both the inlet and the filter trench through an optimization of the test design's geometric structure. Furthermore, moving toward real-world application, an evaluation of the separation efficiency with varying hematocrit levels in blood samples will be essential. In the end, the system's applicability extends beyond NT-proBNP detection and can be applied to a broader range of clinically relevant blood biomarkers.

5.5 References

1. Chen X, Gole J, Gore A, He Q, Lu M, Min J, Yuan Z, Yang X, Jiang Y, Zhang T, Suo C, Li X, Cheng L, Zhang Z, Niu H, Li Z, Xie Z, Shi H, Zhang X, Fan M, Wang X, Yang Y, Dang J, McConnell C, Zhang J, Wang J, Yu S, Ye W, Gao Y, Zhang K, Liu R, Jin L (2020) Non-invasive early detection of cancer four years before conventional diagnosis using a blood test. Nat Commun 11:3475. https://doi.org/10.1038/s41467-020-17316-z

2. Anderson NL, Anderson NG (2002) The human plasma proteome: history, character, and diagnostic prospects. Mol Cell Proteomics MCP 1:845–867. https://doi.org/10.1074/mcp.r200007-mcp200

3. Sharma S, Zapatero-Rodríguez J, Estrela P, O'Kennedy R (2015) Point-of-Care Diagnostics in Low Resource Settings: Present Status and Future Role of Microfluidics. Biosensors 5:577–601. https://doi.org/10.3390/bios5030577

4. Adkins JN, Varnum SM, Auberry KJ, Moore RJ, Angell NH, Smith RD, Springer DL, Pounds JG (2002) Toward a human blood serum proteome: analysis by multidimensional separation coupled with mass spectrometry. Mol Cell Proteomics MCP 1:947–955. https://doi.org/10.1074/mcp.m200066-mcp200

5. Sanchez-Giron F, Alvarez-Mora F (2008) Reduction of blood loss from laboratory testing in hospitalized adult patients using small-volume (pediatric) tubes. Arch Pathol Lab Med 132:1916–1919. https://doi.org/10.5858/132.12.1916

6. Biagini RE, Sammons DL, Smith JP, MacKenzie BA, Striley CAF, Snawder JE, Robertson SA, Quinn CP (2006) Rapid, Sensitive, and Specific Lateral-Flow Immunochromatographic Device To Measure Anti-Anthrax Protective Antigen Immunoglobulin G in Serum and Whole Blood. Clin Vaccine Immunol 13:541–546. https://doi.org/10.1128/CVI.13.5.541-546.2006

7. Mielczarek WS, Obaje EA, Bachmann TT, Kersaudy-Kerhoas M (2016) Microfluidic blood plasma separation for medical diagnostics: is it worth it? Lab Chip 16:3441–3448. https://doi.org/10.1039/C6LC00833J

8. Golden A, Steel C, Yokobe L, Jackson E, Barney R, Kubofcik J, Peck R, Unnasch TR, Nutman TB, de los Santos T, Domingo GJ (2013) Extended Result Reading Window in Lateral Flow Tests Detecting Exposure to Onchocerca volvulus: A New Technology to Improve Epidemiological Surveillance Tools. PLoS ONE 8:e69231. https://doi.org/10.1371/journal.pone.0069231

9. Lu Z, Rey E, Vemulapati S, Srinivasan B, Mehta S, Erickson D (2018) High-yield paper-based quantitative blood separation system. Lab Chip 18:3865–3871. https://doi.org/10.1039/C8LC00717A

10. Homsy A, van der Wal PD, Doll W, Schaller R, Korsatko S, Ratzer M, Ellmerer M, Pieber TR, Nicol A, de Rooij NF (2012) Development and validation of a low cost

blood filtration element separating plasma from undiluted whole blood. Biomicrofluidics 6:12804–128049. https://doi.org/10.1063/1.3672188

11. Lenz KD, Jakhar S, Chen JW, Anderson AS, Purcell DC, Ishak MO, Harris JF, Akhadov LE, Kubicek-Sutherland JZ, Nath P, Mukundan H (2021) A centrifugal microfluidic cross-flow filtration platform to separate serum from whole blood for the detection of amphiphilic biomarkers. Sci Rep 11:5287. https://doi.org/10.1038/s41598-021-84353-z

12. Garcia-Rey S, Nielsen JB, Nordin GP, Woolley AT, Basabe-Desmonts L, Benito-Lopez F (2022) High-Resolution 3D Printing Fabrication of a Microfluidic Platform for Blood Plasma Separation. Polymers 14:2537. https://doi.org/10.3390/polym14132537

13. Cheah E, Tran DP, Amen MT, Arrua RD, Hilder EF, Thierry B (2022) Integrated Platform Addressing the Finger-Prick Blood Processing Challenges of Point-of-Care Electrical Biomarker Testing. Anal Chem 94:1256–1263. https://doi.org/10.1021/acs.analchem.1c04470

14. Khatoon S, Ahmad G (2022) A Review on the Recent Developments in Passive Plasma Separators and Lab-on-Chip Microfluidic Devices. Eng Proc 31:37. https://doi.org/10.3390/ASEC2022-13796

15. Wang Y, Nunna BB, Talukder N, Etienne EE, Lee ES (2021) Blood Plasma Self-Separation Technologies during the Self-Driven Flow in Microfluidic Platforms. Bioengineering 8:94. https://doi.org/10.3390/bioengineering8070094

16. Lutz S, Lopez-Calle E, Espindola P, Boehm C, Brueckner T, Spinke J, Marcinowski M, Keller T, Tgetgel A, Herbert N, Fischer T, Beiersdorf E (2017) A fully integrated microfluidic platform for highly sensitive analysis of immunochemical parameters. Analyst 142:4206–4214. https://doi.org/10.1039/C7AN00547D

17. Maurya A, Murallidharan JS, Sharma A, Agarwal A (2022) Microfluidics geometries involved in effective blood plasma separation. Microfluid Nanofluidics 26:73. https://doi.org/10.1007/s10404-022-02578-4

18. Chin CD, Linder V, Sia SK (2012) Commercialization of microfluidic point-of-care diagnostic devices. Lab Chip 12:2118. https://doi.org/10.1039/c2lc21204h

19. Hauser J, Lenk G, Hansson J, Beck O, Stemme G, Roxhed N (2018) High-Yield Passive Plasma Filtration from Human Finger Prick Blood. Anal Chem 90:13393–13399. https://doi.org/10.1021/acs.analchem.8b03175

20. Thorslund S, Klett O, Nikolajeff F, Markides K, Bergquist J (2006) A hybrid poly(dimethylsiloxane) microsystem for on-chip whole blood filtration optimized for steroid screening. Biomed Microdevices 8:73–79. https://doi.org/10.1007/s10544-006-6385-7

21. Ho Son J, Hun Lee S, Hong S, Park S, Lee J, M. Dickey A, P. Lee L (2014) Hemolysis-free blood plasma separation. Lab Chip 14:2287–2292. https://doi.org/10.1039/C4LC00149D

22. Kuroda C, Ohki Y, Ashiba H, Fujimaki M, Awazu K, Tanaka T, Makishima M (2014) Microfluidic sedimentation system for separation of plasma from whole blood. In: 2014 IEEE SENSORS. pp 1854–1857

23. Dimov IK, Basabe-Desmonts L, Garcia-Cordero JL, Ross BM, Ricco AJ, Lee LP (2011) Stand-alone self-powered integrated microfluidic blood analysis system (SIMBAS). Lab Chip 11:845–850. https://doi.org/10.1039/C0LC00403K

24. Yang C-H, Hsieh Y-L, Tsou P-H, Li B-R (2019) Thermopneumatic suction integrated microfluidic blood analysis system. PLOS ONE 14:e0208676. https://doi.org/10.1371/journal.pone.0208676

25. Maria MS, Rakesh PE, Chandra TS, Sen AK (2016) Capillary flow of blood in a microchannel with differential wetting for blood plasma separation and on-chip glucose detection. Biomicrofluidics 10:054108. https://doi.org/10.1063/1.4962874

26. (2023) A Quick-Reference Tool for Hemolysis Status | Division of Vector-Borne Diseases | NCEZID | CDC. https://www.cdc.gov/ncezid/dvbd/specimensub/hemolysis-palette.html. Accessed 9 Jan 2024

27. Popel AS, Johnson PC (2005) Microcirculation and Hemorheology. Annu Rev Fluid Mech 37:43–69. https://doi.org/10.1146/annurev.fluid.37.042604.133933

28. Vemulapati S, Erickson D (2018) H.E.R.M.E.S: rapid blood-plasma separation at the point-of-need. Lab Chip 18:3285–3292. https://doi.org/10.1039/C8LC00939B

29. Montague SJ, Lim YJ, Lee WM, Gardiner EE (2020) Imaging Platelet Processes and Function-Current and Emerging Approaches for Imaging in vitro and in vivo. Front Immunol 11:78. https://doi.org/10.3389/fimmu.2020.00078

30. Shrirao AB, Schloss RS, Fritz Z, Shrirao MV, Rosen R, Yarmush ML (2021) Autofluorescence of blood and its application in biomedical and clinical research. Biotechnol Bioeng 118:4550–4576. https://doi.org/10.1002/bit.27933

31. Kim H-N, Januzzi JL (2011) Natriuretic Peptide Testing in Heart Failure. Circulation 123:2015–2019. https://doi.org/10.1161/CIRCULATIONAHA.110.979500

5.6 Supporting Information

5.6.1 Fluid control system

The fluid control consisted of a metal housing that houses 1) a LFA mold, 2) an Arduino Due board, 3) and a miniaturized vacuum pump. The fluid control system was linked to a computer via USB and managed using an Arduino code. To initiate the immunoassay the fluid control was mounted on top of the outlet port of the LFA. The setup consists of a micropump that is mechanically positioned on the test strip using a suction cup. The pump works on the basis of the piezo effect. There are two piezoceramics in a pump that deform when a voltage is applied, allowing the transportation of liquid. These piezo actuators enable the pumping of liquid in a specific direction.

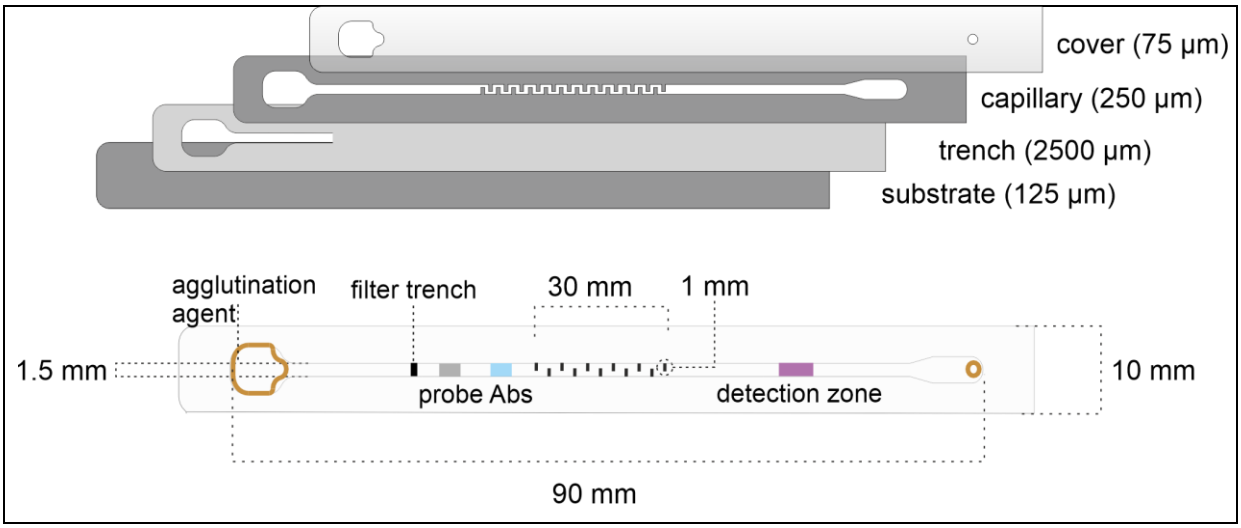

Figure S1: Lateral flow build-up. The lateral flow channel consists of four layers: (1) the substrate, (2) the trench, (3) the capillary and (4) the cover. Purple shape represents the detection zone, brown shape represents the agglutination agent, gray and blue shapes represent probe capture and probe detection antibody labeled fluorescence NP.

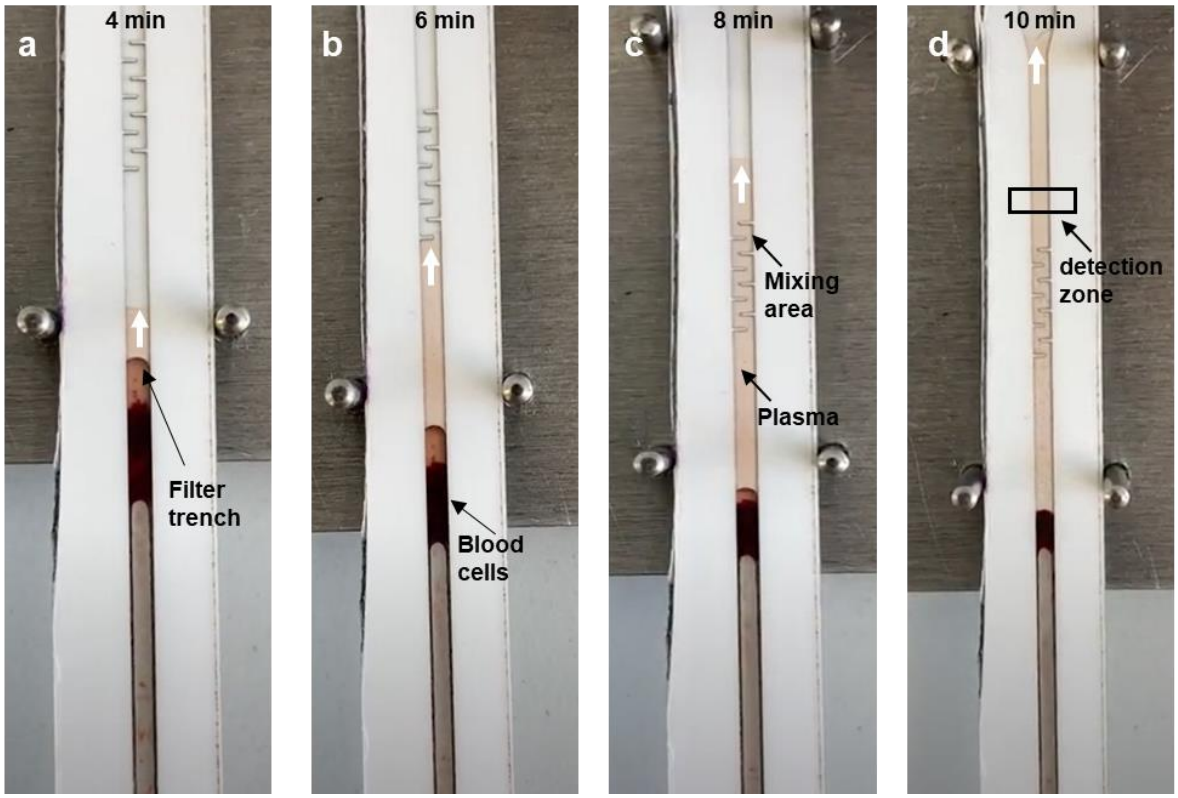

Figure S2: Snapshots showing plasma extraction along the plasma separation channel within 10 minutes. Agglutinated red blood cells are trapped inside the filter trench, eventually resulting in separation of plasma (a). The separated plasma is routed to the mixing area (b). Mixing of plasma and rehydrated probe-specific fluorescent-labeled antibodies, result in the formation of immune-complexes (c). The biotinylated immune-complex is captured in the streptavidin-rich detection zone for the fluorescence read-out (d).

6 Conclusion and Future Perspectives

POCT has gained significant importance during the COVID-19 pandemic. Beyond the pandemic, POCT continues to be a critical component in clinical analysis, particularly in the early diagnosis of diseases. The LFA is the most widely used format for self-testing and facilitates straightforward one-step assays, including optical detection. LFAs easy working mechanism is usually based on membrane and fleece materials for reagent storage, protein immobilization, and sample transportation. However, these materials are prone to inevitable inconsistency in the fabrication process. Additionally, the high inherent sample absorption properties necessitate extra-large sample volumes or additional operational steps, thereby excluding finger prick sampling and compromising failure-safe operation. Therefore, alternative test formats, such as the membrane-free LFA approach presented here, are now being employed. Simple execution of the testing procedure is crucial, especially for untrained personnel or home-testing. In addition, the development of miniaturized pumps and additional equipment facilitates their use in resource-limited settings. Storing the reagents in dry form on the test allows for simple initiation upon sample application, eliminating additional operational steps, such as reagent application or an extra washing step. To address these limitations, a LFA was developed by replacing the membrane's functionalities, such as protein immobilization and sample transportation. This design incorporates a streptavidin-functionalized PEM and streptavidin-functionalized MNPs, in combination with a micropump. This approach, with its straightforward fabrication, ease of handling, and high stability, is ideally suited for home-testing.

To further improves the on-field application, especially in low-resource settings, where skilled personnel or laboratory equipment is limited, the integration of a blood-plasma separation module was required. Since sample preparation plays a pivotal role in blood analysis, the here developed platform integrates an efficient and straightforward method for blood plasma separation. By leveraging a gravity-based sedimentation approach, it eliminates the need for complex and bulky equipment like centrifuges. This not only simplifies the procedure but also makes it more accessible for POCT in remote or resource-limited settings. Furthermore, the use of an agglutination agent accelerates

the sedimentation process by forming blood cell clusters, enhancing the overall efficiency of plasma separation. This method maintains high performance while ensuring patient comfort, crucial for practical and effective on-field diagnostics.

The fully integrated membrane-free LFA shows great promise for enhancing POCT with its simplified fabrication and operational advantages. However, to realize its full potential, significant improvements are needed to address the high standard deviations observed in current approaches. One major contributing factor is the manual assembly of the platform and the manual pipetting of reagents, both of which introduce variability and affect the consistency of results.

To overcome these challenges, a shift towards automated roll-to-roll fabrication processes is essential. This method can provide a more consistent and scalable production of membrane-free LFAs. Automated reagent application within this process can ensure precise and uniform distribution, significantly reducing variability and improving the reliability of the assays.

Further miniaturization of hardware, such as fluorescence camera and analysis software, is also crucial to fully exploit the potential of this setup. Although adding extra hardware may initially raise the platform's costs, advancements in the Internet of Things (IoT) could make these integrations more cost-effective over time. Enhanced sensor performance and objective read-out capabilities would reduce the likelihood of misinterpretation, thereby increasing the overall accuracy and dependability of the tests.

The ability to measure multiple substances simultaneously from a single sample has gained increasing importance in POCT, recently. Measuring multiple specific biomarkers helps to gain a better understanding and diagnosis of the patient's condition. By dividing the main channel of the developed LFA into multiple smaller channels, it is possible to integrate analyte-specific antibodies in each channel, enabling the simultaneous detection of various biomarkers. This approach enhances the diagnostic capability and provides a more comprehensive analysis of the sample. Implementing these advancements allows membrane-free LFAs to achieve the robustness and reproducibility required for widespread clinical and home-testing applications. This will

not only enhance patient comfort and ease of use but also pave the way for more accurate and dependable POCT solutions in diverse healthcare settings.

Eidesstattliche Erklärung

Ich erkläre hiermit an Eides statt, dass ich die vorliegende Arbeit ohne unzulässige Hilfe Dritter und ohne Benutzung anderer als der angegebenen Hilfsmittel angefertigt habe; die aus anderen Quellen direkt oder indirekt übernommenen Daten und Konzepte sind unter Angabe des Literaturzitats gekennzeichnet.

Weitere Personen waren an der inhaltlich-materiellen Herstellung der vorliegenden Arbeit nicht beteiligt. Insbesondere habe ich hierfür nicht die entgeltliche Hilfe eines Promotionsberaters oder anderer Personen in Anspruch genommen. Niemand hat von mir weder unmittelbar noch mittelbar geldwerte Leistungen für Arbeiten erhalten, die im Zusammenhang mit dem Inhalt der vorgelegten Dissertation stehen.

Die Arbeit wurde bisher weder im In- noch im Ausland in gleicher oder ähnlicher Form einer anderen Prüfungsbehörde vorgelegt.

Ort, Datum Unterschrift